University of Pavia
Department of Molecular Medicine

# PhD course in Translational Medicine

XXXVI cycle

*PhD thesis on*

# Molecular determinants of diaphragm muscle impairment in a mouse model of Spinal Muscular Atrophy and a possible nutraceutical intervention

Tutor:
Prof. Monica Canepari

Candidate:
Dr. Francesca Cadile

Academic year 2020-2023

# Introduction

## 1 Spinal Muscular Atrophy

Spinal Muscular Atrophy (SMA) is an autosomal recessive genetic disorder characterized by the loss of nerve cells called *motor neurons* (MNs) and therefore classified as a motor neuron disease. The disease affects MNs located in the anterior horn of the spinal cord, resulting in weakness and progressive paralysis of proximal muscles, leading to muscle atrophy and respiratory failure (Schroth et al., 2009). SMA is the second most common fatal autosomal recessive disorder after cystic fibrosis in infants. According to a pan-ethnic study, it has an incidence of 1 in 11 000 and the carrier frequency of the disease is 1 in 54 (D'Amico et al., 2011; Bottai et al., 2013).

The first case of SMA was ascertained in 1850 in an adult by the two French doctors François-Amilcar Aran and Guillaume Duchenne. At the end of the same century, in the 1890s, the disease in its most severe form was identified in a child by Werdnig and Hoffmann (Werdnig et al 1891; Hoffmann et al., 1893). But only a century later in 1990, the investigators used linkage analysis to identify the locus of the SMA gene on chromosome 5q13 (Brzustowicz et al., 1990; Lunn et al., 2008). In 1994, were identified deletions of multicopy microsatellites in patients with spinal muscular atrophy; some of which were in linkage disequilibrium with the disease locus. Lastly, in 1995, the spinal motor neuron gene (*smn*) was identified as the disease-causing gene (Lunn et al., 2008).

More than 98% of patients affected by SMA have a homozygous disruption of *smn* gene by deletion, rearrangement, or mutation (Lunn et al., 2008). A lack of functional SMN protein, the product of *the smn* gene, is responsible for the degeneration of MNs in the spinal cord, which arises in muscle weakness and hypotonia; in fact, the loss of strength in proximal muscles is a characteristic of SMA patients. Interestingly, MNs that innervate slow-twitch muscles are more vulnerable than those that innervate fast-twitch muscles (Butchbach et al., 2007; Lunn et al., 2008). In two-thirds of cases, SMA patients develop associated problems such as scoliosis due to the progressive degeneration of MNs and the consequent muscular atrophy, and, depending on the SMA subtype, difficulties swallowing, poor head control and

respiratory insufficiency that causes death in severe cases (*NORD (National Organization for Rare Disorders https://rarediseases.org/)*; Vu-Han et al., 2021).

Although SMN is a ubiquitous protein the major pathological hallmarks of SMA are focused on the neuromuscular system but there are many other organs affected. For example, in some cases of severe (type I) SMA, there are typical atrial and ventricular septal defects that can cause dangerous changes to the normal cardiac rhythm and cause sudden death (Bottai et al., 2013).

It is now known that the pathophysiology of SMA is more complex than thought until a few years ago and muscle cells are not only major players in the development of the main clinical symptoms, but also represent a considerable contributor to SMA pathogenesis.

Numerous studies have demonstrated the presence of muscle defects in SMA disease, indicating that SMN levels are imperative to establish and maintain molecular homeostasis in skeletal muscle (Mutsaers et al., 2011). Different variations in muscle fiber size can be observed at a histological level, with SMA muscle cells showing a decreased cross-sectional area (CSA) due to connective tissue infiltration. This is indicative of muscle cell necrosis (Cifuentes-Diaz et al., 2001). The sarcolemma is also destabilized, as showed by Cifuentes-Diaz and colleagues, leading to the high release of muscle enzymes such as creatine kinase 4 (CK) into the circulating blood of SMA patients. CK, in fact, can typically be used as a biomarker of the disease (Pino et al., 2021). In vitro studies have shown that muscle cells from patients with SMA inhibit neuronal outgrowth and development when co-cultured with wild-type motor neurons, indicating that communication between muscles and neurons is essential for the onset of SMA (Braun et al., 1995; Guettier-Sigrist et al., 2002). It is noteworthy that muscle activity significantly impacts neurogenesis and motor neuron viability due to the release of myokines (Pedersen et al., 2011). These myokines can act as retrograde signals from skeletal muscles through neuromuscular junctions (NMJs) to motor neurons (Braun et al., 1995; Bottai et al., 2013).

In both mouse models of SMA and patients with SMA, degenerative pathologies in NMJs are found. NMJs exhibit three principal pathological features, namely immaturity, denervation, and neurofilament accumulation (Cifuentes-Diaz et al., 2001; Rafii et al., 2002; Kariya et al., 2008). The initial emergence of these deficiencies during the pathogenesis of SMA suggests that they may anticipate MN dysfunction, supporting the hypothesis that NMJs and muscles play an important role in SMA (Cifuentes-Diaz et al., 2001; Kong et al., 2009; Murray et al., 2008; Boido & Vercelli et al., 2016).

Mitochondria appear to play a crucial role in both MNs and muscles within the context of SMA. Under normal circumstances, mitochondria are abundant in presynaptic nerve terminals in animal models, where they play a critical part in modulating the efficacy, plasticity, and presynaptic differentiation of synapses. However, research has shown that there is a compromised axonal transport of mitochondria in SMA. The mitochondrial network seems to be impaired in SMA motor neurons, with the organelles' structure destabilized and displaying signs of fragmentation, edema, and concentric lamellar inclusions even if their density seems to remain unchanged (Miller et al., 2016). Mitochondrial mobility indicates a decrease in retrograde transportation as demonstrated by Miller and colleagues. Furthermore, both basal and maximum mitochondrial respiration in SMA motor neurons show a decline, coinciding with an increase in the level of oxidative stress and impairment of the mitochondrial membrane potential (Miller et al., 2016). These deficits, at least in the mouse model, occur during the pre-symptomatic phase. This implies that they have a significant role in the progression of SMA and are not a result of the disease (Miller et al., 2016). Mitochondria are also known as key activators of the intrinsic apoptosis pathway (Pogmore et al., 2021). The results obtained by apoptotic markers in SMA MNs suggest the occurrence of programmed cell death (Piras et al., 2017).

On the other side, muscle tissue from SMA patients shows both mitochondrial depletion and impaired mitochondrial biogenesis, as evidenced by the fact that mtDNA is significantly reduced, as well as the expression level of PGC1-alpha, the primary cofactor of mitochondrial biogenesis (Montes et al., 2015; Ripolone et al., 2015; Montes et al., 2021). SMA muscle pathology, in both mouse models and patients, is indeed associated with mitochondrial respiration impairments, manifested by a decrease in oxidative phosphorylation enzyme activity, reduced expression of oxidative phosphorylation chain component, and overproduction of reactive oxygen species (ROS) leading to oxidative stress (James et al., 2021).

Current pharmacological and cellular approaches, mainly focused on counteracting alterations at the motor neuron level and overlooking the crucial contribution of muscles and NMJ to the development of the condition, are only partially effective in improving the clinical picture of SMA. It is therefore necessary to develop alternative and parallel intervention sites that, in the near future, could provide new and real expectations for the treatment of SMA, especially for patients who unfortunately cannot be treated with recently discovered drugs (Spinraza, Risdiplam, and Zolgensma).

It is imperative to encompass all aspects relevant to the pathophysiology of SMA when devising a fresh therapeutic strategy.

# 2 SMN – Gene and Protein

## 2.1 Smn Gene

*The smn* gene is part of a 500 kb inverted duplication on chromosome 5q13. This gene is present in multiple copies in the human genome: one *Smn1* (*Smn*T, telomeric) and several *Smn2* (*Smn*C, centromeric). Both genes contain nine exons and eight introns that span about 20 kb genomic region. The telomeric and centromeric copies of this gene are nearly identical and encode the same protein. *Smn1* and *Smn2* differ by a single nucleotide (C→T) within an exon splice enhancer of exon 7 (Lorson et al., 1999; Monani et al., 1999). Transcripts derived from SMN1 contain exon 7 while most of the transcripts from SMN2 lack exon 7. This kind of mutation, which affects an exon splice enhancer, results in the exclusion of exon 7 in most transcripts (90% - SMNΔ7) (Lunn et al., 2008) (**Figure 1**). This means that only 10% of the translated protein is completely functional since the excision of the exon 7 leads to the synthesis of a protein that is less prone to oligomerize concerning its full-length form, exhibiting reduced stability and increased susceptibility to degradation. (Burghes & Beattie et al., 2009; Iyer et al., 2014; Le et al., 2005).

Loss of *Smn1* is essential to the pathogenesis of SMA, while the severity of the disease is primarily related to the number of copies of *Smn2* (D'amico et al., 2011).

SMA disease is phenotypically very heterogeneous and is classified into five types (0-IV) based on 3 parameters: the age of onset, the severity of motor decline, and life expectancy.

Most SMA type I patients have two copies of SMN2 (Gavrilov et al., 1998), three SMN2 copies are common in SMA type II, while type III and IV generally have three or four (Feldkötter et al., 2002; Rudnik-Schöneborn et al., 2009).

Unlike humans, mice carry only one *Smn* gene (m*Smn*) which is equivalent to *Smn1* (DiDonato et al., 1997; Viollet et al., 1997). Loss of m*Smn* results in embryonic lethality in the mouse suggesting that the m*Smn* gene product is essential for cell function and survival (Schrank et al., 1997).

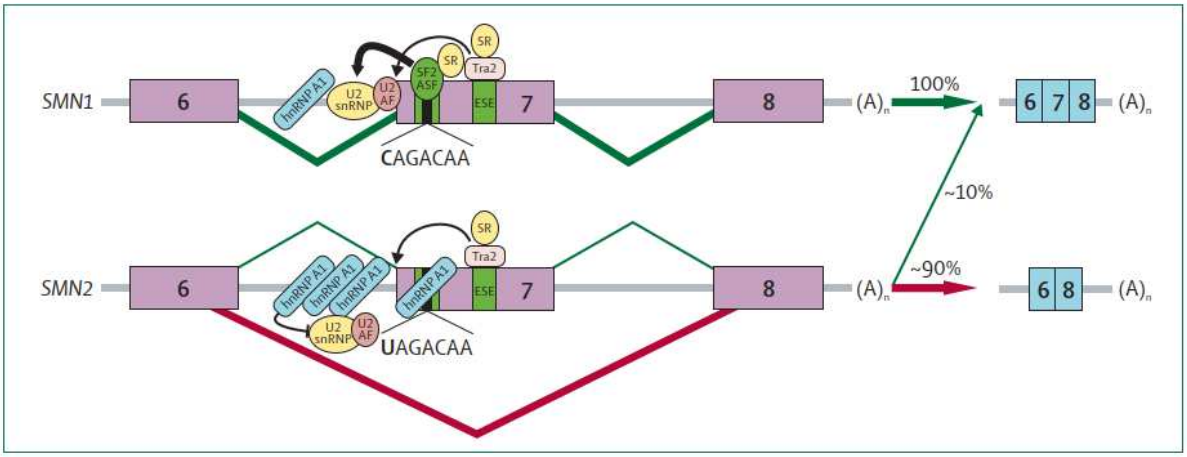


**Fig.1** Representation of pre-mRNA splicing of SMN1 and SMN2 genes (Lunn et al., 2008).

## 2.2 SMN Protein

Survival of motor neuron or survival motor neuron (SMN) is a protein that in humans is encoded by the *Smn1* or *Smn2* genes. SMN protein was first highlighted as a protein of interest when mutations in its coding gene were linked to the SMA (Lefebvre et al., 1995). SMN encodes a 38 kDa protein with 294 amino acids, ubiquitously expressed and localized in the cytoplasm and the nucleus, and is particularly abundant in motor neurons of the spinal cord (Coovert et al., 1997). The SMN protein is expressed in all somatic tissues and is highly conserved in all living things (Paushkin et al., 2000; Miguel-Aliaga et al., 1999). SMN is a fundamental protein especially in the nucleus where it is involved in the assembly of small nuclear ribonucleoprotein complexes (snRNPs), thus being responsible for the correct RNA maturation and metabolism (Piras et al., 2017; Bowerman et al., 2012). The Tudor domain (a highly conserved motif with a function in protein-protein interactions) of SMN is responsible for interaction with coilin, a marker of Cajal bodies (CBs) (Hebert et al., 2001). Mutations in this domain, are often found in SMA patients. Inside the nucleus SMN protein is condensed in dot-like structures linked with coiled Cajal bodies, named “gems” (Liu et al., 1996), which are coilin negative as opposed to CBs. The gem’s function is still unclear, but it has been observed that SMA patients are characterized by a reduced number of them in their nuclei concerning controls (Lunn et al., 2008). How the reduced amount of SMN impacts the formation of CBs or gems and how this affects the severity of SMA must be determined (Lunn et al., 2008).

SMN1 contains nine exons, with exon 8 remaining untranslated. SMN2 differs from SMN1 at 5 bases, and a C-to-T transition in exon 7 of SMN2 favors skipping of exon 7 during splicing, resulting in the majority of SMN2 products being a truncated isoform referred to as SMNΔ7 (Lorson et al., 1999; Chaytow et al., 2018). However, it is known that the missing SMN protein can be partly offset by SMN2, in fact, the number of copies of SMN2 is inversely proportional to the severity of the pathology (Lorson et al., 1999). Other SMN isoforms have been found in various tissues (**Figure 2, 3**): an SMN6B protein can be translated from both the *Smn1* and *Smn2* genes by the inclusion of an intronic Alu sequence as an alternative exon following exon 6 (Seo et al., 2016). SMN6B is tracked both in the nucleus and cytosol and is twofold more stable than SMNΔ7 but twofold less stable than full-length SMN. Another isoform, SMNΔ5 is present in muscle and the central nervous system (Gennarelli et al., 1995). Finally, an axonal-SMN (a-SMN) has also been proposed, being produced from intron 3 retention during splicing; it is localized to the axon, and its expression is enhanced in the spinal cord and the brain (Chaytow et al., 2018).

SMN is not only a common protein linked to genetic disease, but it turned out to be important in multiple fundamental cellular homeostatic pathways, including a well-characterized role in the assembly of the spliceosome and the biogenesis of ribonucleoproteins. The SMN protein appears to be involved in multiple functions, including the resolution of R-loops. These are structures that arise during transcription where DNA-RNA hybrids form. If these structures go unresolved, it can result in genome instability and DNA damage. SMN associates with both RNApolII and the helicase SETX during transcription, which are responsible for resolving these structures (Lomonte et al., 2020).

SMN deficiency has been associated with alterations in oxidative status, dysfunction of mitochondria, and impairment of bioenergetic pathways. More recent studies have shown that SMN is also involved in other housekeeping processes, including mRNA trafficking and local translation, cytoskeletal dynamics, endocytosis, and autophagy (Chaytow et al., 2018). Moreover, SMN can influence the function of the ubiquitin-proteasome system, it is also involved in various cellular signaling pathways and the dynamic regulation of membranes and the cytoskeleton; all of these functions of SMN are crucial for mitochondrial biogenesis, transport, and dynamics, and for $Ca^{2+}$ homeostasis and cell signaling, (Zilio et al., 2022) **(Figure 4**).

The in-depth study of the SMN protein regarding its ubiquitous presence and multiple functions in all eukaryotic cells has led to the conclusion that SMA is not purely an MNs

disorder but it's something more complex (Burr et al., 2023). It is still uncertain why MNs are particularly susceptible to low levels of SMN protein. One theory has been put forward to try to answer this question: the disruption of snRNP formation affects the splicing of a specific set of genes that are important for MN circuitry. To date, the issue remains unresolved (Burghes & Beattie et al., 2009; Fallini et al., 2012).

| SMN isoform | Splicing | Protein isoform | Expression | Localisation |
|---|---|---|---|---|
| Full-length SMN (FL-SMN) | Exons 1, 2a, 2b, 3, 4, 5, 6, 7, 8 | Functional SMN protein | High expression during development, decreasing into the adult CNS | Nuclear gems and cytosolic, including axons, dendrites and synapses |
| SMNΔ7 | Exons 1, 2a, 2b, 3, 4, 5, 6, 8 | Degradation signal introduced by the change in C-terminal | High expression during development, decreasing into the adult CNS | Nuclear accumulation |
| Axonal-SMN (a-SMN) | Inclusion of intron 3 | Truncated protein due to premature stop codon on the boundary of exon 3/intron 3 | Expressed during development, not detected in the adult CNS | Motor neuron axons |
| SMN6B | Inclusion of an Alu element forming exon 6B | Truncated protein due to premature stop codon after exon 6B | Unknown | Nuclear and cytosolic |
| SMNΔ5 | Exclusion of exon 5 | Unknown | Expressed in the mature CNS | Unknown |

**Fig. 2** Main isoforms of SMN (Chaytow et al., 2018).

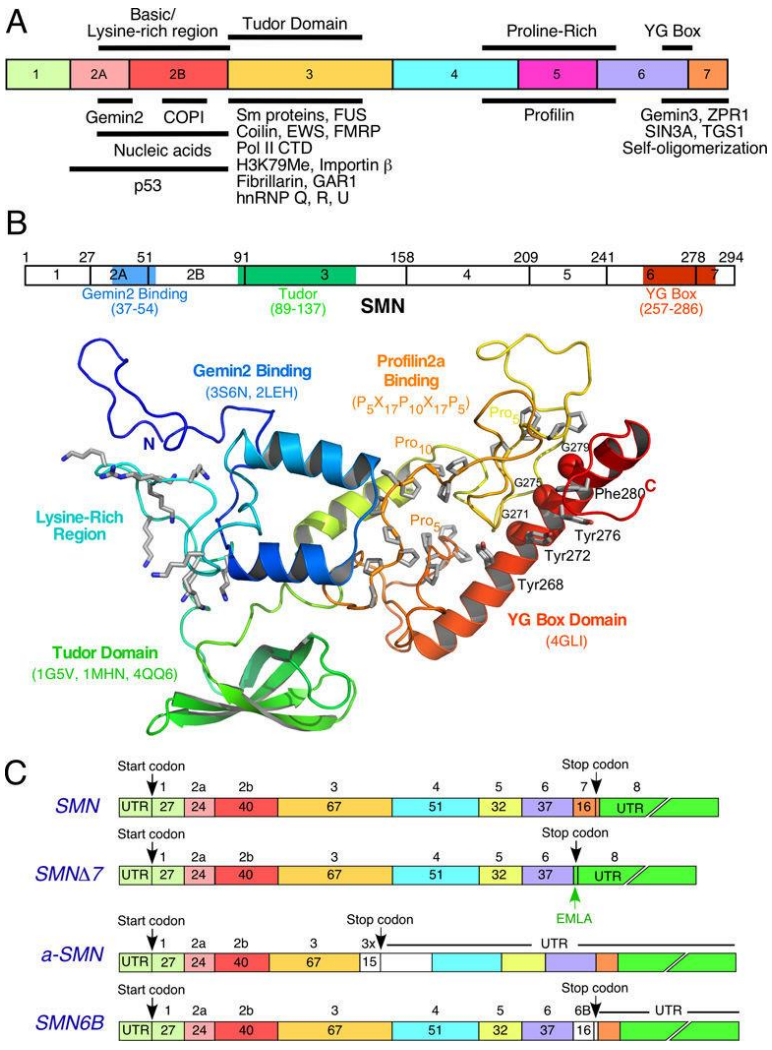


**Fig.3** Structure of SMN protein and *SMN* transcripts (Singh et al., 2017)

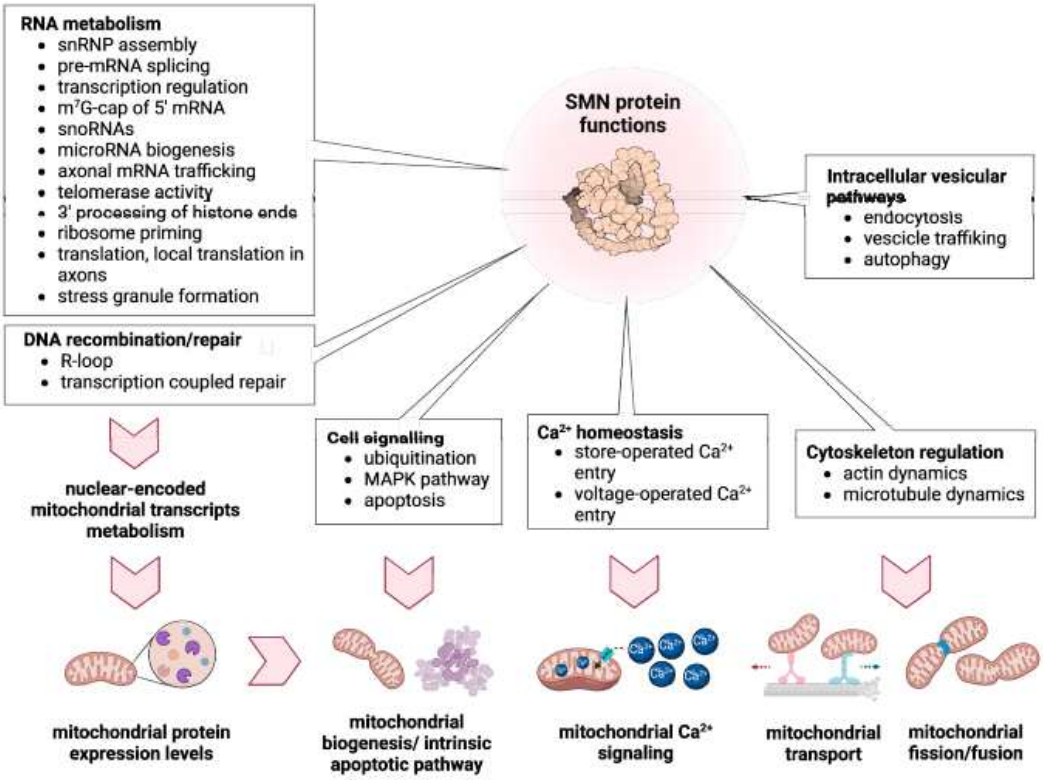


**Fig.4** Different SMN functions (Zilio et al., 2022).

# 3 Spinal Muscular Atrophy Classification

SMA presents itself in a heterogeneous way ranging from death within weeks of birth to mild proximal weakness developing during adulthood. The disease has been categorized into four distinct types due to the detailed clinical reports collected over the last 125 years that describe the clinical manifestations and the wide range of clinical severity of SMA. These reports were compiled and registered into a categorization scheme in 1991 by the International Consortium on Spinal Muscular Atrophy, encompassing numerous phenotypes. Initially, the classification separated SMA into three distinct categories based on the patient's ability to stand or sit and the age of pathology development. Later, a fourth category was introduced for adult patients who developed the disease belatedly. Subsequently, a fifth category was necessary to include patients with prenatal onset resulting in death within weeks (Kolb et al., 2016). Over time, the classification and description of all types of SMA have become increasingly specific, with the understanding that the severity of the pathology is inversely proportional to the number of copies of SMN2 (Smeriglio et al., 2020; Burr et al., 2022) (**Figure 5**).

## 3.1 Type 0 (Congenital SMA)

The newborns diagnosed with type 0 SMA represent the most severe phenotype; they typically only possess one copy of the *Smn2* gene and do not survive for more than a few weeks despite extensive respiratory support (Singh et al., 2021). SMA type 0 defines neonates who exhibit severe weaknesses and hypotonia and who have a medical history of reduced fetal movements. It is believed that the weakness is of prenatal origin. Infants with this condition typically exhibit areflexia, facial diplegia, atrial septal defects, and joint contractures. Life expectancy is shortened, and the majority do not survive past six months of age (Kolb et al., 2016).

## 3.2 Type I (Werdnig-Hoffmann disease)

SMA Type I, also known as Werdnig-Hoffmann disease, is a severe condition that usually presents around six months of age. Individuals affected typically possess 2 to 3 copies of the *Smn2* gene. These patients exhibit decreased muscle tone, along with severe and progressive muscle weakness, abnormal swallowing and speech, weakened sucking ability, and respiratory failure. SMA Type 1 is characterized by rapid loss of MNs and it leads to fatal outcomes or the need for permanent ventilator assistance in over 90% of patients (Singh et al., 2021). The infants never attain the capability to sit independently, the profound hypotonia they experience can result in a "frog-leg" posture when lying down and poor to absent control of their head movements. The weakness in the intercostal muscles, with the diaphragm being relatively spared, results in a chest with a bell-like shape and a pattern of breathing that is paradoxical, commonly known as "belly breathing". Infants diagnosed with type 1 SMA typically experience respiratory failure before the age of two years old. Assisted ventilation can increase survival rates among patients with weak coughs that heighten the risk of mucus aspiration. Such occurrences directly correlate to an amplified chance of recurrent pulmonary infections and even suffocation-related death. In severe cases, tracheostomy and antibiotics may be necessary to manage pneumonia and potential pulmonary complications (Kolb et al., 2016; Darras et al., 2015). SMA Type I can be subcategorized into IA (or type 0), IB with onset less than 3 months, and IC with onset from 3 to 6 months (Burr et al., 2023).

## 3.3 Type II (Dubowitz disease)

SMA-II, Dubowitz disease, or intermediate type typically emerges between 6 and 18 months of age. Most children affected with SMA-II typically possess three copies of the *Smn2* gene. Patients attain the ability to sit without support, and some also gain the ability to stand, but not to walk independently. SMA-II patients exhibit difficulties sitting without support or standing until they reach one year of age (Singh et al., 2021). This intermediate type of SMA typically presents as gradual weakness in the proximal legs that exceeds weakness in the arms. Progressive scoliosis and weakness of the intercostal muscles lead to restrictive lung disease. In these children, cognition is normal (Kolb et al., 2016). Approximately 70% of patients survive up to 25 years of age, with some surviving into their third decade; respiratory compromise is the leading cause of death (Burr et al., 2023).

## 3.4 Type III (Kugelberg-Welander disease)

SMA-III, also referred to as Kugelberg-Welander disease, a mild SMA, is typified by varying degrees of muscle weakness. Patients with SMA-III possess 3-4 copies of the *Smn2* gene. The incidence of SMA-III accounts for 30% of all cases of SMA in the population (Singh et al., 2021). After 18 months, patients present with symptoms similar to type II, including progressive proximal weakness that affects the legs more than the arms. Despite this, patients can walk, but as the disease progresses, they may require a wheelchair. Patients may also experience tremors or exhibit polyminimyoclonus in their hands. In certain instances, prominent calves may be observed. Life expectancy is around adulthood. SMA Type III can be further divided into IIIA, which presents between 18 months and 3 years, and IIIB, which presents after 3 years (Burr et al., 2023; Zerres et al., 1997).

## 3.5 Type IV (adult SMA)

SMA type IV manifests in later life (typically around the age of thirty) and less than 5% of all SMA patients are affected by it. In this type of SMA, patients possess 4-8 copies of the *Smn2* gene. It is a mild form of spinal muscular atrophy that does not significantly impact the patient's life expectancy (Singh et al., 2021). Patients are ambulatory and present with mild leg weakness and develop progressive proximal weakness (Burr et al., 2023).

| SMA Type | Subtype | Age of Onset | Level of Motor Functions | Life Expectancy | *SMN2*cn (%) |
|---|---|---|---|---|---|
| 0/1a | | pre-natal | Need respiratory assistance | <1 month | |
| 1 | | 0–6 mo. | Cannot sit independently | <2 years | 2 (73.4%) |
| | 1b | | Absence of head control and ability to roll over | | |
| | 1c | | Sometimes gain head control or the ability to roll from supine to prone position | | |
| 2 | | <18 mo. | Cannot stand independently | >2 years | 3 (81.8%) |
| | 2a | | Independent sitting lost | | |
| | 2b | | Independent sitting conserved | | |
| 3 | | >18 mo. | Able to stand and walk independently | Adulthood | 3–4 (50.6%; 45.5%) |
| | 3a | 18 mo.–3 y. | | | |
| | 3b | >3 y. | | | |
| 4 | | >20 y. | Weaknesses in lower limbs | Adulthood | |

**Fig. 5** Current classification of SMA patients in 5 types (Smeriglio et al., 2020).

## 3.6 Non-5q SMAs forms

About 95% of cases of SMA result from homozygous deletions occurring in exons 7 and 8 of the *Smn1* gene located on chromosome 5q13. This deletion leads to the development of 5q-SMA, the most common form of the disease. The remaining approximately 5% of cases are attributed to mutations in various other genes, comprising the non-5qSMA spectrum. Non-5qSMA is currently associated with 16 genes and one unresolved locus (Axente et al., 2021). Non-5q forms of SMA are rare and they exhibit genetic and clinical heterogeneity. Typically, they are classified based on the mode of inheritance (autosomal dominant, autosomal recessive, or X-linked) and the distribution of muscle weakness (proximal, distal, or bulbar) (Peeters et al., 2014; Darras et al., 2015). One such form is spinal muscular atrophy with respiratory distress (SMARD); it is an extremely rare neuromuscular disorder. Generally, it manifests between two and six months of life. It is characterized by paralysis of the diaphragm muscles and generalized muscle weakness. Other early clinical features identified in affected children are growth retardation during fetal development, premature birth, weak crying, and foot deformities. The illness is a variant of spinal muscular atrophy type 1, but compared to the latter, the respiratory deficit is more serious. From the beginning, affected children require mechanical ventilation; many are fed through a gastric probe. It is an autosomal recessive disorder caused by mutations affecting the *ighmbp2* gene located on chromosome 11, which encodes a protein known as immunoglobulin μ-binding protein 2 (IGHMBP2) or

immunoglobulin S-μ-binding protein 2 (SμBP-2). This protein is associated with the RNA processing machinery in both the cytoplasm and the nucleus in a similar way to the SMN protein (Zerres et al., 2003; Perego et al., 2020). Important clinical differences with 5q-SMA consist of diaphragm involvement within the first few weeks of life, which is initially unaffected in SMA, and weakness distribution that is distal instead of proximal (Zambon et al., 2023).

One other form is pontocerebellar hypoplasia type 1 (PCH1) which is an autosomal recessive condition and it is a major cause of non-5q spinal muscular atrophy. The range of phenotypes in patients can include neonatal death to survival into puberty. Several symptoms can affect patients, such as lower and upper motor neuron signs, ataxia, visual and hearing impairment, seizures, or contractures. Additionally, a reduced cerebellar size is always observed, while the shape remains unaltered (Ivanov et al., 2018; Zerres et al., 2003). In over 50% of cases, PCH1 results from mutations that affect the EXOSC3 gene (PCH1B form), which encodes subunit 3 of the human exosome complex, the primary machinery responsible for processing RNA. Therefore, it can be deduced that RNA processing is the root cause of both classical and non-classical forms of SMA. PCH1C is similar to the PCH1B form, it arises from mutations in the *Exosc8* gene that encodes an additional subunit of the aforementioned complex. Few cases of mutations affecting *slc25a46* (a gene that encodes a mitochondrial carrier protein) have been reported. It interacts with a protein complex involved in the maintenance of mitochondrial cristae junctions, has pro-fission capacity, and acts in mitochondrial dynamics (Bagli et al., 2017; Ivanov et al., 2018). VRK1 (vaccinia-related kinase) also can cause PCH. It encodes a ubiquitously expressed protein that controls several processes, such as cell cycle regulation or chromatin organization (Peeters et al., 2014).

# 4 Diagnosis and treatment of SMA

Unfortunately, due to the variation in age and severity of symptoms, there may be a delay in making an initial diagnosis of SMA. Individuals with SMA may be identified by three methods, namely preconception carrier screening, fetal prenatal testing, and post-birth testing. Carrier screening is pertinent for individuals with or without a positive family history of SMA, given the relatively high carrier frequency of deletions in SMN1. Prenatal testing of the fetus

can be carried out through chorionic villus sampling or amniocentesis, or potentially through the extraction of fetal cells from the maternal circulation. Newborns can undergo testing for SMA shortly after birth through targeted diagnostic testing if they have a positive family history of the disease, using commonly available testing laboratories, or through unbiased population screening (Mercuri et al., 2022). Diagnostic tests, such as further genetic testing, electromyography, or a blood test to measure creatine kinase, an enzyme released from damaged muscles, may be required for children. Unlike a genetic molecular blood test, these assays cannot accurately confirm a diagnosis of SMA, but they can be used to rule out also other forms of muscle disease. To confirm the diagnosis of SMA a molecular genetic blood test must be carried out to see if the child has a specific mutation in the *Smn1* gene in fact this test is also called as "*Smn* gene deletion test". This test has a dual function as it also measures the copy number of the *Smn2* gene, which indicates the severity of the disease and plays a fundamental role in identifying SMA conditions accurately. In cases of atypical SMA or negative genetic testing for both *Smn1* deletion and mutations, electromyography is a fundamental tool (Naveed et al., 2021; Iftikhar et al., 2021). In any case, early diagnosis of disease is crucial as it enhances treatment effectiveness.

The therapeutic options for SMA depend on the specific case and are determined by the type and severity of the disease. The most severe forms of SMA result in extreme muscle atrophy and weakness, necessitating urgent therapeutic interventions (Singh et al., 2021).

Currently, several SMA therapy possibilities exist (**Table 1**) and the main ones will be explained below.

| Treatment | Modality |
|---|---|
| Nusinersen | SMN2 mRNA splicing modifier |
| Risdiplam | SMN2 mRNA splicing modifier |
| Onasemnogene abeparvovec | SMN1 replacement via AAV9 vector |
| Stem cells | Stem cells therapy |
| Reldesemtiv | enhances the sensitivity of the troponin complex in fast skeletal muscles to calcium |
| Apitegromab | inhibits pro-myostatin and enhances motor function |
| Olesoxime | promotes the survival of purified MNs lacking neurotrophic factors |
| Histone deacetylase inhibitors | increase the expression of SMN |
| Indoprofen, TC007, Azithromycin, inhibition of the proteasome | Stabilize the SMN protein |

**Table 1** Treatment for SMA

## 4.1 Splicing modification of SMN-2 gene

### 4.1.1 Nusinersen

Nusinersen (SPINRAZA) is the first licensed drug for treating SMA in both child and adult patients. The US Food and Drug Administration (FDA) approved it in December 2016, while the European Medicines Agency approved it in June 2017. Nusinersen is an antisense oligonucleotide (ASO) developed to increase the expression of the SMN protein by modulating the splicing of the SMN2 precursor messenger RNA (pre-mRNA) to make a full-length mature messenger RNA (mRNA) from the SMN2 pre-mRNA (Gidaro et al., 2018; Bennett et al., 2019). In 2006, Singh et collegues discovered Intronic Splicing Silencer N1 (ISS-N1), an intron-7 ISS in the *Smn1/2* genes of humans. This component is crucial in regulating alternative splicing of SMN exon 7 and it is associated with SMA pathogenesis (Li et al., 2020). The most optimum site for ASO targeting was identified within intron 7, located approximately 10 nucleotides downstream of the 5'-splice site. The binding of this molecule results in the shifting of the splicing suppressor proteins hnRNP A1/A2. This then permits U1 small nuclear ribonucleoproteins to bind to the 5′-splice site, thereby promoting the inclusion of SMN2 exon 7 into mRNA (Bennet et al., 2019). Specifically, Nusinersen allows the incorporation of exon 7 into the mRNA of SMN2 (Chiriboga et al., 2016) (**Figure 6**).

The recommended dose for both adults and children entails a single administration of 12 mg in 5 mL via the intrathecal route through a lumbar puncture because antisense oligonucleotides cannot cross the blood-brain barrier (Messina et al., 2022; Aartsma-Rus et al., 2017). Four initial loading doses are required, with the first three doses administered at 14-day intervals before the fourth dose is given 30 days after the third dose. One dose every four months is the required maintenance dose (Singh et al., 2021).

Clinical trials have demonstrated that SMA type 1 afflicted patients display considerable enhancements in their motor capabilities after a brief interval following treatment, with these outcomes affirmed by a decline in the concentrations of markers for axonal damage in both blood and cerebrospinal fluid (Bianchi et al., 2021). Other studies have indicated the favorable outcomes of Nusinersen's treatment. Specifically, 51% of patients demonstrated significant advancements in motor functions, such as achieving full head control and independent sitting, whilst only 1% of cases showed standing ability (Finkel et al., 2017). Additionally, overall survival rates were improved (Messina et al., 2022). Recently, a two-year phase IV study with an open-label design was conducted to assess the safety and clinical outcomes of Nusinersen therapy in infants and toddlers diagnosed with SMA, who require further medical assistance following gene therapy treatment. Interim efficacy results from 29 participants treated with Nusinersen indicated that the majority of patients demonstrated increased motor function measured by the mean total score on the Hammersmith Infant Neurological Examination Section 2 (Hine-2) scale, which showed improvements compared to the baseline. Nusinersen has been approved in over 60 countries as a treatment for spinal muscular atrophy in individuals ranging from infants to adults. (https://www.osservatoriomalattierare.it/).

Nusinersen could be administered to patients with type I SMA to extend their survival. However, further investigations are required to determine whether it can improve muscle function (Aartsma-Rus et al., 2017). No relevant adverse reactions were detected: levels of CK and transaminases remained stable, indicating the absence of muscle injury or hepatic abnormalities.

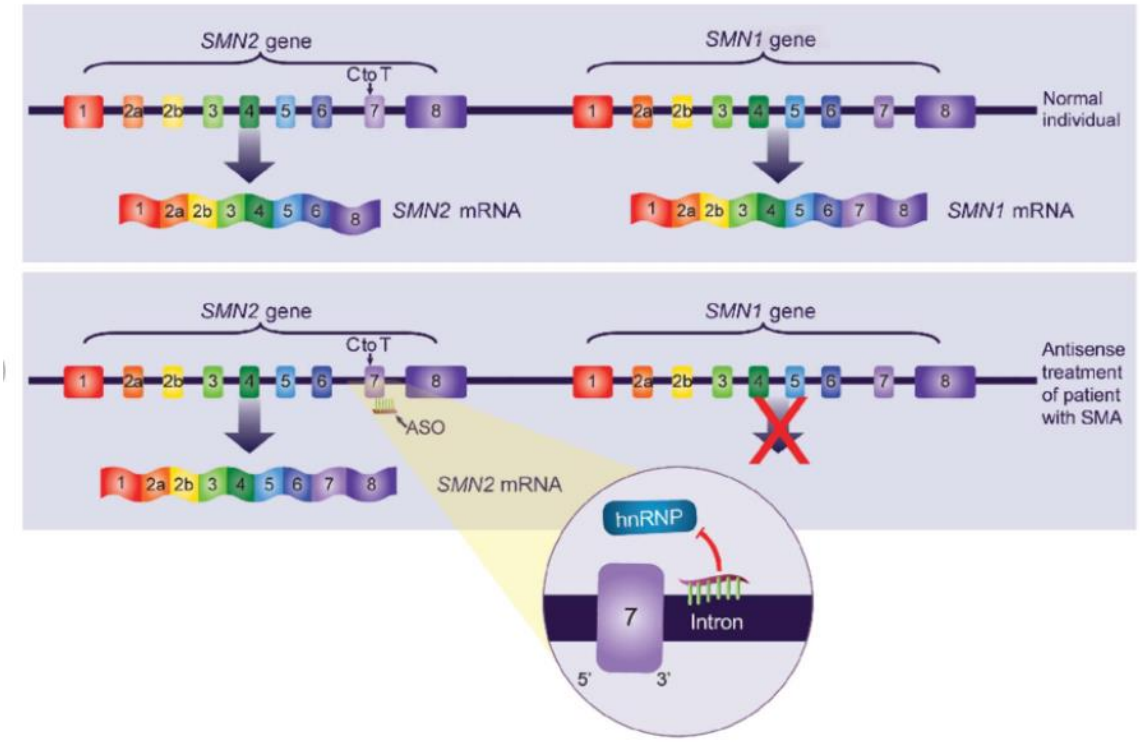


**Fig. 6** Mechanism of action of Nusinersen (Chiriboga et al., 2016).

### 4.1.2 Risdiplam

Risdiplam was granted FDA approval in August 2020 for treating SMA patients aged 2 months and above. Risdiplam is taken orally once a day after a meal, at about the same time each day. During pre-mRNA splicing of SMN2, Risdiplam aids in the precise incorporation of exon 7 into the mature transcript. This inclusion allows to production of adequate quantities of functional SMN proteins required to counteract the loss of SMN1 function observed in SMA patients (Ratni et al., 2021). In 2023 the European Commission approved to extension of the marketing authorization of Risdiplam for the treatment of children below two months old diagnosed with spinal muscular atrophy (SMA) type 1, 2, or 3, or with one to four SMN2 gene copies. The decision was based on provisional results from the Rainbowfish study of pre-symptomatic infants with SMA type 1 aged between zero and six weeks. The Rainbowfish study involved six children with either 2 or 3 copies of the *Smn2* gene who participated in the study for at least one year. After one year of treatment with Risdiplam, 100% (6/6) of the

participants were able to sit, 67% (4/6) were able to stand, and 50% (3/6) could walk independently. All children survived without permanent ventilation at 12 months (https://www.osservatoriomalattierare.it/).

## 4.2 Gene-therapy Onasemnogene abeparvovec

Onasemnogene abeparvovec (Zolgensma®) formerly known as AVXS-101, is a drug based on gene therapy approved by the FDA in 2019 and EMA in 2020 for pediatric SMA 5q-patients who have up to three copies of SMN2 (Messina et al., 2022). Administered via a single intravenous infusion, Onasemnogene abeparvovec utilizes the adeno-associated virus (AAV9) vector to introduce a functional copy of the human survival motor neuron *Smn1* gene into motor neuron cells **(Figure 7)**. AAVs are small non-pathogenic viruses that can efficiently transfect the central nervous system by targeting MNs and astrocytes. A particular AAV serotype, namely serotype 9, can be delivered systemically or through intrathecal injection, as it can cross the blood-brain barrier. Therefore, this allows for the noninvasive administration of the therapy (Parente and Corti et al., 2018). Onasemnogene abeparvovec was well-tolerated overall. While hepatotoxicity is a recognized risk, it can generally be reduced with prophylactic prednisolone (Blair et al., 2022). Patients who have received treatment exhibit enhanced motor and respiratory capabilities compared to the control group, especially when treatment is administered at an early age, emphasizing the significance of prompt diagnosis and treatment (Naveed et al., 2021).

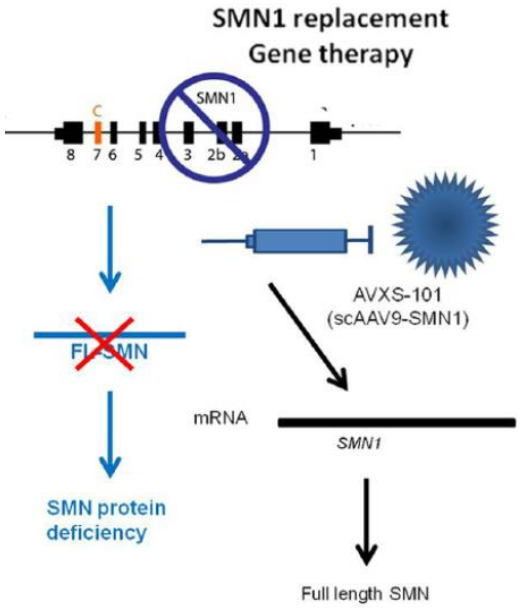


**Fig. 7** Representation of gene therapy approach for SMA with scAAV9 vector (Parente & Corti et al., 2018).

## 4.3 Stem cells

Stem-cell therapies may yield distinct therapeutic advantages, including the safeguarding of unimpaired motor neuron function, the modulation of environmental toxicity, as well as the replacement of both neuronal and non-neuronal cellular populations. It has previously been demonstrated that the transplantation of neural stem cells or motor neuron precursors into the spinal cord or intrathecally into the cerebrospinal fluid improves the phenotype of the SMA mice model (Parente & Corti et al., 2018). Embryonic stem cells can be differentiated into neural stem cells through the use of retinoic acid, sonic hedgehog, and neurotrophic factors. iPSC lines were produced from two patients with type I SMA through nucleofection of adult fibroblasts with reprogramming factors using a non-viral vector method. The transplant into a severe SMA mouse model resulted in an improvement in the disease phenotype, remedying muscle connections and enhancing the physical appearance of the mice. Their weight increased by approximately 50%, and their lifespan was also slightly extended, by around 40%. Although stem cell therapy looks promising, it is currently not comparable to the results obtained with gene or molecular therapy (Zanetta et al., 2014). Zeng and colleagues have generated two iPSC lines from two SMA type I patients with homozygous SMN1 mutations and confirmed their pluripotency and ability to differentiate into three germ layers. These iPSC lines may be used to generate skeletal muscles to model muscle atrophy in SMA that

persists after the treatment of motor neurons. Furthermore, they will serve as a complementary platform for in vitro drug screening (Zeng et al. 2023). Even so, the safety and efficacy of cell therapy must be carefully demonstrated in a preclinical setting before it can be used in humans (Zanetta et al., 2014). In conclusion, the hope is that stem cell therapy in the future could also be used in combination with other therapies to significantly improve SMA symptoms, thus achieving the best possible therapeutic outcome.

However, whenever we think about using stem cells, we face several problems, such as their limited accessibility and difficulty in obtaining them, as well as issues related to immunosuppression.

Moreover, it has never been clarified how long the cells can persist in the adult body and whether they can cause damage (Ahmadian-Moghadam et al., 2020; Zanetta et al., 2014).

## 4.4 Targeting SMN – independent factors

### 4.4.1 Reldesemtiv

Reldesemtiv (CK-2127107) is a second-generation fast skeletal muscle troponin activator (FSTA). It enhances the sensitivity of the troponin complex in fast skeletal muscles to calcium, leading to increased muscle strength in response to neuronal stimuli. It also delays and reduces the onset and severity of muscle fatigue. Patients treated with this small molecule exhibit benefits in a variety of parameters, such as the maximum ventilatory volume or the ability to walk (Hwee et al., 2014; Messina et al., 2022).

### 4.4.2 Apitegromab

Apitegromab (SRK-015) is a monoclonal antibody designed to inhibit pro-myostatin and enhance motor function in patients with SMA. SRK-015 has a specific binding affinity to myostatin preforms, namely, pro myostatin and latent myostatin, leading to the inhibition of myostatin activation. It is suggested for use as a monotherapy or an additional therapy to enhance muscle function in affected individuals. It has been demonstrated that mono- and multiple-ascending doses of Apitegromab are safe and well tolerated at doses up to 30 mg/kg in healthy volunteers (Barrett et al., 2021). Inhibition of myostatin may prove to be a

potentially beneficial treatment for patients affected by milder forms of the condition (Long et al., 2019).

### 4.4.3 Olesoxime

Olesoxime (TRO19622) is a mitochondrial-targeted neuroprotective compound that is part of a group of cholesterol-oximes that have been discovered for their ability to promote the survival of purified MNs lacking neurotrophic factors. Olesoxime aims at the proteins found on the outer mitochondrial membrane and accumulates in mitochondria to avoid the opening of the permeability transition pore caused by oxidative stress, among other things. Olesoxime has demonstrated considerable neuroprotective effects in several in vitro and in vivo models (Bordet et al., 2010). Analyses indicated that Olesoxime may assist in maintaining motor function in patients with Types 2/3 SMA. However, recent studies have unfortunately not confirmed the results obtained in phase 2 clinical trials. Therefore, it is currently challenging to determine the therapeutic efficacy of Olesoxime for SMA, particularly when compared to the latest-generation medications (Muntoni et al., 2020).

## 4.5 Non-specific therapies to increase SMN levels

### 4.5.1 Histone deacetylase inhibitors

Histone deacetylase (HDAC) remodeling through acetylation and/or deacetylation is crucial to the transcriptional regulation of eukaryotic cells. HDAC inhibitors selectively modify gene transcription by remodeling chromatin and altering transcription factor complex protein structure. HDAC inhibitors have been found to increase *SMN2* promoter activity. Valproic acid, a classic class I HDAC inhibitor, has demonstrated advantageous outcomes in SMA mouse models increasing the expression of SMN. Another class I HDAC inhibitor, phenylbutyrate, demonstrated significant SMN expression elevation in patient fibroblasts. However, the drug showed highly varied outcomes in patients. While these molecules demonstrated success in mice models of SMA, they have not progressed to clinical trials. In conclusion, HDAC inhibitors alone do not provide the same level of therapeutic benefit as SMN replacement (Mohseni et al., 2013; Chaytow et al., 2021).

### 4.5.2 Stabilizing the SMN protein

Avoiding the degradation of SMNΔ7, the product of SMN2 would permit low-level expression to have a more pronounced effect on intracellular pathways, which could be therapeutic. Indoprofen is a non-steroidal anti-inflammatory drug (NSAID), which was discovered through an SMN2-luciferase screen to raise SMN protein levels in patient fibroblasts. This screening process was additionally utilized to establish further compounds that enhance SMN expression in vitro and in vivo. A new aminoglycoside, TC007, has been discovered to function as a read-through compound for exon 8 of SMN2, causing an increase in the number of nuclear gems found in patient fibroblasts. Furthermore, it may slightly enhance the survival rate of the severe SMA mouse model. Azithromycin has shown efficacy in the animal model of SMA too. The inhibition of the proteasome may offer another alternative means to enhance SMN levels. Notwithstanding, none of these approaches have yet undergone clinical trials for SMA (Chaytow et al., 2021).

# 5 Animal models

The treatments for SMA that we know of today have been made possible by different animal models that have allowed the discovery of new therapeutic strategies. The nematode Caenorhabditis elegans (C. elegans) is a powerful model for studying the function of several disease-related genes. The C. elegans genome has a single SMN ortholog, *Smn1*, which encodes for an SMN protein with 36% identical characteristics to its human orthologue. SMN is found essential for the survival of C. elegans animals. The C. elegans *Smn1* mutants serve as a proficient tool for identifying modulators of SMN function via large-scale screening. The genome of Drosophila also encodes a single copy of the SMN ortholog *Smn* and it exhibits a 41% sequence homology to human SMN1. Drosophila models carrying various mutations of *Smn* have undergone thorough development and analysis.

Another example is the zebrafish which is well suited to the examination of neuromuscular dysfunction and motor neuron disease because of its well-established motor neuron circuitry

and comparatively uncomplicated neuromuscular setup. Many techniques, including transgenesis and gene knockdown/knockout, are feasible in zebrafish, which enhances the model's potency for genetic studies.

The mouse, like most mammals, contains only one copy of SMN (unlike man, who contains two). Homozygous deletion of *Smn1* in mice results in significant cell death during embryonic blastocyst development, leading to lethality. This indicates the crucial biological roles of the SMN protein. To establish the genetic basis of human SMA, various mouse models have been created via gene targeting or transgenesis to express varying copies of human SMN2 on a homozygous disruption background of *Smn1*. The phenotypic presentations of severe (type I), intermediate (type II), and mild (type III) forms of SMA in various mouse models demonstrate a direct correlation with SMN expression levels and this finding aligns with clinical observations in humans (Edens et al., 2015). For these reasons, mouse models are predominantly used as animal models for studying SMA.

## 5.1 SMNΔ7 mice model

The most widely used SMA mouse model is the Smn1−/−; SMN2tg/tg; SMNΔ7tg/tg called SMA Δ7 mice by Jackson Laboratory stock #005025 (Le et al. 2005). This mouse model carries two transgenic alleles and one targeted null mutant. The Tg(SMN2*delta7)4299Ahmb transgene comprises an SMA cDNA without exon 7, while the Tg(SMN2)89Ahmb transgene comprises the complete human SMN2 gene. The Smn-targeted mutant lacZ reporter allele substitutes endogenous *Smn* expression with lacZ expression (https://www.jax.org/strain/005025). SMNΔ7 is not harmful as it demonstrates a prolonged survival rate of SMA mice from 5.2 to 13.3 days and exhibits symptoms and neuropathology comparable to patients suffering from intermediate type II SMA (Le et al., 2005; Edens et al., 2015) (**Figure 8**). SMNΔ7 SMA mice are significantly smaller than their carrier and normal littermates (**Figure 9**). They demonstrate deficits in surface righting, negative geotaxis, and cliff aversion reflex responses. Furthermore, SMNΔ7 SMA mice demonstrate deficits in their motor function manifested by lowered spontaneous activity levels (fewer grids crossed and fewer pivots), prolonged latency in showing a crawling/walking response, and impaired homing test response. Finally, these mice exhibit weakened muscle strength, indicated by a considerable decrease in their grasping response (Butchbach et al., 2007).

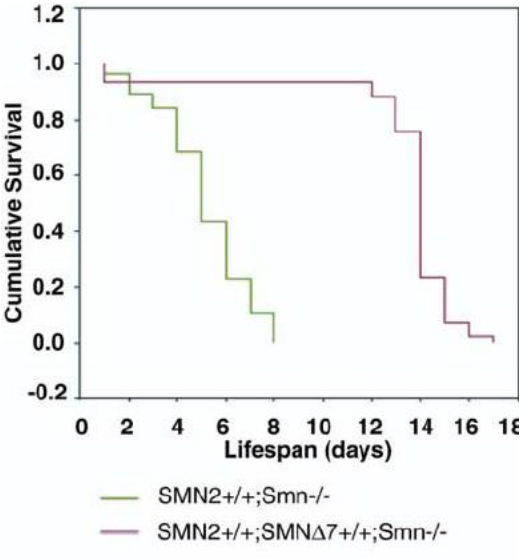


**Fig 8** Cumulative survival of SMN2+/+; SMN -/- compared to SMN2+/+; SMNΔ7 +/+ SMN -/- (Le et al., 2005).

**Fig. 9** SMNΔ7 SMA mouse with spinal muscular atrophy (left) and a control mouse (right) at 11 days old.

# 6 SMA and skeletal muscle

Whilst the fundamental importance of MNs in SMA is widely acknowledged the more severe forms of SMA demonstrate the involvement of many other tissues and organs (Sleigh et al., 2011; Simone et al., 2016) and the muscular tissue, as already mentioned, is the most affected tissue next MNs.

Pathological alterations in the skeletal muscle system in SMA mice models and patients with SMA have been extensively documented in the scientific literature and a plausible direct involvement of muscle in the pathogenesis of SMA has been postulated (Mutsaers et al., 2011; Lee et al., 2011; Kim et al., 2020). Available data indicate a myotube maturation delay (Martinez-Hernandez et al., 2009) and a disruption in the skeletal muscle molecular composition, along with an increase in the activity of the cell death pathway (Lee et al., 2011). Additionally, abnormal differentiation in muscle satellite cells has been reported (Hayhurst et al., 2012). Skeletal muscle fibers from mice with muscle-specific SMN knockout showed a disorganized sarcolemma and mice had reduced lifespan without displaying any overt neuropathology (Cifuentes-Diaz et al., 2001). Histological analysis revealed also marked variation in muscle fiber size, degenerative changes as internal nuclei, proliferation of interstitial connective tissue, and necrosis leading to high serum CK levels (Namba et al., 1970; Mastaglia and Walton et al., 1971). In vitro experiments have shown that muscle cells from SMA patients displayed a reduction in fusion (Arnold et al., 2004), which can inhibit neuronal outgrowth and development when co-cultured with wild-type motor neurons, suggesting that degeneration of muscle-neuron communication is involved in the development of SMA (Braun et al., 1995; Guettier-Sigrist et al., 2002). The decrease in muscular force produced by SMA muscles is attributed to their small muscle fiber size rather than any deficiencies in their innervation. Significant muscle weakness is associated with the delayed expression of mature isoforms of specific proteins, such as ryanodine receptors and sodium channels. Concurrently, there is increased expression of the perinatal myosin isoforms, accompanied by decreased expression of the adult ones (Lee et al., 2011).

The significance of SMN protein to muscle function is intrinsic as studies have shown that reintroducing SMN to muscle, even in advanced stages of pathology, can help alleviate the condition (Kim et al., 2020).

The effect of SMA on the skeletal muscle system is not uniform, and the muscle groups that are affected by the disease and those spared are similar in both human and mouse models of SMA (Durmus et al., 2017). Abnormalities and dysfunction in NMJs have been also discovered leading to an overt phenotype that compromises survival.

Severe denervation affecting numerous muscles essential for vital motor functions (such as maintaining head posture, respiration, and mastication) was observed in end-stage SMA mice models similar to what we observe in human SMA patients (Ling et al., 2012). Denervation is more prevalent in the muscles located in the head and trunk; however, it also occurs in the muscles situated in the proximal and distal limbs (Ling et al., 2012). Mice SMA models exhibit aberrant synaptic protein expression, delayed post-synaptic maturation, impairment in the development of acetylcholine receptor (AChR) clusters together with impaired release of synaptic vesicles (Jablonka et al., 2007; Kariya et al., 2008; Murray et al., 2008; Kong et al., 2009; Ling et al., 2010; Ruiz et al., 2010; Torres-Benito et al., 2011). This is accountable for the halted post-natal development of the NMJ and maturation of motor units and also contributes to muscle weakness (Voigt et al., 2010).

The presence of mitochondrial disturbances in the locomotor muscles of patients and mice models of SMA was also observed. It has been demonstrated, in fact, that muscle pathology in SMA is connected to a decrease in mitochondrial respiration, reduced activity in enzymes for oxidative phosphorylation, and a simultaneous reduction in the expression of subunits for oxidative phosphorylation machinery that are encoded in both the nucleus and mitochondria (James et al., 2021). Analysis of muscle biopsy samples from patients with SMA-II compared to age-matched controls indicated evidence of mitochondrial dysfunction in skeletal muscle as a decreased COX activity in the limb muscles and paraspinal muscles (Ripolone et al., 2015). Defects in mitochondrial activity in SMA muscle impede proper muscle fiber maturation and contraction, hence leading to patient weakness and hypotonia. It is interesting to note that myoblasts and differentiated myotubes from SMA patients showed an intrinsic energy deficit characterized by an increased reliance on mitochondrial ATP production (James et al., 2021).

Finally, electron microscopy analysis has revealed the presence of mitochondrial swelling and vacuolar degeneration, with various grades, with a concentric, onion-like arrangement of mitochondrial cristae in SMA mice models with *Smn1* deficiency in muscle leading to

autophagy/mitophagy alterations and finally defective mitochondrial clearance (Chemello et al., 2023).

## 6.1 Diaphragm muscle in SMA

Although muscle atrophy and severe muscle weakness are the classic features of SMA, the diaphragm muscle deserves a separate chapter.

Respiratory involvement plays a major role in morbidity and mortality in children (LoMauro et al., 2016) and mice (Michaud et al., 2010) with SMA. Severe SMA mouse models exhibit defects in breathing patterns with smaller ventilation volume, longer breath duration, and greater apnea frequency and duration (Michaud et al., 2010). Intercostal and paraspinal muscles are more impacted than the diaphragm, which is relatively less affected (Crawford et al., 2003). Based on clinical evaluations, patients with intermediate type II SMA were found to have relatively intact diaphragm strength. However, these patients also showed an increase in fatigue sensitivity which can lead to acute respiratory failure, particularly during sleep (Fauroux et al., 2020). This suggests that the diaphragm serves as the primary muscle upon which the entire respiratory process relies and, as a result, experiences heightened fatigue. Diaphragmatic fatigue was detected by Fauroux and colleagues in SMA type 2 patients above 10 years of age. The rapid increase in the burden on the diaphragmatic muscles, coupled with the mechanical hindrance caused by spinal deformity, worsens lung compliance (Khirani et al., 2013).

As has long been known, muscular fatigue is strongly linked to mitochondrial function (Schiaffino & Reggiani et al., 2011). Mitochondria could influence muscle fatigue, predominantly through the modulation of energy production and/or through ROS accumulation and consequently the oxidation of cellular proteins including myofilaments, DHPR, RyR1 receptors, and SERCA pumps (Wan et al., 2017).

Very few studies analyzed the human SMA diaphragm at the molecular level. No clear damage at the mitochondrial level was found in one postmortem diaphragm muscle sample from a patient with SMA type I (Ripolone et al., 2015).

Degenerative changes of NMJs in the diaphragm have been described. At the molecular level, the majority of NMJs in the diaphragm of mice with SMA exhibit suboptimal terminal

arborization, as well as neurofilament buildup and a decreased quantity of AchRs (Neve et al., 2016; Kariya et al., 2008). The axons of the phrenic nerve innervating the SMA diaphragm degenerate, but functionally, however, this muscle appears to be comparatively preserved, which may be a paradox that can be explained by the diaphragm's ability to tolerate a much higher loss of healthy motor units than other nearby muscle groups (Kariya et al., 2008).
Moreover, pronounced swelling and disintegration of mitochondria have been observed in both the postsynaptic areas and the presynaptic axon terminal of mice diaphragm (Voigt et al., 2014). Finally, a proteomic study evidenced altered expression of several proteins involved in diverse mechanisms, including the respiratory electron transport chain, mitochondrial transport, proteolysis, oxidative phosphorylation, protein acetylation, and apoptosis at the level of sub-synaptic regions (Neve et al., 2016).
These changes seem to be degenerative rather than developmental. In fact, the diaphragm must be highly efficient at birth to expand and clear the lungs, as movement is very limited in the first few days of life. The maturation of the neuromuscular components of the trunk proceeds in a neck-to-tail direction during embryogenesis. This means that the occurrence of SMA-dependent pathological changes may be contingent upon the maturation of motor units, despite the fact that these changes are not developmental in and of themselves. This stage would be reached earlier in the diaphragm than in the lower limbs (Voigt et al., 2010; Voigt et al., 2014; Mcgovern et al., 2008).

# 7 SMA and Nervous System

SMN deficiency plays a major role in MNs' development and maintenance, which could result in the intrinsic deterioration of skeletal muscle due to MNs death in SMA.
The rapid degeneration of MNs during disease onset results in postnatal NMJ impairments both in mice and humans.
As already mentioned NMJ pathology in SMA mice involves the accumulation of neurofilaments and insufficient axonal growth, causing denervation and disrupted calcium homeostasis that leads to decreased motor neuron excitability, reduced terminal arborization, and inhibited synaptic vesicle release (Kariya et al., 2008; Shababi et al., 2014). Interesting studies indicate that these impairments could arise as a secondary outcome of intrinsic MNs

pathology, as synapse loss is inhibited by a selective increase of SMN levels in MNs (Gogliotti et al., 2012). Specific deficiencies comprise hindered acquisition of excitatory synaptic inputs of MNs and mature firing patterns of MNs; radial growth of motor axons, ensheathment, and myelination of Schwann cells (Mercuri et al., 2022). Mitochondria in the MNs of SMA-afflicted mice displayed functional impairment and fragmentation, along with reduced respiration and ATP synthesis, defective retrograde transport, lower membrane potential, and increased ROS production (Miller et al., 2016).

The low levels of SMN could also impact certain phases of brain maturation and maintenance. Low SMN levels disturb cell proliferation and neurogenesis in SMA mice (Wishart et al., 2010). The most notable morphological changes were qualitatively observed in the hippocampus, with a particularly striking effect on the hippocampal dentate gyrus. Wishart and colleagues showed evidence of reduced hippocampal cellular proliferation and neurogenesis after birth in severe SMA mice models, alongside changes in protein expression levels that control proliferation, migration, and developmental process of neuronal cells.

Nevertheless, cognitive function remains preserved in chronic SMA, and clinical observations suggest that infants with SMA Type II exhibit earlier speech development compared to typically developing toddlers (Shababi et al., 2014).

Moreover, the brain shows a high sensitivity to oxidative stress; consequently, the maintenance of redox homeostasis in the brain is crucial for the regular function of the central nervous system (CNS). The redox imbalance might cause tissue damage and initiate neurodegenerative disorders (NDDs). In the brain, mitochondria play a key role in ATP supply to cells via oxidative phosphorylation, as well as the synthesis of essential biological molecules. Inefficient oxidative phosphorylation may generate ROS. Mitochondrial metabolism, phospholipid metabolism, and proteolytic pathways are the potential and major sources of free radicals. A lower concentration of ROS is essential for normal cellular signaling, whereas the higher concentration and long-time exposure of ROS cause damage to cellular macromolecules such as DNA, lipids, and proteins, ultimately resulting in necrosis and apoptotic cell death. Various neurodegenerative diseases such as Parkinson's disease (PD), Alzheimer's disease (AD), Huntington's disease (HD), and amyotrophic lateral sclerosis (ALS), among others, can be the result of biochemical alteration due to oxidative stress (Singh et al., 2019; Jurcau et al., 2021). Most likely these alterations are also present in SMA (Hayashi et al., 2002; James et al., 2021).

Ultimately, it can be said that increased ROS and oxidative stress in SMA pathology, with any exceptions indicating that tissue/cell-type differences and the type of ROS examined, are important (Acsadi et al., 2009).

# 8 Hericium erinaceus and Ergothioneine

Hericium erinaceus also known as Yamabushitake (in Japanese), Houtou (in Chinese), or "lion's mane", is an edible and medicinal mushroom belonging to the class Basidiomycetes, subclass Holobasidiomycetidae, order Hericiales, and family Hericiaceae. It has been used in traditional Chinese medicine for centuries (Gravina et al., 2023). H. erinaceus synthesizes at least 70 distinct bioactive metabolites including β-glucans, erinacines, hericenones, alkaloids, sterols, and volatile aroma compounds. H. erinaceus has many health-promoting properties such as antibiotic, anticancer, antioxidant, antifatigue, antisenescence, neuroprotective, antidepressant, and anti-anxiety activities. It has been demonstrated that the inclusion of H. erinaceus in the diet proved effective in increasing hippocampal neurotransmission, enhancing locomotor performance and recognition memory in normal mice, and improving recognition memory in frail mice during aging (Ratto et al., 2019; Rossi et al., 2018; Brandalise et al., 2017). Additionally, it induced hippocampal and cerebellar neurogenesis (Roda et al., 2021). The impacts of H.erinaceus are not limited to the nervous system. It has been noted that administering this mushroom to mice enhances muscle endurance and boosts mitochondrial function (Komiya et al., 2019).

Of all the components found in H. erinacius, Ergothioneine is undoubtedly one of the most significant. L-Ergothioneine (ERGO) is a thiol derivative of histidine that occurs naturally (Tang et al., 2018) (**Figure 10**). It is named after the Ergot fungus which was responsible for its first identification (Cheah et al., 2017). ERGO arises naturally in the human diet and is synthesized by most mushrooms, cyanobacteria, and numerous types of soil bacteria, although not by animals or plants (Ames et al., 2018). However, it is actively absorbed from the diet of both humans and animals by an intestinal transporter, OCTN1, (encoded by the gene *slc22a4* or *Octn1)* that has a high degree of specificity. This suggests that ERGO serves a useful function. It is also not quickly metabolized or excreted in urine so it can be found in a variety of human tissues and bodily fluids (Halliwell et al., 2018). Numerous in vitro studies have

indeed demonstrated that ERGO has many functions. It is capable of scavenging ROS and Reactive Nitrogen Species (RNS), such as hydroxyl radicals, hypochlorous acid, singlet oxygen, and peroxynitrite; can also modulate inflammation, chelate divalent metal cations like iron and copper (thus reducing their potential to cause oxidative damage), and protect various sources of damage (Cheah et al., 2017). In addition, ERGO may protect mitochondrial DNA from oxidative damage caused by hydrogen peroxide or UV exposure. The therapeutic benefits of ERGO are thought to be mediated through mitochondrial protection (Cheah et al., 2021). It has been suggested that ERGO accumulates and acts as an adaptive antioxidant for the protection of injured tissues. Human studies confirm these effects (Ames et al., 2018). This accumulation appears to be linked to a rise in the expression of the *Octn1* gene, causing an increase in transporter activity (Halliwell et al., 2018). The deletion of the *Octn1* transporter gene in mice or zebrafish leads to oxidative damage to DNA and lipids, highlighting its essential role. Moreover, ERGO promotes the differentiation of neuronal stem cells, which could be crucial for the development and maintenance of the central nervous system (Cheah et al., 2017). The available evidence indicates that ERGO could potentially safeguard the brain from oxidative damage, neuro-inflammation, and toxic amyloid accumulation, and target underlying pathologies in neurodegeneration. Regarding its distribution in the organism, Ergo is capable of crossing the blood-brain barrier, this includes breast milk and even the placenta (Halliwell et al., 2018). ERGO is currently being used as a human food supplement for its antioxidant, cell protection, vision, and heart health properties (Halliwell et al., 2018).

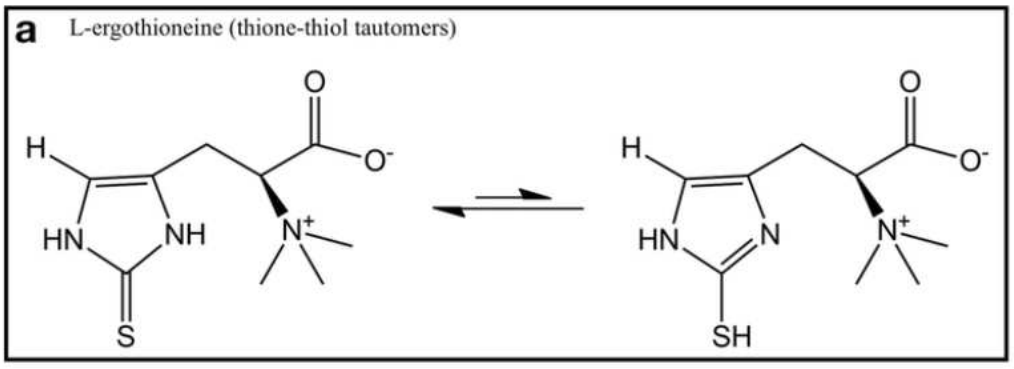


**Fig. 10** Structure of Ergothioneine (Tang et al., 2018).

# Aims and Objectives

The relevance of respiratory muscles to the clinical picture of patients with SMA and the lack of data on the intrinsic contractile capacity of the diaphragm warrant investigations. The main goal of this study is to perform a comprehensive analysis of intrinsic diaphragm functionality and underlying molecular adaptations by integrating functional, biochemical, and molecular analyses of isolated diaphragm muscle from the SMNΔ7 mouse of 11 days. By utilizing a SMA mouse model, we could investigate the diaphragm muscle, which for obvious ethical reasons, cannot be studied at the molecular level in humans. To further understand the diaphragm muscle defects could be of importance for the prevention and effective management of respiratory complications in SMA patients.

The second aim of the study was to test the effect of ERGO, a very potent natural antioxidant molecule, on SMA mice in vivo. The identification of a natural supplement capable of improving the life quality in SMA mice and possibly in SMA patients could be a valuable tool to be combined with the current therapies.
In order to answer this aim, a dietary supplementation will be carried out in pregnant/mothers by adding ERGO to drinking water during pregnancy and feeding time, and the life quality and the lifespan of the newborns were analyzed.

The effectiveness of ERGO treatment was evaluated also on the isolated diaphragm. Based on the antioxidant and protective actions of ERGO on mitochondrial constituents and properties, the hypothesis that oxidative/metabolic damage in diaphragm muscle may play a major role in SMA phenotype could be validated.

Finally, in collaboration with Dr. Daniele Bottai, a neurobiologist with great experience in neural stem cells and neurodegenerative diseases, molecular and cellular analyses on Neural Stem Cells (NSCs) prepared from the subventricular zone of the brain of SMNΔ7 mice were also performed. Studying the impact of ERGO on NSCs and diaphragm muscle will allow us to understand whether the effect in vivo is only due to a peripheral action or can be achieved by a concomitant action at a central level.

# Material and methods

## 1 Animals and treatment

Mice showing SMA phenotype and control littermate mice 11 days of age were used (SMNΔ7 mice from Jackson Laboratory stock #005025). This time point was adopted as a compromise to obtain a higher number of sick animals that are alive, given that the median survival age of SMNΔ7 mice is approximately 13 days. SMNΔ7 mice have undergone genetic modification to serve as carriers. They have been engineered to contain two transgenic genes: the *Smn1* gene, which lacks exon 7 (SMNΔ7), and the human *Smn2* allele, as well as the mutated *Smn1* gene. These models are created through Genome Editing techniques and are employed to develop disease models by inserting specific mutations in one or several genes. Transgenic animals are essential for studying gene expression and conducting biomedical research. In our particular case, we can replicate human symptoms of a genetic disease, enabling us to study it in depth.

Heterozygous SMNΔ7 mice for the null allele (SMN+/−) were bred, resulting in offspring with the following genotypes:

1. Homozygous for both transgenes and heterozygous for the null allele (7SMN+/+; SMN2 +/+; SMN+/−—50%). These mice do not show SMA phenotype and are used as breeders.
2. Homozygous for both transgenes and homozygous for the null allele (7SMN+/+; SMN2 +/+; SMN+/+—25%). These mice do not show SMA phenotype and are used as control mice (WTs).
3. Homozygous for both transgenes and homozygous for the null allele (7SMN+/+; SMN2 +/+; SMN−/−—25%). These mice show SMA phenotype (SMAs).

To evaluate the effect of ERGO, a dietary supplementation will be carried out in heterozygous SMNΔ7 pregnant/mother by adding ERGO (20 μg/die) to drinking water during pregnancy and feeding time. As already mentioned, ERGO is capable of crossing the blood-brain barrier, this includes breast milk and even the placenta (Halliwell et al., 2018).

From mating with a heterozygous male, we obtained:

1. Treated homozygous for both transgenes and heterozygous for the null allele (7SMN+/+; SMN2 +/+; SMN+/−—50%). These mice after washing out were used as breeders.
2. Treated homozygous for both transgenes and homozygous for the null allele (7SMN+/+; SMN2 +/+; SMN+/+—25%). These mice were named WT+ERGO.
3. Treated homozygous for both transgenes and homozygous for the null allele (7SMN+/+; SMN2 +/+; SMN−/−—25%). These mice were named SMA+ERGO.

Mice were genotyped utilizing a PCR assay.

They were euthanized using cervical dislocation. The lower part of the thorax was excised, and the muscle of the diaphragm was dissected.

All procedures were approved by the Animal Care and Use Committee at the University of Pavia (protocol reference number 280/2021-PR) and were communicated to the Ministry of Health and local authorities by Italian law.

## 2 Genotyping

A piece of the tail was taken from each newborn as a sample for testing. Each sample was transferred in a 1.5 ml tube, where 500 µl of Lysis buffer final volume of100mL (10mL of Tris HCl 1 M pH 8.5, 5mL EDTA 100 mm pH 8, 1ml of 20% SDS, 20mL of NaCl 1M) and 30 µl of Proteinase K, an enzyme belonging to the S8 family of proteases, commonly used in molecular biology to purify the preparations of nucleic acids digesting contaminant proteins have been previously added. The presence of Protein K is required because it inactivates nucleases (in this case DNases) that might degrade DNA during the purification. Each sample tube was placed in a thermostatically controlled bath at 55ºC overnight. Following this, the samples underwent centrifugation for 10 minutes at 14000 rpm under room temperature, and the resultant supernatant was then added to 500 µl of isopropanol to allow the recovery of the DNA in solid form. Further centrifugation is performed at the maximum speed for 5 min at room temperature. Subsequently, the supernatant is discarded. 1 mL of 70% ethanol was added to each DNA sample, followed by a third centrifugation at 14000 rpm for 10 minutes at room temperature. Subsequently, the supernatant was removed once again. The pellets obtained from each sample were resuspended in 200 µl of TE final volume 100 ml (1mL of Tris HCl 1 M PH 8.5, 1ml of EDTA 100 mm PH 8). Each sample was then incubated in a bath at 55°C for 5 hours while agitating. The DNA thus obtained was then quantified, (ng/µl) using a NanoPhotometer N60/N50 (IMPLEN, Westlake Village, CA, USA). The next stage involves the use of PCR, or polymerase chain reaction, a molecular technique that enables us to amplify fragments of nucleic acids. However, we must be aware of the initial and terminal nucleotide sequences.

Offspring were genotyped using a PCR-based test carried out on tail DNA samples. The mouse *Smn* knock-out allele was detected using the primers (Sigma Aldrich, St. Louis, MO, USA) in **Table 2**. The procedure for PCR involved heating for 5 minutes at 94 ◦C, following which there were 40 cycles, each consisting of 1 minute at 94 ◦C, 1 minute at 53 ◦C, and 1 minute at 72 ◦C. After PCR, electrophoresis was performed on a 1.5% agarose gel. This method is commonly utilized for examining and isolating nucleic acids by capitalizing on the charges inherent in DNA or RNA molecules (which are negatively charged) to encourage their migration, under the influence of an electric field, through the agarose gel. The samples for analysis have been placed in specific vertical slots, known as "wells". As DNA is a polyanion,

fragments are inclined to migrate towards the positive pole of the gel. To enable the visualization of nucleic acids, several dyes are available for use. Ethidium bromide is the most commonly used dye. This molecule is intercalated between DNA bases and emits fluorescent light when it is exposed to ultraviolet light (300 nm). Ethidium bromide can be used in the gel preparation process. After running we proceed to the acquisition of the bands on the gel using UV transillumination system ImageMaster® VDS. The 800 kDa band corresponds to the WT phenotype, while the 500 kDa band corresponds to the SMA phenotype. The presence of both bands indicates the heterozygous phenotype. On the eleventh day of the life of mice, WT and SMA animals are sacrificed, and the diaphragm is collected for functional or molecular studies.

| | |
|---|---|
| *SMN1* WT FORWARD | 5′CTCCGGGATATTGGGATTG 3′ |
| *SMN1* WT REVERSE | 5′ TTTCTTCTGGCTGTGCCTTT 3′ |
| *SMN1* MUTANT REVERSE | 5′ GGTAACGCCAGGGTTTTCC 3′ |
| *SMN2* WT FORWARD | 5′ CTGACCTACCAGGGATGAGG 3′ |
| *SMN2* TRANSGENE | 5′ GGTCTGTTCTACAGCCACAGC 3′ |
| *SMN2* WT REVERSE | 5′CCCAGGTGGTTTATAGACTCAGA 3′ |
| *SMNΔ7* TRANSGENE 01 | 5′ TCCATTTCCTTCTGGACCAC 3′ |
| *SMNΔ7* TRANSGENE 02 | 5′ ACCCATTCCACTTCCTTTTT 3′ |
| *SMNΔ7* POSITIVE CTRL FORWARD | 5′ CAAATGTTGCTTGTCTGGTG 3′ |
| *SMNΔ7* POSITIVE CTRL REVERSE | 5′ GTCAGTCGAGTGCACAGTTT 3′ |

**Table 2** Primers used for PCR assay to genotype offspring (Cadile et al., 2023).

# 3 Ex Vivo Functional Analysis

The mice were sacrificed by cervical dislocation, the lower part of the chest was removed, and the diaphragm (**Figure 11**) was sectioned and immersed in an oxygenated Krebs solution (NaCl 120 mM, KCl 2,4 mM, $CaCl_2$ 2,5 mM, $MgSO_4$ 1,2 mM, Glucose 5,6 mM, $KH_2PO_4$ 1,2 mM, $NaHCO_3$ 24,8 mM, pH 7,4). A stereomicroscope (with a magnification range of ×10 to ×60) was employed for the dissection of diaphragm strips (with a width of 1–2 mm) that encompassed the central tendon. The diaphragm strips were transferred to the myograph and secured using hooks between a force transducer (AME801; Aksjeselkapet Mikkroelektronik, Horten, Norway) and a movable shaft that is used for adjusting the muscle length. The strips

were fastened by creating small apertures in between the ribs and reinforcing them using ligatures of silk thread (Rossi et al., 2001). At a stable temperature of 22°C, the samples were transferred to an organ bath containing Krebs solution enriched with 95% $O_2$ and 5% $CO_2$, and connected to a force transducer (FT-03, Astromed, West Warwick, RI USA). Platinum electrodes, linked to a stimulator (stimulator S48, AstroMed, Warwick, RI, USA), were situated on either side of the perfusion bath, around 2 mm from the sample. The preparations were stretched to Lo (the length at which maximum twitch force is observable), and their reaction to electrical stimulation was measured (**Figure 12**). Strips were stimulated for approximately 30 minutes using supra-maximal and low-frequency stimuli (0.03 Hz). The maximum force of contraction, the time at the peak tension (TTP), and the relaxation time (TTR) were measured. Afterward, tetanic isometric contractions (110 Hz, 500 ms, supramaximal amplitude) were evoked at Lo. The fatigue index was calculated by measuring the reduction in maximum absolute tetanic force following 20 successive contractions using a ramp protocol at frequencies of 0.03, 0.09, 0.3, and 0.9 Hz (Careccia et al., 2021; Mahmoodzadeh et al., 2021). The normalized tetanic force was expressed as the maximal tetanic force/muscle cross-sectional area (CSA) ($mN/mm^2$), while the fatigue index was expressed as a percentage of the maximal tetanic force. The voltage transducer's output signals underwent analog-to-digital conversion (A/D) and were stored in a personal computer (PC) for subsequent analysis. The analysis was performed using the CEA Spike2 software (CED, Cambridge, UK) and the Cambridge Electronic Design (CED) 1401 A/D electronic converter. The functional experiments were repeated after incubating for 30 minutes in Krebs solution augmented with 0.4% of a water solution that contained 20µg of ERGO, to demonstrate the capacity of this molecule to confer advantages on muscle functions. The dosage of ERGO was selected from relevant literature (Roda et al., 2021) and adjusted to facilitate a translational comparative study with human subjects taking ERGO as a dietary supplement.

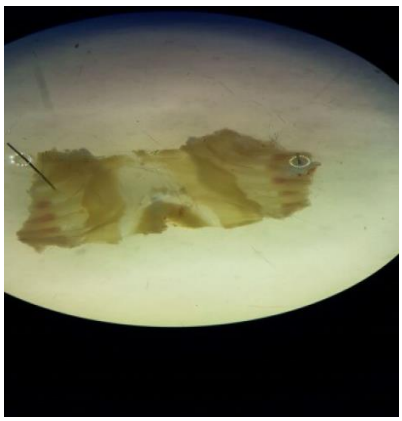

**Fig. 11** Isolated mouse diaphragm.

**Fig. 12** The diaphragm strips in the organic bath.

# 4 Oxyblot Analysis

Frozen diaphragm samples were homogenized at 4 °C in a buffer consisting of protease inhibitors (1:50), β-mercaptoethanol (1,5% v/v), Tris-HCl 0.5M pH 7.6, NaCl 1M, EDTA 100 mM pH 7, and 0.1% NP40. The suspension of protein underwent centrifugation at a speed of 13,500 rpm for 20 min at 5 ◦C. Following the recovery of the supernatant, protein concentration was determined using the RC DC Protein Assay from Bio-Rad Laboratories via spectrophotometric analysis. Oxyblot Protein Oxidation Detection Kit (purchased from Millipore, Vimodrone, Italy) was utilized to detect the protein carbonylation level, using reagents to detect carbonyl groups in the protein side chain. Six micrograms of protein lysate were denatured by the addition of 12% SDS, resulting in a final SDS concentration of 6%. Samples were derivatized, through incubation for 10 min with 2,4-dinitrophenylhydrazine (DNPH), to 2,4 dinitrophenylhydrazone (DNP hydrazone). The derivatization reaction was then blocked by the addition of 7.5 µl of a neutralization solution. Lastly, beta-mercaptoethanol (5% v/v) was added to each sample. The DNP-derivatized protein samples were separated using polyacrylamide gel electrophoresis (4–20% SDS precast gels, Biorad, Hercules, CA, USA) and subsequently subjected to Western blotting. One-dimensional electrophoresis was then performed on 15% SDS-polyacrylamide gel (running gel: Acrylamide (40% solution) 37.8%, bis (2% solution) 20.2%, Tris-HCl (1.5 M solution pH

8.8) 870 mm, SDS 0.5%, ammonium persulphate 0.3%, TEMED 0.075%; staking gel: Acrylamide (40% solution) 11.4%, bis (2% solution) 6%, Tris-HCl (1 M solution pH 6.8) 350 mm, SDS 0.5%, ammonium persulphate 0.5%, TEMED 0.1%). The proteins were subsequently transferred onto nitrocellulose membranes at 100V 400 mA 100 W for a total duration of 2 hours. The membranes were first stained with Ponceau Red and then incubated with a 3% BSA/T-PBS 1X solution (Aspecific Bond Block Solution) at room temperature with stirring for 2 hours to achieve blocking. Subsequently were incubated with a primary antibody that specifically targeted the DNP moiety of the proteins. This was succeeded by an HRP-antibody conjugate that targeted the primary antibody (second antibody: goat anti-rabbit IgG). Protein detection was performed using the Amersham ECL Select™ detection system (Cytiva Life Sciences, ex GE Healthcare, Marlborough, MA, USA), which highlights the HPR substrate through a chemiluminescent reaction. Membranes were obtained using ImageQuant™ LAS 4000 analysis software (GE Healthcare Life Sciences, Milwaukee, WI, USA) and the densitometric analysis was carried out using Photoshop 7 (Adobe) software. Protein oxidation was measured by determining the oxidative index (OI), which is the ratio of densitometric values of the OXYBLOT bands to those stained with Ponceau Red. The OI was compared between different experiments by expressing it relative to the control samples.

# 5 Gene Expression Analysis

Frozen muscle tissues were pulverized using a sterile pestle and mortar previously treated with RNase Zap (Merck, Germany) to remove any trace of RNase presence. The powder resulting from each sample was used for RNA extraction using a specific kit (SV Total RNA Isolation System, Promega, Italia). The concentration of RNA was evaluated by using NanoPhotometer N60/N50 (IMPLEN, Westlake Village, CA, USA). The protocol was as follows: in 300 ng of RNA of each sample were added 2 µL of reaction mix composed by 1 µL of random primers and 1 µL of deoxyribonucleosides (dATP, dGTP, dCTP, and dTTP 10 mM each at neutral pH) and 6.5 µL of a second mix composed by First-Strand Buffer 5x, DTT 0.1 M, RNaseOUT Recombinant RNase Inhibitor (40 U/µL) and SuperScript III RT (200 U/µL). The mixture thus composed was incubated at 25°C for 5 min, and at 50°C for 60 min (annealing and extension steps). Afterward, the reaction was inactivated by increasing the

temperature to 70°C for 15 minutes. The cDNA obtained was analyzed by real-time PCR (Applied Biosystems 7500, Waltham, MA) with the SYBR Green PCR kit (Applied Biosystems, Waltham, MA). A mixture, containing 15 µL of SYBR Green PCR Master Mix, 0.6 µL of oligo primers specific to each gene, 3 µL of cDNA mold of each sample, and 12 µL of sterile H2O, was prepared. The protocol for amplifying the gene involved a four-step process: A pre-incubation cycle of ten minutes at 95°C is necessary for activating the Hot-Start-Taq polymerase and denaturing the DNA. Forty amplification cycles, with each one divided into:

I. First, the samples were subjected to denaturation by being brought to a temperature of 95°C for 15 seconds.
II. A 60-second step was taken at 60°C, during which the primer was annealed.
III. A 30-second stage at 72°C was performed, during which the DNA strand underwent elongation.

**Table 3** presents oligonucleotide primers implemented for real-time PCR. The concentration of the target gene was quantified concerning the housekeeping gene (GAPDH) concentration. The ΔCt was computed by deducting the threshold cycles (Ct) values of each sample from the Ct value of the reference sample for both the housekeeping genes and target genes. The values obtained from the target genes were normalized against the values obtained from the housekeeping gene.

| | Forward Primer | Reverse Primer |
|---|---|---|
| *SERCA1* | TGTTTGTCCTATTTCGGGGTG | AATCCGCACAAGCAGGTCTTC |
| *SERCA2* | GAGAACGCTCACACAAAGACC | CAATTCGTTGGAGCCCCAT |
| *PGC1α* | ACCCCAGAGTCACCAAATGA | CGAAGCCTTGAAAGGGTTATC |
| *SIRT1* | CCGCGGATAGGTCCATATACT | AACAATCTGCCACAGCGTCA |
| *NRF1* | GCACCTTTGGAGAATGTGGT | CTGAGCCTGGGTCATTTTGT |
| *NRF2* | TTCTTTCAGCAGCATCCTCTCCAC | ACAGCCTTCAATAGTCCCGTCCAG |
| *BNIP3* | TTCCACTAGCACCTTCTGATGA | GAACACCGCATTTACAGAACAA |

**Table 3** Oligonucleotide primers used for real-time PCR (Cadile et al., 2023).

# 6 Western Blot Analysis

Frozen muscles were pulverized using a ceramic pestle in a steel mortar while keeping it frozen with a continuous supply of liquid nitrogen to preserve the integrity of muscle components. The obtained powder was homogenized using a lysis buffer containing Tris-HCl 20 mM, Triton X-100 1%, glycerol 10%, NaCl 150 mM, EDTA 5 mM, NaF 100 mM, and NaPPi 2 mM supplemented with protease inhibitor 5x (Protease Inhibitor Cocktail, Sigma-Aldrich, St. Louis MO), phosphatase inhibitors 1x (phosphatase Inhibitor Cocktail, Sigma-Aldrich, St. Louis MO), and phenylmethylsulfonyl fluoride (PMSF) 1 mM. Tissue lysis was carried out on ice for a duration of 40 minutes. The homogenate was centrifuged at 13,500 rpm for 20 minutes at 4°C. Subsequently, the supernatant was transferred to clean Eppendorf tubes and kept at -80°C until required. The protein concentration in the lysates was ascertained utilizing the reducing agent and detergent compatible (RC-DC) protein assay (Bio-Rad, Hercules, CA). It is a colorimetric assay utilized for the determination of protein in the presence of reducing agents and detergents. Equal amounts of muscle samples were loaded on 4–20% gradient precast gels purchased from BioRad (Bio-Rad, Hercules, CA) and subjected to electrophoresis. Electrophoresis was conducted for two hours at a constant current of 100 V in a running buffer with pH 8.8 (Tris 25 mM, glycine 192 mM, SDS 1%). To monitor protein separation, a marker of protein molecular weight (Prestained Protein Ladder Marker, Bio-Rad, Hercules, CA) comprising a mixture of proteins with known molecular weight was loaded onto the gel. Proteins were electro-transferred to polyvinylidene fluoride (PVDF) membranes using a constant voltage of 100 V for 2 hours at 4°C in a transfer buffer comprising Tris 25 mM, glycine 192 mM, and methanol 20%. The effective protein transfer to the membrane was the membrane was confirmed by staining with Ponceau Red (Merck, Darmstadt, Germany) in acetic acid (Ponceau Red 0.2% in acetic acid 3%) for 15 minutes with stirring at room temperature. Non-specific binding sites on the PVDF membrane were saturated using a blocking solution consisting of 5% fat-free milk in solution with Tris 0.02 M, NaCl 0.05 M, and Tween-20 0.1% (Tris-buffered saline-Tween 20, TBS-T) for 2h at room temperature with constant agitation. After incubation, the membrane underwent three washes of TBS-T, each lasting 10 minutes. Afterward, the membranes were incubated with specific primary antibodies (**Table 4**) overnight at 4°C. Subsequently, the membranes were incubated with appropriate horseradish peroxidase (HRP)-conjugated secondary antibodies.

Protein detection was carried out using an advanced chemiluminescence detection system (GE Healthcare Life Sciences, Little Chalfont, UK) that identifies the substrate of horseradish peroxidase (HRP) by chemiluminescence reaction (**Figure 13**). The membrane was analyzed using ImageQuant LAS 4000 analysis software (GE Healthcare Life Sciences, Little Chalfont, UK). The content of each protein investigated was assessed by determining the brightness-area product of the protein band as previously described (Gondin et al., 2011). The levels of the target protein were standardized using a housekeeping protein (tubulin). The phosphorylation levels of some proteins were calculated by the ratio between phosphorylated and unphosphorylated total forms of the same protein.

The five mitochondrial complexes comprising the respiratory chain can be detected on a single PVDF membrane by a five-antibody cocktail targeting the corresponding proteins. Five micrograms of quantified proteins were loaded onto precast gradient acrylamide/bisacrylamide gels from Bio-Rad, and electrophoresis was performed. Electrophoresis was then conducted at a constant current (100 V) for 2 hours in a running buffer. At the end of the gel run, gels were transferred on a PVDF membrane at 100 V for 2 h at 4C or a constant 35 mA overnight (O/N) in a cold transfer buffer. After saturation with a 5% fat-free milk (in TBS-T 1x) blocking solution for 2 h at room temperature, membranes were incubated O/N at 4°C with the specific primary antibody against the mitochondrial complexes of the respiratory chain in 5% fat-free milk in TTBS 1x. Subsequently, the membranes were incubated for one hour at room temperature and agitated while using the HRP-conjugated donkey anti-mouse secondary antibody in 5% fat-free milk. Protein detection was performed using the Amersham ECL Select detection system (Cytiva Life Sciences, formerly known as GE Healthcare) and membranes obtained through the ImageQuant LAS 4000 software (GE Healthcare Life Sciences). The exposure time is automatically adjusted or can be edited depending on the intensity of the signal emitted. Subsequently, to visualize the overall protein quantity on the membrane, they underwent Coomassie PVDF-specific staining (0.1% Coomassie blue R-250, 50% methanol, 10% acetic acid) for 20 min and destained with a destaining solution composed by 40% methanol and 10% acetic acid. Air-dried membranes were then digitized with a scanner and analyzed. Data were reported as the ratio brightness area product (BAP) for each of the five complexes to the total amount of protein stained with Coomassie (in arbitrary units).

| Primary Antibody | Species | Dilution | Supplier |
|---|---|---|---|
| p-AMPK | Rabbit | 1:1000 | Cell Signaling |
| AMPK | Rabbit | 1:1000 | Cell Signaling |
| PGC1α | Rabbit | 1:1000 | Abcam |
| TOM20 | Rabbit | 1:1000 | Santa Cruz |
| DRP1 pSer637 | Rabbit | 1:1000 | Cell Signaling |
| DRP1 | Rabbit | 1:1000 | Cell Signaling |
| SOD1 | Rabbit | 1:1000 | Abcam |
| Catalase | Rabbit | 1:1000 | Abcam |
| PRDX3 | Rabbit | 1:1000 | Abcam |
| LC3B | Rabbit | 1:1000 | Sigma |
| p62 | Rabbit | 1:2000 | Cell Signaling |
| PARKIN | Mouse | 1:2000 | Invitrogen |
| Tubulin | Mouse | 1:2000 | Sigma |
| SERCA1 | Rabbit | 1:1000 | Cell Signaling |
| SERCA2 | Rabbit | 1:1000 | Cell Signaling |
| GPX | Rabbit | 1:1000 | Abcam |

**Table 4** Antibody used for WB assay.

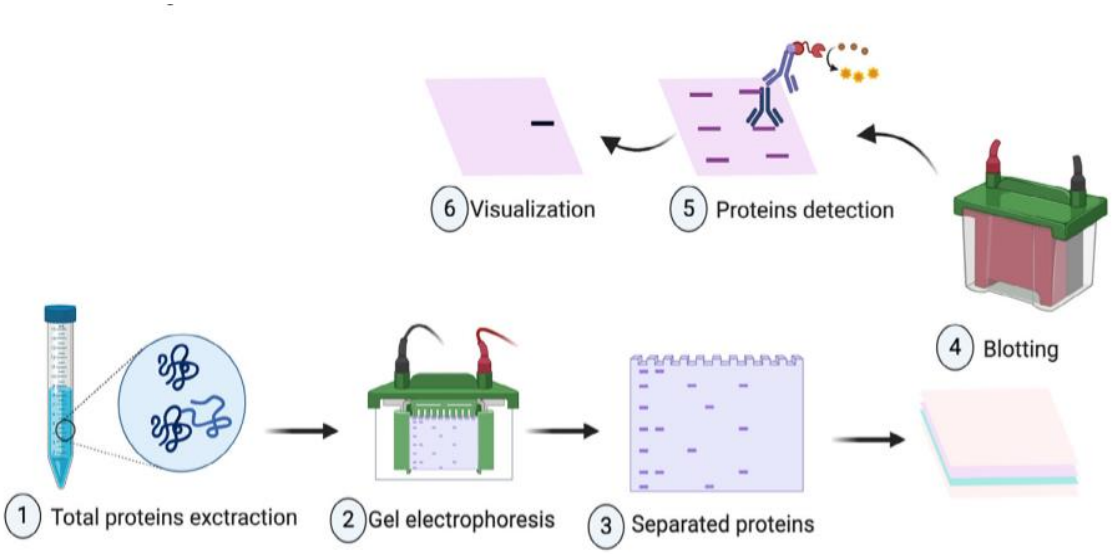


**Fig. 13** Workflow of Western blot assay (Meftahi et al., 2020).

# 7 Oxygraph-2k for High-Resolution Respirometry (O2k HRR)

Mitochondrial respiration was measured using the Oxygraph-2k (O2k, OROBOROS Instruments, Innsbruck, Austria) (**Figure 14A, B**). For each mouse, the diaphragm muscle was properly dissected and divided into two parts in ice-cold BIOPS buffer (biopsy preservation solution: 7.23 mM $K_2$EGTA, 5.77 mM $Na_2$ATP, 2.77 mM Ca$K_2$EGTA, 6.56 mM $MgCl_2$•$6H_2O$, 20 mM Taurine, 15 mM $Na_2$Phosphocreatine, 20 mM Imidazole, 0.5 mM Dithiothreitol (DTT), 50 mM MES, pH 7.1) at 0 ◦C. Both pieces were used for the analysis in duplicate during the day.

Pieces of diaphragm were washed in ice-cold BIOPS for 10 min, permeabilized with 20 µg/mL Saponin (Merck) in BIOPS in agitation at 4 ◦C, and finally washed with mMiR05 buffer (mitochondrial respiration medium: 3 mM $MgCl_2$, 60 mM lactobionic acid 0.5 mM EGTA, 20 mM taurine, 10 mM $KH2PO_4$, 20 mM 4-(2-hydroxyethyl) piperazine-1-ethane sulfonic acid (HEPES), 110 mM D-sucrose, and 1 g·L-1bovine serum albumin (pH 7.1)). Muscle samples were transferred into Oroboros-O2k chambers; The experiment was conducted in Mir05 solution at 37 °C with an oxygen concentration ranging from 400 to 250 µM to prevent respiratory $O_2$ limitation. The medium was re-oxygenated with pure gaseous $O_2$ whenever the oxygen concentration fell below the 250 µM threshold. Additionally, the measurements were carried out while utilizing Blebbistatin, an inhibitor of myosin II-ATPase, at a concentration of 25 µM, which was dissolved in a 5 mM stock solution of DMSO (Perry et al., 2011) to prevent spontaneous contraction in the respiratory medium of muscle samples. Calibration at air saturation was executed every day before commencing experiments. Respiration was assessed using substrate-uncoupler-inhibitor titration (SUIT) protocols previously described with modifications (Zuccarelli et al., 2021; Makrecka-Kuka et al., 2015). Glutamate and malate (10 mM and 4 mM, respectively) are added to measure non-phosphorylating resting mitochondrial respiration in the absence of adenylates, to assess oxygen consumption, which is primarily determined by proton leakage through the inner mitochondrial membrane (known as "LEAK" respiration). Succinate (10mM) facilitated the convergent electron flow into Complexes I and II through the Q-junction, thereby determining the LEAK of both Complexes I and II. ADP was added until a final concentration of 10 mM

was reached to achieve maximal ADP-stimulated mitochondrial respiration (OXPHOS capacity). Titrations using FCCP, the uncoupler protonophore carbonylcyanide-p trifluoromethoxyphenylhydrazone (a few steps of 1 µM), were conducted to ascertain the capacity of the electron transfer system (ETS). Rotenone (Rot, 0.5 µM added to inhibit Complex I) and Antimycin A (AmA, 2.5 µM to inhibit Complex III and thus the mitochondrial respiratory chain) were added for the determination of maximal respiratory uncoupled efficiency and residual oxygen consumption (ROX), respectively, independently by mitochondria. Before administering AmA, the chambers were supplemented with Cytochrome C (10 µM) to assess the integrity of the outer mitochondrial membrane. A rise in oxygen flow exceeding 15% would signify compromised organelles. At the end of each experiment, muscle samples were removed from the chambers, washed in PBS, centrifuged at 14,000× g for 10 minutes at 4 °C, and frozen in liquid nitrogen before being stored at −80 °C until further determinations. All mitochondrial respiration parameters have been adjusted for residual O2 consumption (ROX) and normalized using the value of citrate synthase activity (see below) (Larsen et al., 2012).

## 7.1 Citrate Synthase Activity

CS activity was determined using the Citrate Synthase Activity Assay Kit (Merck, Darmstadt, Germany). Muscle samples were homogenized in an ice-cold CS Assay Buffer provided by the kit, kept on ice for 40 min, and centrifuged at 10,000 g for 20 min at 4C to obtain a protein extract. Protein concentration was assessed using the RC-DC protein assay (Bio-Rad, Hercules, CA), and 5 µg of protein lysate was utilized to assess CS activity. The initial absorbance ($T_{initial}$) was measured at 412 nm after the addition of the appropriate Reaction Mix by a plate reader (CLARIOstar Plus, BMG Labtech, Ortenberg, Germany). Subsequently, the absorbance (A412) was measured at 5-minute intervals for 45 minutes. CS enzyme activity was measured by interpolating the final reading at the time ($T_{final}$) on a standard curve with scalar concentrations of a solution of a known concentration (2 nmol/L) of GSH Standard solution. Values for citrate synthase activity were used to normalize the parameters evaluated by using O2k HRR.

**A** **B**

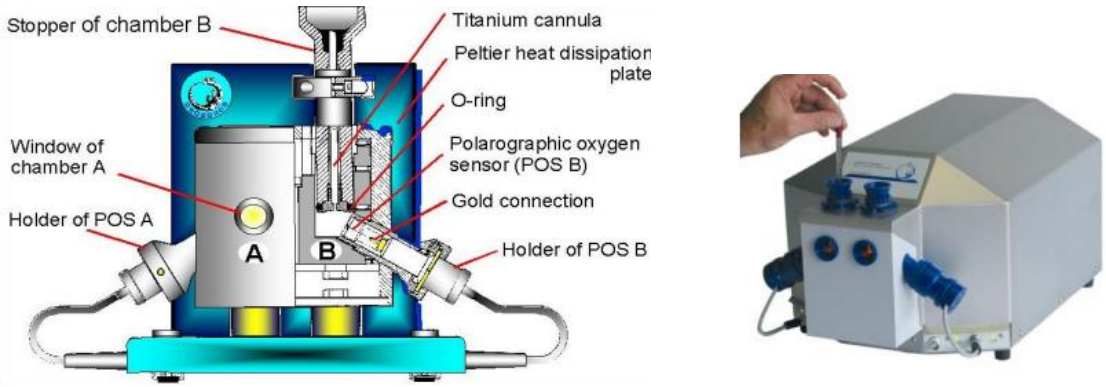


**Fig.14A, B** Oxygraph-2k (Mitochondrial Physiology Network 06.01: 1-18 (2011)).

# 8 Electron Microscopy (EM)

Intact diaphragms were fixed at room temperature with 3.5% glutaraldehyde in 0.1M Na Cacodylate buffer, pH 7.2 for several hours. Small pieces of fixed diaphragms were then postfixed in 2% $OsO_4$ in the same buffer for 2 hrs and then blockstained in aqueous saturated uranyl acetate. After dehydration, specimens were embedded in an epoxy resin (Epon 812). Ultrathin sections (~50 nm) were cut using a Leica Ultracut R microtome (Leica Microsystem) with a Diatome diamond knife (Diatome Ltd.) and double-stained with uranyl acetate and lead citrate. Sections were viewed and photographed using a 120 kV JEM-1400 Flash Transmission Electron Microscope (Jeol Ltd., Tokyo, Japan) equipped with a CMOS camera (Matataki and TEM Center software Ver. 1.7.22.2684 (Jeol Ltd., Tokyo, Japan)) (Boncompagni et al., 2009).

## 8.1 EM Quantitative analyses

For all quantitative EM analyses, micrographs of non-overlapping regions were randomly collected from longitudinal sections of internal areas of diaphragm fibers. The number of mitochondria was evaluated in longitudinal sections and reported as an average number/ 100

μm$^2$, while the size of mitochondria was measured using TEM Center Software and reported as Average Mitochondrial Size (μm$^2$).

# 9 In vivo tests

Survival, muscle function, and other selected phenotypic tests to quantify key features and drug effects in the neonatal SMA Δ7 mice model were evaluated. A battery of straightforward, easy-to-perform, rapid, and moderate throughput tests of motor function, and indices of neonatal well-being were performed on mice from birth to to the last day of life (El-Khodor et al., 2008).

All the in vivo tests were conducted in the four groups: WT, WT+ ERGO, SMA, SMA + ERGO.

## 9.1 Survival

Survival evaluation was performed using the Kaplan–Meier method which is a non-parametric statistical method employed to assess the survival function derived from data on lifetimes. It displays the likelihood of a subject surviving up to a particular time point (Jager et al., 2008). The curve is created by graphing the survival probability over time. In medical research, it is often used to measure the fraction of patients living for a certain amount of time after treatment. The Kaplan-Meier survival curve approximates survival probabilities from data that are missing, censored, or truncated.

The estimator of the survival probability or survival function S(t) is given by:

$$\widehat{S}(t) = \prod_{i:\, t_i \le t} \left(1 - \frac{d_i}{n_i}\right),$$

with a time when at least one event happened, $d_i$ the number of events (e.g., deaths) that happened at time, and the individuals known to have survived (have not yet had an event or been censored) up to time The survival rate of two animal groups, SMA and SMA +ERGO, was compared from the day of birth until their natural death. The statistical significance of the curve was assessed by the log-rank test.

## 9.2 The hind-limb suspension test

The hind-limb suspension test or the tube test is a new non-invasive motor function assessment specifically created for neonatal rodents. This test evaluates the proximal hind-limb muscle strength, weakness, and fatigue in mouse or rat neonates. Furthermore, it evaluates overall neuromuscular performance, muscle strength, and body posture. During each trial, the mouse is suspended upside down by its hind limbs in a 50 ml plastic centrifuge tube with a cotton ball. The experiment typically consists of two consecutive trials, but extra trials can be done to evaluate the progression of muscle exhaustion in animals. Padding at the base to safeguard the animal's head in the event of a fall. Hind-limb score (HLS) which assesses the positioning of the legs and tail (El-Khodor et al., 2008) (**Figure 15**). Pups belonging to the 4 groups: WT, WT+ ERGO, SMA, and SMA + ERGO are tested daily.

The scoring of the adopted posture was based on the following criteria: a score of 4 denotes a normal posture, typical hind-limb separation with an elevated tail. A score of 3: The animal displays signs of weakness, with its hind limbs positioned closely together but rarely touching each other. Score 2: Hind limbs are near each other, often in contact. A score of 1: Weakness is evident, and hind limbs are frequently in a clasped position with the tail raised. The HLS score provides an objective measurement of the extent of hind-limb extension during the first 10-15 seconds of hanging onto the tube lip. The score remains constant even if the animal displays a higher or lower score later on.

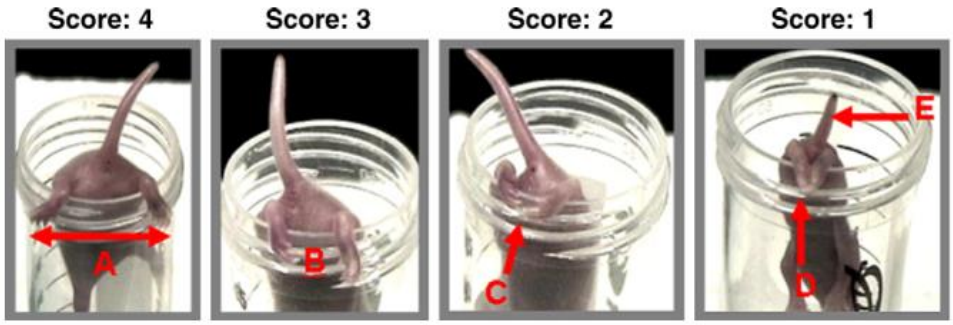


**Figure 15** The tube test and the scoring criteria for the hind-limb score (HLS) (El-Khodor et al., 2008).

## 9.3 Body weight and growth of hair

The weight and the growth of hair of mice belonging to the 4 groups: WT, WT+ ERGO, SMA, and SMA + ERGO have been monitored daily.

## 9.4 Righting Reflex

Pups belonging to the 4 groups: WT, WT+ ERGO, SMA, and SMA + ERGO are tested daily. They are positioned on their back on a level surface, and their ability to move to a dorsal position was evaluated Release the pups and record the duration of time it takes until they return to the prone position, including the direction of their righting (left or right) (**Figure 16**). A maximum of one minute is allotted for each trial if necessary. As this test is a reflex, there is no learning component and it can be repeated throughout the experimentation period (Feather-Schussler et al., 2016).

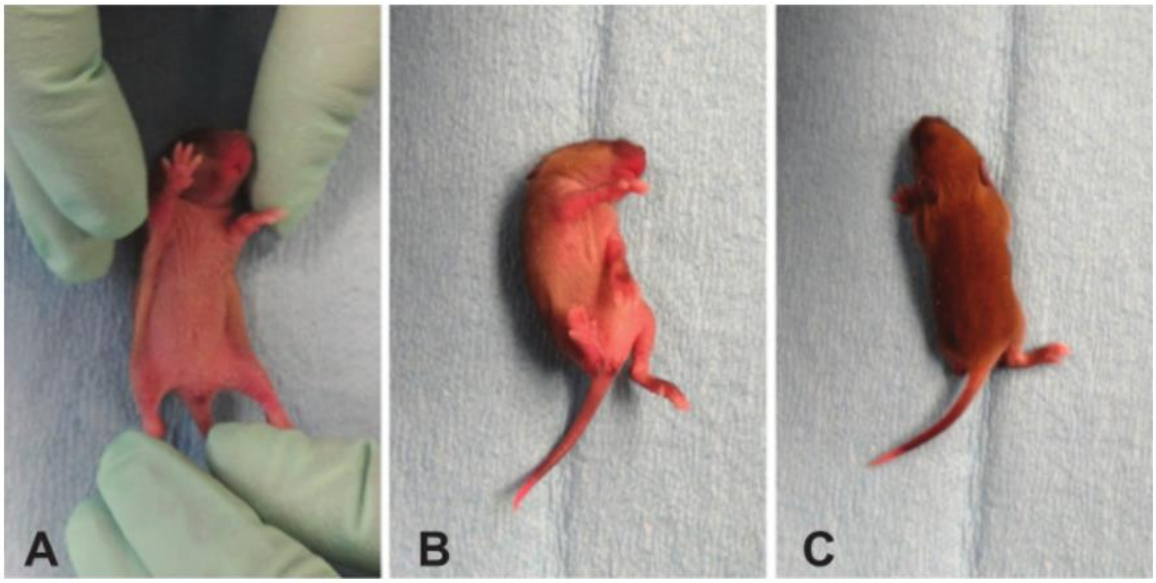


**Fig. 16** Phases of surface Righting (Feather-Schussler et al., 2016).

## 9.5 Open Arena Test

The animals were placed in a 63x42 cm arena for 5 minutes, after which their performances were recorded by a SMART video tracking system (2 Biological Instruments, Besozzo,

Varese, Italy) and a Sony CCD color video camera (PAL). Using this software, the total distance covered by the mice in centimeters was measurable.

## 9.6 Calculation of scores

Scores ranging from 1 to 4 were assigned to each of the above four parameters (hindlimb suspension test, weight, righting reflex, and total distance in open arena). Scores were assigned to each mouse, with a value of 1 indicating poor performance or low weight, while a value of 4 indicating maximum performance or weight. Scores of 2 and 3 represented intermediate values (**Table 5,6,7,8**).
To the last parameter: hair, only two scores were assigned. A value of 1 in the case of absence or 2 in the case of the presence of hair (**Table 9**).

All the individual scores ( hindlimb suspension test, weight, righting reflex, total distance in open arena, and hair growth) were then added up and the total value indicated the quality of life of the mouse. The overall score, which is a summation of individual five scores, ranges from 5 (minimum) to 18 (maximum). A score of 5 indicates a poor quality of life, while a score of 18 denotes an excellent quality of life.

| | |
|---|---|
| **Score 1** | Very poor performance |
| **Score 2** | Poor performance |
| **Score 3** | Intermediate performance |
| **Score 4** | Excellent performance |

**Table 5** Hindlimb suspension test and relative scores.

| | |
|---|---|
| **Score 1** | 0-3 gr |
| **Score 2** | 3,01- 4,34 gr |
| **Score 3** | 4,35—5,68 gr |
| **Score 4** | >5,69 gr |

**Table 6** Weight and relative scores.

| | |
|---|---|
| **Score 1** | 0-10 cm |
| **Score 2** | 10,1-40 cm |
| **Score 3** | 40,1-100 cm |
| **Score 4** | >100 cm |

**Table 7** Total distance in an open arena with relative scores.

| | |
|---|---|
| **Score 1** | >15 s |
| **Score 2** | 5,1-15 s |
| **Score 3** | 3-5 s |
| **Score 4** | 0-2,9 s |

**Table 8** Righting Reflex and scores.

| | |
|---|---|
| **Score 1** | No hair |
| **Score 2** | Hair |

**Table 9** Hair growth and scores.

# 10 NSCs preparation

## 10.1 Dissection of the brain and isolation of the SVZ

The cells used in the experiments were derived from the brains of delta 7 SMA and WT mice sacrificed on day 11 of life. Dissection and isolation operations involve removing the brain from the skull, washing it several times with PG solution (50 mL PBS 10X, 5 mL Penicillin-streptomycin (final concentration100 U/ml), 10 mL Glucose 30% (final concentration 0.6%) for the final volume of 500 mL) and then surgically isolating the regions of interest (Adami et al., 2018). The part of the brain used in the experiments is the subventricular zone (SVZ), which extends between the lateral walls of each ventricle and the hippocampus. These are two

brain regions that contain neural stem cells (NSCs), which generate new neurons in the olfactory bulb, to which the NSCs migrate by differentiating (Bottai et al., 2003). To harvest both SVZs, place the brain under a dissecting microscope and make a coronal cut approximately 4 mm from the olfactory bulbs, then make a second cut approximately 2-3 mm posteriorly to obtain a 2 mm slice containing the SVZ (Daniela et al., 2007). Afterwards, the samples are transferred to a 15 mL falcon containing PG solution and stored at 4°C until the dissection of all mice is completed.

## 10.2 Dissociation of brain tissue and primary cultures

The brain tissue is cut into small fragments, using special scissors and for juvenile mice, as in our study, the usage of the papain digestion protocol is unnecessary due to the fragile nature of the tissue, which can be easily broken down. The tissue can be readily broken down by placing it in a 1 ml EBSS solution and dissociating it mechanically. This can be achieved by passing it through the tip of a 1000 µl Gilson pipette approximately 30 times. Then we add 5 ml of EBSS solution and centrifuge at 123 rpm for 10 minutes. Once the supernatant has been removed, leaving approximately 200 µl in the falcon, gently dissociate the pellet using a 200 µl Gilson pipette set at 180 µl by passing through the tip 20-25 times, then add 5 mL of EBSS and centrifuge for 10 minutes at 123 rpm. At this point, the supernatant is completely removed and the cells are resuspended in 0.5 ml of DB1 proliferation medium (2 mM L-glutamine, 0,6% Glucose, 9,6 µg/ml Putrescein, 0,025 mg/ml Insulin, 6,3 ng/ml Progesterone, 0,1 mg/ml Apo-transferrin, 5,2 ng/ml sodium selenite, 20 ng/ml EGF, 10 ng/ml FGF-2, 4 mg/L Heparin, 1:100 Penicillin/streptomycin) and counted using trypan blue as a dye to exclude dead or damaged cells. The cells are plated at a density of about 3500 cells/$cm^2$ in the growth medium (DB1) using 6-well plates (3 ml of medium) or 25 $cm^2$ culture flasks (5 ml DB1). Subsequently, they are placed inside a cell culture incubator set at 37°C and 5% $CO_2$ for cultivation (Daniela et al., 2007). The medium used for DB1 cell proliferation consists of DB0, a medium base, which is a control medium, to which growth factors such as EGF and FGF2. DB0 also forms the basis of other media such as F (**Table 10**) and CTRL (**Table 11**) media used for the differentiation of NSCs.

| | |
|---|---|
| L-glutamine | 2 mM |
| Glucose | 0,6% |
| Putrescein | 9,6 µg/ml |
| Insulin | 0,025 mg/ml |
| Progesterone | 6,3 ng/ml |
| Apo-transferrin | 0,1 mg/ml |
| sodium selenite | 5,2 ng/ml |
| FGF-2 | 10 ng/ml |
| Heparin | 4 mg/L |
| Penicillin/streptomycin | 1:100 |

**Table 10** F medium.

| | |
|---|---|
| L-glutamine | 2 mM |
| Glucose | 0,6% |
| Putrescein | 9,6 µg/ml |
| Insulin | 0,025 mg/ml |
| Progesterone | 6,3 ng/ml |
| Apo-transferrin | 0,1 mg/ml |
| sodium selenite | 5,2 ng/ml |
| Fetal Bovine serum (FBS) | 2% |
| Heparin | 4 mg/L |
| Penicillin/streptomycin | 1:100 |

**Table 11** CTRL medium.

## 10.3 Cell cultures and proliferation

Five to seven days after seeding, the cells form spherical structures derived from a single stem cell (i.e. they are clones). These are mechanically dissociated into single cells and replated in the appropriate plates with a proliferation medium in a volume appropriate to the plate (Bottai et al., 2008). These spheres, called neurospheres, are heterogeneous structures that include: neural stem cells, apoptotic cells, mature progenitor cells, differentiating cells, and differentiated cells. They tend to grow in suspension, but sometimes can also grow attached to the plate, forming elongated structures. These spheres increase in size due to the continuous

division of NSCs, but also due to the increase in the number of progenitors and other cells. Once they reach a considerable size, usually around 100-150 µm, it is appropriate to dissociate them so that their big size does not prevent medium trophic factors from entering the innermost regions of the spheres, a mechanical dissociation is done to obtain single cells again so that they can be counted and their growth progress assessed. To allow the proliferation of these cells, it is necessary to provide them with a regular supply of growth factors, made possible by the addition of a new medium every 2 days (DB1) and the storage of plates in an incubator at a constant temperature of 37°C and 5% partial pressure of $CO_2$.

## 10.4 Mechanical dissociation of neurospheres

The choice of the ideal time for dissociation is a compromise between a high number of neurospheres and their size, which must never be exceeded as this would prevent the diffusion of nutrients into the interior, and is usually between 5-10 days. This is done by harvesting the cells and centrifuging them at 123g for 10 minutes. The supernatant, consisting of the spent medium, is then removed, leaving at the bottom approximately 200 µl consisting of the pellet (cells) and a small residue of the medium. At this point, we proceed to the mechanical dissociation step using a 200 µl Gilson pipette set at 180 µl, the contents of the Falcon are passed through the tip approximately 100 times.

Dissociation occurs due to the friction generated between the liquid coming out of the tip and the wall of the test tube. Once the dissociation is complete, continue counting; dilute a small aliquot taken from the residue in the falcon in trypan blue by performing a dilution proportional to the number of cells contained in the 200 µl; usually starting with a 1:2 dilution (5µl of suspension in 5µl of trypan blue) and increasing to 1:10 if the cells were highly concentrated in previous dilutions. Counting is performed under a video microscope (100X magnification) after placing the aliquot of cells and stain in the Burker counting. In this device, you count the cells that do not appear colored, because trypan blue enters in the cells with damaged plasma membrane (dying). The count allows the total cell content of the 200 µl to be determined in one simple operation:

Cell concentration (cell/µl) = n°cell/0.1µl*10*Dilution factor

As the individual squares in the counting chamber subtend 0.1µl, multiplication by 10 and the dilution factor gives the number of cells contained in 1µl. To find the total number of cells,

simply multiply this value by the volume of residue in the tube: total cells = (n°cells/µl)*200 µl.
Once the counting is complete and the total number of cells is obtained, the cells are plated on plates chosen according to the total number of cells and the surface area of the plate itself.

## 10.5 Growth curves

The proliferative capacity of the cells is assessed using the proliferation assay (growth curves) obtained from 10 samples (5 WT and 5 SMA). At each passage, the cells are mechanically dissociated when the spheres reach the appropriate size (approximately 0.1 mm) and plated at a density of 10000 cells/$cm^2$ (Adami et al., 2018). This assay uses 6-well multiwells, each with a surface area of 9 $cm^2$, each plated with 90000 cells. The total number of cells is calculated by multiplying the proliferation rate obtained from the ratio of live cells counted to plated cells (90000) by the total number of cells from the previous passage (Adami et al., 2018).

## 10.6 Ergothioneine dose-response curve

This assay is used to determine the concentration of ERGO that induces a greater increase in NSCs proliferation. The assay is performed in a 48-well multi-plate with 10000 cells seeded in each well with 300µL of DB1 medium and different concentrations of ERGO were added to a final concentration of: 2.5 µM, 5 µM, 10 µM, 20 µM, 50 µM, 100µM and 200 µM which were dissolved in water, a control containing the vehicle ($H_2O$) was included). Each sample was run in duplicate. After 5 days, the neurospheres were dissociated to obtain single cells, which were then counted to determine the concentration of ERGO at which the number was greatest.

## 10.7 MTT Assay

This is an assay to measure the metabolic activity of cells, an indicator of their proliferation and viability. It is performed in a 96-well multiwell plate divided into vertical columns so that each sample is quadruplicated. Five thousand cells are seeded into each well and 100 µL DB1 is added. Samples are divided into CTR (vehicle-treated and ERGO-treated 0.5µM.
After 3 days, 10µL of MTT (0.5mg/ml) is added and left for 3 hours (Adami et al., 2018). At the end of the three hours required for the reaction to take place, all the medium is removed,

taking care not to remove the cells. Finally, the spectrophotometer is used to analyze the cell viability.

## 11 Statistical Analysis

The data were expressed as mean ± S.D. The statistical significance of the differences between the averages was determined with the Student t-test; a probability of less than 5% ($p < 0.05$) was considered significant. The statistical analysis was performed using GraphPad Prism 9.0 software. The sample size was predetermined based on the published literature and chosen to use the fewest number of animals to achieve statistical significance.

# Results and Discussion part I

The main objective of my PhD thesis was to explore the key functional, biochemical, and molecular, differences between SMA and WT diaphragm of SMNΔ7 mice model 11 days old. The study of the diaphragm in this pathology is, as mentioned above, very limited, but at the same time of fundamental interest in order to improve the life quality of SMA patients.
These experiments have been published in “International Journal of Molecular Sciences” (Cadile et al., 2023).

International Journal of
*Molecular Sciences*

MDPI

*Article*

# Diaphragm Fatigue in SMNΔ7 Mice and Its Molecular Determinants: An Underestimated Issue

**Francesca Cadile [1], Deborah Recchia [2], Massimiliano Ansaldo [1], Paola Rossi [2], Giorgia Rastelli [3], Simona Boncompagni [3,4], Lorenza Brocca [1], Maria Antonietta Pellegrino [1] and Monica Canepari [1,*]**

[1] Department of Molecular Medicine, via Forlanini 6, University of Pavia, 27100 Pavia, Italy; francesca.cadile01@universitadipavia.it (F.C.); massimiliano.ansaldo01@universitadipavia.it (M.A.); lorenza.brocca@unipv.it (L.B.); map@unipv.it (M.A.P.)
[2] Department of Biology and Biotechnology "L. Spallanzani", University of Pavia, 27100 Pavia, Italy; deborah.recchia@unipv.it (D.R.); paola.rossi@unipv.it (P.R.)
[3] Center for Advanced Studies and Technology, University G. d'Annunzio of Chieti-Pescara, 66100 Chieti, Italy; giorgia.rastelli@unich.it (G.R.); simona.boncompagni@unich.it (S.B.)
[4] Department of Neuroscience, Imaging and Clinical Sciences, University G. d'Annunzio of Chieti-Pescara, 66100 Chieti, Italy
* Correspondence: canepari@unipv.it

**Abstract:** Spinal muscular atrophy (SMA) is a genetic disorder characterized by the loss of spinal motor neurons leading to muscle weakness and respiratory failure. Mitochondrial dysfunctions are found in the skeletal muscle of patients with SMA. For obvious ethical reasons, the diaphragm muscle is poorly studied, notwithstanding the very important role that respiratory involvement plays in SMA mortality. The main goal of this study was to investigate diaphragm functionality and the underlying molecular adaptations in SMNΔ7 mice, a mouse model that exhibits symptoms similar to that of patients with intermediate type II SMA. Functional, biochemical, and molecular analyses on isolated diaphragm were performed. The obtained results suggest the presence of an intrinsic energetic imbalance associated with mitochondrial dysfunction and a significant accumulation of reactive oxygen species (ROS). In turn, ROS accumulation can affect muscle fatigue, cause diaphragm wasting, and, in the long run, respiratory failure in SMNΔ7 mice. Exposure to the antioxidant molecule ergothioneine leads to the functional recovery of the diaphragm, confirming the presence of mitochondrial impairment and redox imbalance. These findings suggest the possibility of carrying out a dietary supplementation in SMNΔ7 mice to preserve their diaphragm function and increase their lifespan.

**Keywords:** SMA; diaphragm muscle; muscle fatigue; ergothioneine



**Citation:** Cadile, F.; Recchia, D.; Ansaldo, M.; Rossi, P.; Rastelli, G.; Boncompagni, S.; Brocca, L.; Pellegrino, M.A.; Canepari, M. Diaphragm Fatigue in SMNΔ7 Mice and Its Molecular Determinants: An Underestimated Issue. *Int. J. Mol. Sci.* **2023**, *24*, 14953. https://doi.org/10.3390/ijms241914953

Academic Editor: Daniel Taillandier

Received: 11 September 2023
Revised: 29 September 2023
Accepted: 3 October 2023
Published: 6 October 2023



## 1. Introduction

SMA is an autosomal recessive genetic disorder characterized by loss of spinal motor neurons leading to muscle atrophy, weakness, and respiratory failure [1]. SMA has an incidence of about one in 10,000 live births [2]. It is caused by mutations in the SMN1 gene, which encodes the Survival Motor Neuron (SMN) protein, essential for the survival and normal functioning of motor neurons [3].

In humans, there are two SMN genes, the telomeric SMN1 coding for a ubiquitous protein (full-length SMN), and its centromeric homolog SMN2 mostly generating a protein lacking exon7 (SMNΔ7), which is not functional: the SMN2 gene produces a limited amount of functional protein that can modulate SMA severity [4].

Although the key role of motoneurons in determining the most severe symptoms of SMA is widely recognized, the presence of defects in other cell/tissue types in SMA models indicates the complexity of this disease [5–7]. Pathological changes in the SMA skeletal muscle system have been widely reported, and a direct contributing role of muscle in SMA

was also hypothesized [8,9]. Besides denervation, available data also indicate the presence of mitochondrial disturbances in the locomotor muscles of patients and mouse models of SMA [10–12].

The effect of SMA on the skeletal muscle system is not uniform, and the muscle groups that are affected by the disease and those spared are similar in both humans and mouse models of SMA [13]. Respiratory involvement plays an important role in morbidity and mortality in children [14] and mice [15] with SMA. It is, in fact, necessary to monitor respiratory muscle performance in order to avoid acute and/or chronic respiratory failure [16]. Despite the relevance of this aspect, for obvious ethical reasons, very few studies have characterized the diaphragm muscle in patients with SMA. Specifically, based on clinical evaluations, relatively well-preserved diaphragm strength was found in patients with intermediate type II SMA as well as an increase in fatigue sensitivity that eventually leads to acute respiratory failure, especially during sleep [16]. Very few studies have analyzed the molecular level of the human SMA diaphragm. Degenerative changes in neuromuscular junctions (NMJs) in the diaphragm have been described in 6-month-old patients [17], and no clear damage was found in one post-mortem diaphragm muscle sample from a patient with SMA type I [10].

Several murine models of SMA have been generated, mostly based on Smn1 (murine homolog of human SMN1) gene inactivation and the introduction of more copies of the human SMN2. Severe SMA mouse models exhibit defects in breathing patterns with smaller ventilation volume, longer breath duration, and greater apnea frequency and duration [15]. Moreover, pronounced swelling of mitochondria [18] and alteration in the expression of proteins with an important role in the mitochondrial respiratory chain were found at the level of sub-synaptic regions [19].

The relevance of respiratory muscles to the clinical picture of patients with SMA and the lack of data on the intrinsic contractile capacity of the diaphragm warrant further investigations. An understanding of the diaphragm muscle defects could be important for preventing and effectively managing respiratory complications in SMA patients.

The central goal of this study was to carry out a comprehensive analysis of the intrinsic diaphragm functionality and the underlying molecular adaptations, combining functional, biochemical, and molecular analyses on isolated diaphragm muscle of SMNΔ7 mice. This model is, to date, one of the lines of SMA mice most widely used in numerous laboratories around the world. Ref. [20] exhibited symptoms and neuromuscular pathology similar to that of patients with intermediate type II SMA [21,22]. In this mouse model of SMA, ultrastructural study revealed features of NMJ alterations in diaphragm muscle [18], but no information about its contractile function is available. The results obtained in this study showed high fatigue sensitivity related to a redox imbalance in the diaphragm from SMNΔ7 mice. Interestingly, exposure of the diaphragm muscle to ergothioneine, a potent antioxidant molecule, seems able to restore diaphragm function.

## 2. Results

### *2.1. Ex Vivo Functional Analysis*

The contractile performance was assessed on diaphragm muscles isolated from SMNΔ7 (SMA) and control (WT) mice. Twitch time parameters, i.e., time to peak (TTP) and half relaxation time (TTR), showed a significant prolongation in the SMA diaphragm. Consequently, the isometric specific tension developed in twitch was increased, while specific tetanic tension was not changed (Figure 1a). Importantly, the fatigue test showed that the fatigue resistance was significantly reduced in SMA diaphragm in comparison with WT (Figure 1b).

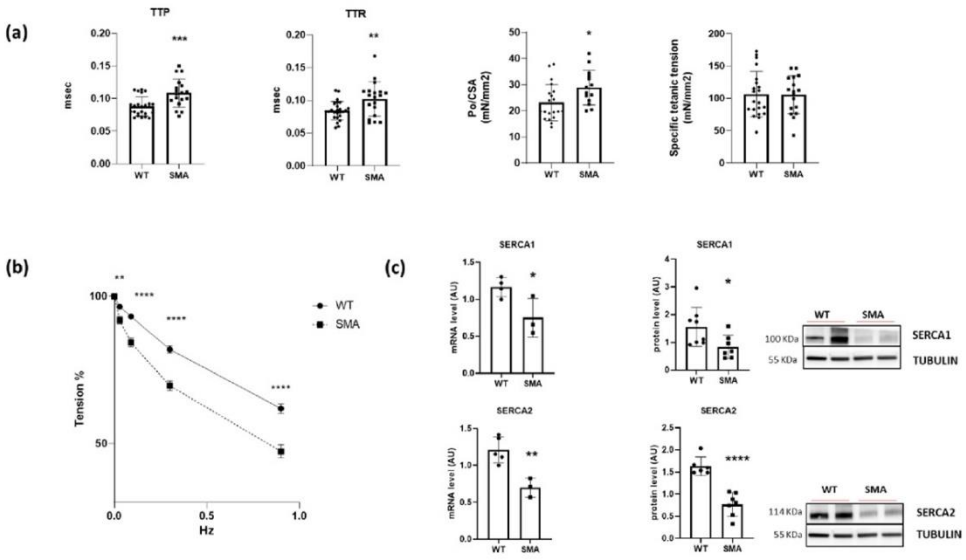


**Figure 1.** Alterations of contractile functions in SMA diaphragm. (**a**) Mean values of twitch time to peak (TTP), twitch half relaxation time (TTR), twitch specific tension (Po/CSA), and specific tetanic tension determined in ex vivo functional analysis in the diaphragm muscles (WT, n = 21; SMA, n = 17). (**b**) Fatigue index (percentage of the maximal tetanic force) (WT, n = 12; SMA, n = 12). (**c**) Gene (by RT-PCR) expression (WT, n = 5; SMA, n = 3) and protein (by Western blot) expression (WT, n = 8; SMA, n = 7) of sarcoplasmic reticulum $Ca^{2+}$ ATPase pumps (SERCA1 and 2). The level of protein target was normalized against the level of the housekeeping tubulin measured in the same blot. Representative Western blots are shown. Bars represent means± SD. Individual data are represented as scatter plots. * $p \leq 0.05$ ** $p \leq 0.01$ *** $p \leq 0.001$**** $p \leq 0.0005$.

The kinetics of force development and relaxation are mainly dictated by Ca2+ handling in the cell. A significant decrease in sarcoplasmic reticulum (SR) Ca2+ ATPase (SERCA1 and 2) pump gene and protein expression was found (Figure 1c).

### *2.2. Energy Imbalance and Oxidative Metabolism*

A significantly increased phosphorylation of the energy sensor AMPK was found in the SMA diaphragm (Figure 2a), suggesting a higher AMP/ATP ratio in the muscle and the presence of energy imbalance. Gene expression of PGC1α, Sirtuin1, and NRF1, involved in the regulation of oxidative metabolism by stimulating mitochondrial biogenesis, and the PGC1α protein expression were found significantly downregulated in the SMA diaphragm (Figure 2b,c). Unexpectedly, however, the protein expression of mitochondrial import receptor subunit TOM 20 was significantly higher (Figure 2c) in the SMA diaphragm, suggesting an increased mitochondrial mass. In agreement, the key components of the mitochondrial respiratory chain (OXPHOS complex), in particular, complex I, III, and IV (Figure 3), were significantly up-regulated. To evaluate whether the increased level of mitochondrial complexes leads to enhanced mitochondrial function, we compared the respiratory capacity of the diaphragms of SMA and WT mice. No changes were found in leak cellular respiration, oxidative phosphorylation (OXPHOS), and electron transfer system capacity (ETS) sustained by complex I, complex II, and by the contribution of both (Figure 4).

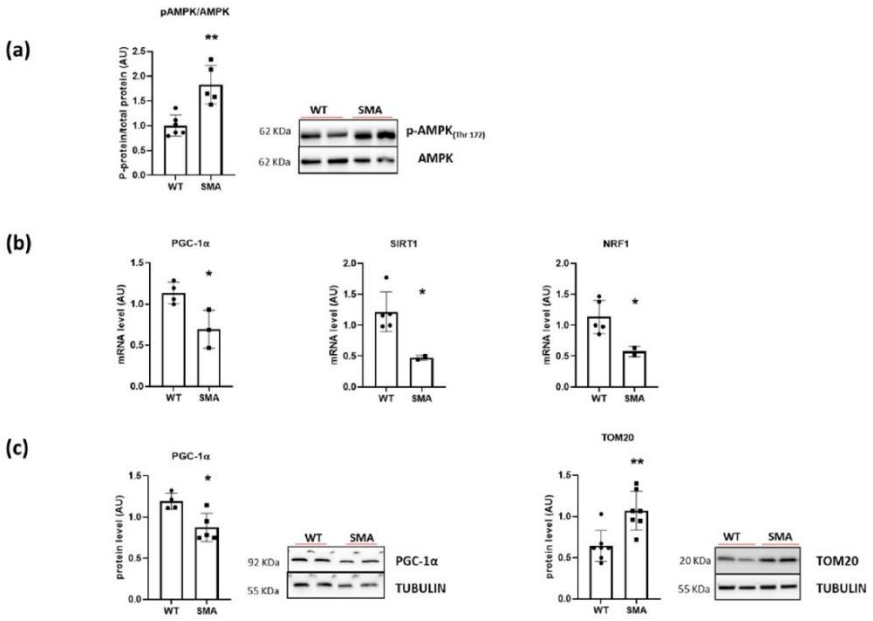


**Figure 2.** Energy imbalance in SMA diaphragm. (**a**) Mean values of the ratio between the content in the phosphorylated (p) and total forms for AMPK determined by Western blots (WT, n = 6; SMA, n = 5). (**b**) Gene expression of PGC1α, Sirtuin1 (SIR1) and NRF1 by RT-PCR (WT, n = 5; SMA, n = 3). (**c**) Protein expression of PGC1α (WT, n = 4; SMA, n = 5) and mitochondrial import receptor subunit TOM-20 (WT, n = 7; SMA, n = 7) determined by Western blots. The level of protein target was normalized against the level of the housekeeping tubulin measured in the same blot. Representative Western blots are shown. Bars represent means ± SD. Individual data are represented as scatter plots. * $p \leq 0.05$ ** $p \leq 0.01$.

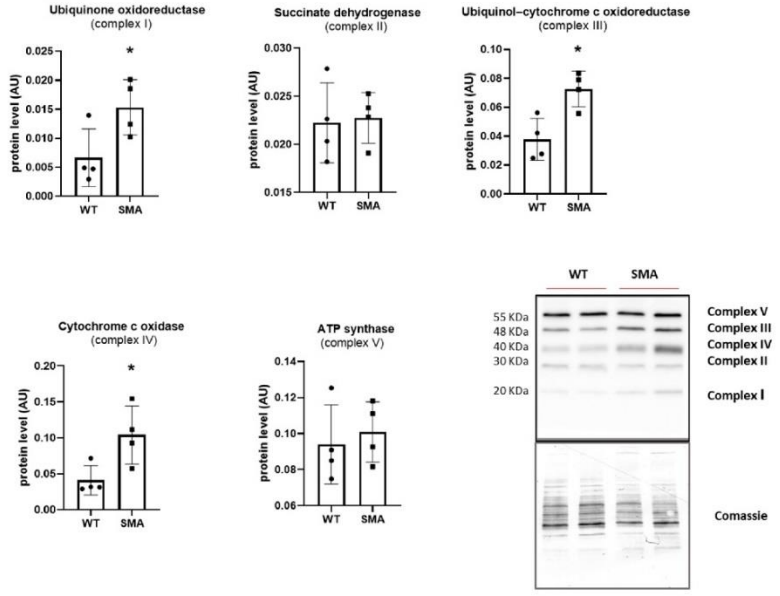


**Figure 3.** Up-regulation of OXPHOS complexes in SMA diaphragm. Experiments were performed on controls (WT, n = 4) and SMA phenotype (SMA, n = 4) diaphragms. Mean values of the components of the mitochondrial respiratory chain determined by Western blots. The level of protein target was normalized against the level of the same blot. stained with Comassie. Representative Western blots are shown. Bars represent means ± SD. Individual data are represented as scatter plots. * $p \leq 0.05$.

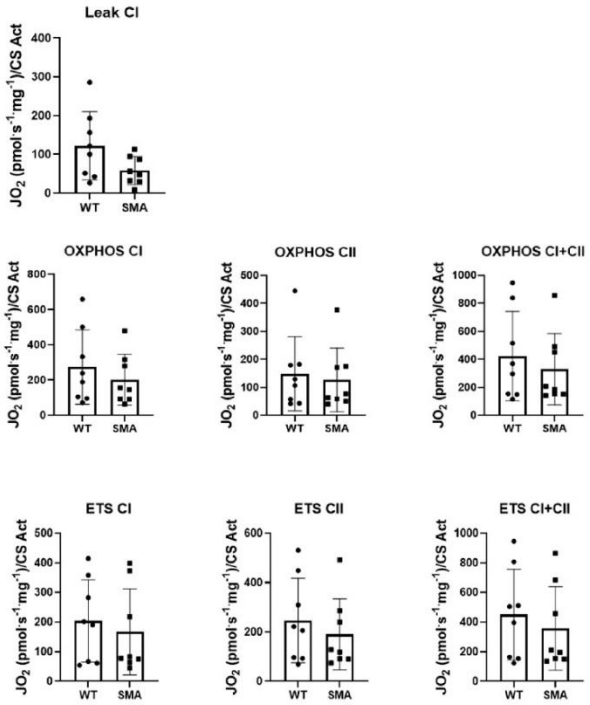


**Figure 4.** Mitochondrial respiration indices (LEAK—Resting non-phosphorylating electron transfer, OXPHOS—Oxidative phosphorylation, ETS—electron transfer system) are not changed in the complexes evaluated (Complex I—CI and Complex II—CII, both complexes—CI + CII) in SMA diaphragm. Experiments were performed on controls (WT, n = 8) and SMA phenotype (SMA, n = 8) diaphragms. Mean values of the mitochondrial respiration indices. Bars represent means ± SD. Individual data are represented as scatter plots.

To better characterize mitochondrial adaptations in the diaphragm of SMA mice, markers of mitochondrial dynamics were analyzed. Expression of pro-fusion proteins (OPA1, MNF1, MNF2), proteins involved in mitochondrial fission (FIS1, and the phosphorylate form of DRP1 at serine 616) showed no changes except for a significant increase in phosphorylation at serine 637 in DPR1 (Figure 5a,b).

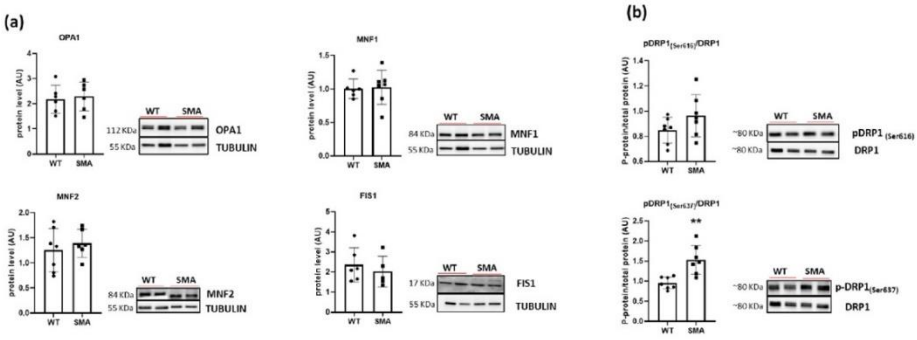


**Figure 5.** Alteration of markers of mitochondrial dynamics in SMA diaphragm. (**a**) Protein levels of OPA1, MNF1, MNF2 and FIS1 determined by Western blots (WT, n = 6; SMA, n = 6). (**b**) Phosphorylation of serine 616 and serine 637 of DPR1 (WT, n = 7; SMA, n = 7). The level of protein target was normalized against the level of the housekeeping tubulin measured in the same blot. Representative Western blots are shown. Bars represent means ± SD. Individual data are represented as scatter plots. ** $p \leq 0.01$.

### 2.3. Autophagy and Mitophagy

To assess the activation of the autophagy process, the ratio between the active and the inactive forms of LC3B (LC3BII/LC3BI) and the protein level of p62 were determined. The significant induction of the active form LC3BII, together with the decrease in p62 expression (Figure 6a), suggest the activation of the autophagy flux, which, however, does not result in an increased mitophagy activation. Indeed, a decrease in gene expression of BNIP3 (Figure 6b) and of PARKIN protein content, both involved in promoting the selective autophagy of depolarized mitochondria, was found (Figure 6c).

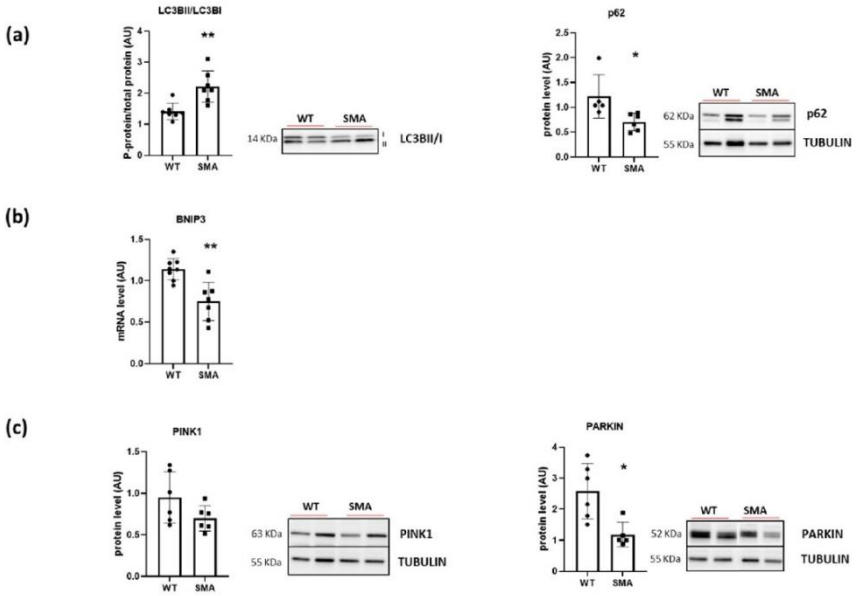


**Figure 6.** Alteration in autophagy and mitophagy processes in SMA diaphragm. (**a**) The ratio between the active form and the inactive form of LC3B (LC3BII/LC3BI) (WT, n = 7; SMA, n = 7) and protein levels of p62 (WT, n = 5; SMA, n = 6), determined by Western blots. (**b**) Gene expression of BNIP3 by RT-PCR (WT, n= 8; SMA, n= 7). (**c**) Protein levels of mitophagy makers PINK1 and PARKIN (WT, n = 6; SMA, n = 6), determined by Western blots. The level of protein target was normalized against the level of the housekeeping tubulin measured in the same blot. Representative Western blots are shown. Bars represent means ± SD. Individual data are represented as scatter plots. * $p \leq 0.05$ ** $p \leq 0.01$.

### 2.4. Redox Imbalance

Redox imbalance was investigated by evaluating the level of protein carbonylation, the level of ROS scavenger protein superoxide dismutase 1 (SOD1), catalase, Heat Shock Protein 27 (HSP27), Heat Shock Protein 70 (HSP70), Peroxiredoxin 3 (PRDX3) and gene expression of NRF2, the major sensor of cell redox balance. A significant increase in carbonylated proteins in the SMA diaphragm was revealed by Oxyblot analysis (Figure 7a). No induction of NRF2 (Figure 7b) and no changes in SOD1, catalase, HSP27, and HSP70 content were found. Peroxiredoxin 3 (PRDX3) was the only protein of antioxidant defense systems that revealed a significant increase in its expression (Figure 7c).

### 2.5. Effect of Exposure to the Antioxidant Molecule Ergothioneine

To test the impact of redox imbalance on contractile function, the determination of the contractile performance was repeated after incubation of the diaphragm in Krebs (for 30 min) and with 0.4% of water solution of ergothioneine (ERGO) added. Importantly, the exposure to ERGO restored TTP and TTR values to the WT level (Figure 8a) and reduced SMA diaphragm fatigability (Figure 8b).

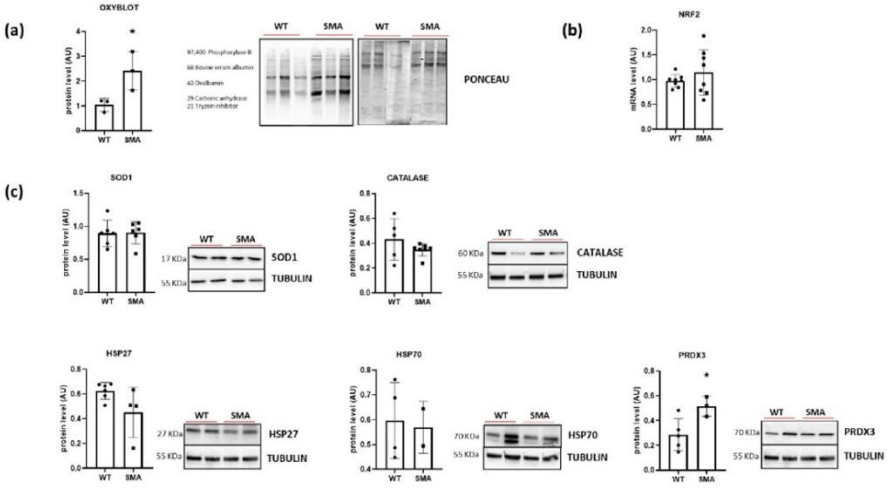


**Figure 7.** Presence of redox imbalance and ROS accumulation in SMA diaphragm. (**a**) Protein levels of carbonylated proteins revealed by Oxyblot analysis (WT, n= 3; SMA, n= 3). (**b**) Gene expression of NRF2 by RT-PCR (WT, n = 8; SMA n = 7). (**c**) Protein levels of SOD1 (WT, n = 6; SMA, n = 6), Catalase (WT, n = 5; SMA, n = 7), HSP27 (WT, n = 6; SMA, n= 4), HSP70 (WT, n = 4; SMA, n = 2) and Piroxiredoxin 3 (PRDX3) (WT, n= 5; SMA, n= 3), determined by Western blots. The level of protein target was normalized against the level of the housekeeping tubulin measured in the same blot. Representative Western blots are shown. Bars represent means ± SD. Individual data are represented as scatter plots. * $p \leq 0.05$.

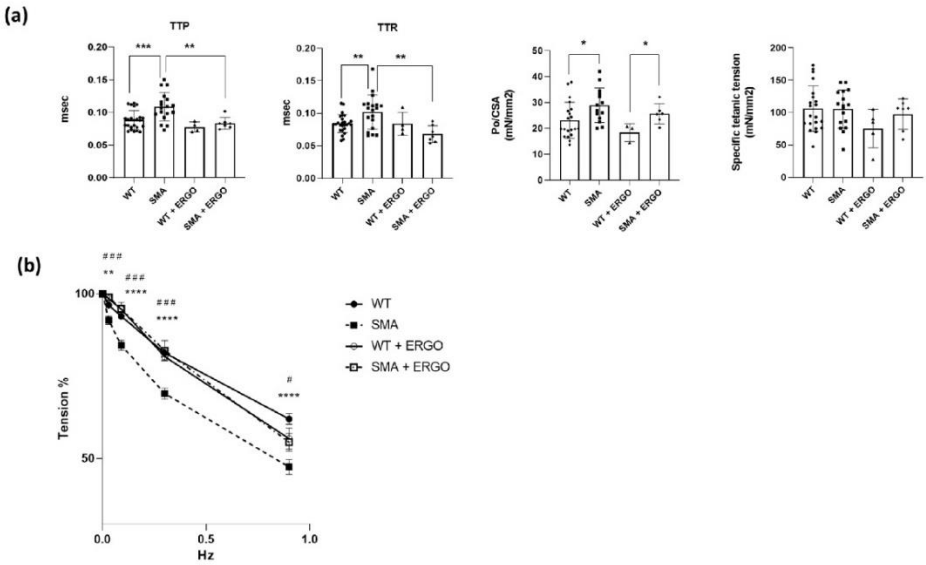


**Figure 8.** Recovery of contractile functions in SMA diaphragm following ergothioneine exposure. Experiments were performed on diaphragms of controls (WT), SMA phenotype (SMA), controls treated with ergothioneine (WT + ERGO), and SMA phenotype treated with ergothioneine (SMA + ERGO). (**a**) Mean values of twitch time to peak (TTP), twitch half relaxation time (TTR), twitch specific tension (Po/CSA) and specific tetanic tension (WT, n = 21; SMA, n = 17; WT + ERGO, n = 5 and SMA + ERGO, n = 7). (**b**) Fatigue index (percentage of the maximal tetanic force) (WT, n = 12; SMA, n = 12, WT + ERGO, n = 3 and SMA + ERGO, n = 8). Bars represent means ± SD. Individual data are represented as scatter plots. * $p \leq 0.05$ ** $p \leq 0.01$ *** $p \leq 0.001$ **** $p \leq 0.0005$ SMA vs. WT; # $p \leq 0.05$ ### $p \leq 0.001$ SMA vs. SMA+ERGO.

## 3. Discussion

### 3.1. SMA Diaphragm Exhibits Reduced Fatigue Resistance

The lack of variation in specific tetanic tension (Figure 1a) suggests the function of the myofibrillar contractile machinery is preserved in the SMA diaphragm. This is in agreement with studies in patients with SMA demonstrating that the diaphragm function is quite spared [16]. Notwithstanding the capacity to develop tension, a significant increase in both time to peak tension and time to half relaxation of single twitch in diaphragms from SMNΔ7 mice was found. Kinetics of force development and relaxation are mainly dictated by $Ca^{2+}$ handling in the cell. The rate of release of calcium ions by the sarcoplasmic reticulum (SR) depends on the activity of dihydropyridine and ryanodine receptors, whereas the rate of calcium reuptake is modulated by the activity of the SR calcium ATPase (SERCA) pumps. These pumps are particularly prone to suffer activity alterations, since they are characterized by an average life of 30–40 days, making these proteins potentially susceptible to oxidative damage [23]. In the present study, a significant reduction in gene and protein expression of SERCA1 and SERCA2 was found (Figure 1c). A very interesting result was the finding of a higher fatigability in diaphragm isolated from SMA mice (Figure 1b). This result is in accordance with the paper of Fauroux and colleagues suggesting that, in SMA patients, the inspiration relies mainly on the diaphragm that maintains its capacity to develop force but increases its fatigue sensitivity [16]. Therefore, our attention was focused on molecular determinants of diaphragm fatigue.

### 3.2. Energy Balance in SMA Diaphragm

One of the multiple factors leading to muscle fatigue could be a decrease in available ATP [24], as suggested by the finding of the activation of the energy sensor AMPK (Figure 2a). A decrease in available ATP could act on SERCA pumps and account for a longer timing of the single twitch. Moreover, a decrease in available ATP and a metabolic impairment could explain the greater sensitivity to fatigue observed in the diaphragm of SMA mice. The main source of ATP in the muscle is the oxidative phosphorylation that takes place in mitochondria. Our results showed that PGC1α, Sirtuin1, and NRF1 were significantly reduced in SMNΔ7 diaphragm, suggesting a defect in mitochondrial biogenesis (Figure 2b,c). Several indications of mitochondrial defects were found in the tibialis anterior muscle from SMNΔ7 mice [25,26] and muscle-specific Smn1 knockout mice [12], and in several skeletal muscles but not the diaphragm in patients with SMA [10]. Notice that only one diaphragm post-mortem was analyzed in these patients [10]. Interestingly, Chemello and colleagues demonstrated, in the tibialis anterior muscle of muscle-specific Smn1 knockout mice, the presence of dysfunctional mitochondria together with several unaltered mitochondria and higher mitochondrial protein levels [12]. Recently, it has been reported that mitochondrial activity was increased in an SMN depletion cell model [27]. In our study, an increased expression of mitochondrial import receptor subunit TOM-20 and marker proteins of OXPHOS complexes (Figures 2c and 3), but no changes in basal mitochondrial activity, were found (Figure 4). These apparently conflicting results point to the presence of dysfunctional mitochondria that could account for the increase in mitochondrial proteins but not contribute to an increase in mitochondrial activity.

To ensure optimal function in energy generation, the dynamic properties of mitochondria are critical [28]. Among the mitochondrial-shaping proteins, the contribution of active dynamin-related protein 1 (DRP1) is one of the important factors affecting mitochondrial shape controls, calcium homeostasis, and muscle mass [29], and the phosphorylation plays a crucial role in its activity regulation [30]. Moreover, available evidence indicates that phosphorylation of DRP1 in Ser637 induces mitochondrial elongation against oxidative stress [31,32]. In the present study, a significant increase in Ser637 phosphorylation of DRP1 was found (Figure 5b), suggesting an alteration in mitochondrial shape. Fused mitochondria have been demonstrated in aging [33,34], under nutrient deprivation [35], and in neuromuscular disease [36,37]. In-depth morphological studies are necessary to verify the presence of fused/elongated mitochondria in SMA diaphragm. Preliminary

qualitative EM investigations on SMA diaphragms show the presence of mitochondria of variable shape often clustered in shorter columns scattered within the fiber interior (Figures S1A–C and S2a,b) and the lack of "triadic" mitochondria, i.e., mitochondria coupled to the $Ca^{2+}$ Release Units (CRUs) or triads (Figure S1d–f), supporting their misplaced and uneven distribution [38]. The proper "triadic" association is essential for the bi-directional cross-talk between the two organelles, as the $Ca^{2+}$ released from SR during EC coupling enters into the mitochondrial matrix, stimulating ATP production [39–41].

Mitochondrial quality control is managed by mitophagy. Mitophagy represents, however, an "extreme decision" for a cell because mitochondria are an essential source of ATP. Moreover, to be degraded by autophagosome, the mitochondria must undergo a prior fragmentation process [42]. It was demonstrated that under starvation, mitochondria protect themselves from mitophagy by promoting fusion in order to maximize ATP production [32]. Only upon prolonged starvation do mitochondria undergo degradation and removal by mitophagy. Chemello and co-workers found a decrease in BNIP3 gene expression and an increase in LC3II in tibialis anterior of muscle-specific Smn1 knockout mice. Moreover, they found a reduction in LAMP1 and LAMP2 and a reduction in autophagic flux, leading them to hypothesize dysfunctional mitochondrial clearance [12]. In accordance with this study, a decrease in gene expression of BNIP3 and the protein level of PARKIN (Figure 6b,c) was found in the SMA diaphragm. However, the general autophagy process seemed to be activated, as indicated by a significant increase in the protein level of LC3BII and by a significant decrease in p62 protein expression (Figure 6a). So, the scenario emerging from the results of our study confirms the hypothesis of a reduction in mitochondria renewal also in diaphragm muscle that, on one hand, could meet the muscle need for the supply of ATP to the cells, but, on the other hand, could lead to an increase in ROS production.

### *3.3. Oxidative Stress in SMA Diaphragm*

The presence of redox imbalance and ROS accumulation in SMA mouse diaphragms was revealed by the presence of a great amount of carbonylated proteins (Figure 7a) and by an increase in complexes I and III of the mitochondrial respiratory chain, the main factors responsible for ROS formation (Figure 3) [43]. The increase in ROS production is expected to promote the expression of the antioxidant system composed of NRF2, SOD1, catalase and HSPs, but in the SMA diaphragm, all of these factors were not changed (Figure 7b). The lack of induction of the scavenging system could lead to ROS accumulation. Interestingly, only the expression of mitochondrial antioxidant protein peroxiredoxin 3 (PRDX3), essential for maintaining mitochondrial mass and membrane potential [44], was increased, in accord with the increased TOM20 expression (Figure 7c). Importantly, ROS accumulation could contribute to muscle fatigue, as indicated by an increasing body of evidence [24,45]. Accordingly, the recovery of the contractile performance of the isolated diaphragm after ERGO exposure was found (Figure 8). ERGO is a very water-soluble natural antioxidant molecule accumulating within tissues through the action of a specific organic cation transporter, and it is able to permeate the plasma, placenta and mitochondrial membranes [46,47]. While the exact function of ERGO has yet to be elucidated, it was established as a powerful scavenger mitochondria-derived superoxide species and a protector of mitochondrial constituents from damage by ROS [46,47].

## 4. Materials and Methods

### *4.1. Animals*

SMA (SMNΔ7 mice from Jackson Laboratory stock #005025) and control littermate mice 11 days of age were used. This time point was chosen as a compromise to have a higher number of alive sick animals, since the median age of survival of SMA mice is ~13 days. Heterozygous SMNΔ7 mice for SMN1 (SMN+/−) were crossed together to generate offspring with the following genotypes:

1. Homozygous for both transgenes and heterozygous for the null allele (7SMN+/+; SMN2 +/+; SMN+/−—50%). These mice do not show SMA phenotype and are used as breeders.
2. Homozygous for both transgenes and heterozygous for the null allele (7SMN+/+; SMN2 +/+; SMN+/+—25%). These mice do not show SMA phenotype and are used as control mice (WTs).
3. Homozygous for both transgenes and heterozygous for the null allele (7SMN+/+; SMN2 +/+; SMN−/−—25%). These mice show SMA phenotype (SMAs).

In order to achieve statistical significance, the sample size was chosen to use the smallest number of animals; there were no statistical methods employed to predetermine the sample size. The mice were identified through genotyping, but there was no randomization in the experiments. All procedures were approved by the University of Pavia's Animal Care and Use Committee (protocol reference n° 280/2021-PR) and, in conformity with Italian law, were communicated to the Ministry of Health and local authorities.

### 4.2. Genotyping

A PCR-based assay on tail DNA was used to genotype offspring. The mouse *Smn* knock-out allele was detected using the primers (Sigma Aldrich, St. Louis, MO, USA) in Table 1. The PCR procedure consisted of 5 min of heating at 94 °C, then 40 cycles of 94 °C for 1 min, 53 °C for 1 min, and 72 °C for 1 min, and finally a cycle of 10 min at 72 °C.

**Table 1.** Primers used for PCR assay to genotype offspring.

| | |
|---|---|
| *SMN1* WT FORWARD | 5′CTCCGGGATATTGGGATTG 3′ |
| *SMN1* WT REVERSE | 5′ TTTCTTCTGGCTGTGCCTTT 3′ |
| *SMN1* MUTANT REVERSE | 5′ GGTAACGCCAGGGTTTTCC 3′ |
| *SMN2* WT FORWARD | 5′ CTGACCTACCAGGGATGAGG 3′ |
| *SMN2* TRANSGENE | 5′ GGTCTGTTCTACAGCCACAGC 3′ |
| *SMN2* WT REVERSE | 5′CCCAGGTGGTTTATAGACTCAGA 3′ |
| *SMNΔ7* TRANSGENE 01 | 5′ TCCATTTCCTTCTGGACCAC 3′ |
| *SMNΔ7* TRANSGENE 02 | 5′ ACCCATTCCACTTCCTTTTT 3′ |
| *SMNΔ7* POSITIVE CTRL FORWARD | 5′ CAAATGTTGCTTGTCTGGTG 3′ |
| *SMNΔ7* POSITIVE CTRL REVERSE | 5′ GTCAGTCGAGTGCACAGTTT 3′ |

### 4.3. Ex Vivo Functional Analysis

The mice were sacrificed by cervical dislocation, the lower part of the chest was removed, and the diaphragm was dissected and immersed in an oxygenated Krebs solution. A stereomicroscope (×10 to ×60) was used to dissect the diaphragm strips (width 1–2 mm) including the central tendon. The diaphragm strips were transferred to the myograph and mounted by hooks between a force transducer (AME801; Aksjeselkapet Mikkroelektronik, Horten, Norway) and a movable shaft used to adjust muscle length. The strips were secured by opening small holes between the ribs and strengthening them with silk thread ligatures [48]. At a constant temperature of 22 °C, the preparations were placed in an organ bath that was filled with Krebs solution bubbled with 95% $O_2$ and 5% $CO_2$. The preparations were stretched to Lo (the length at which the maximum twitch force is seen), and their electrical stimulation response was evaluated. If a response could be elicited, the preparation was stimulated for ∼30 min with supramaximal, low-frequency (0.03 Hz) stimuli. Time to peak tension (TTP), and time to half relaxation (TTR) were measured. Subsequently, tetanic isometric contractions were evoked (110 Hz, 500 ms, supramaximal amplitude) at Lo. By calculating the decrease in the force of the maximal absolute tetanic force after 20 repeated contractions in a ramp protocol at 0.03, 0.09, 0.3, and 0.9 Hz, the fatigue index was determined [49,50]. The normalized tetanic force was expressed as the

maximal tetanic force/muscle cross-sectional area (CSA) (mN/mm$^2$), while the fatigue index was expressed as a percentage of the maximal tetanic force. The functional experiments were repeated following incubation for 30 min in Krebs augmented with 0.4% of a water solution containing 20µg of ergothioneine (ERGO), a naturally occurring amino acid derivative of histidine. ERGO has a powerful antioxidant action [51,52], and the dose was chosen based on data present in the literature [53] and modified to allow a translational comparison with human subjects taking ERGO as a dietary supplement.

### 4.4. OXYBLOT Analysis

Frozen diaphragm samples were homogenized at 4 °C in a buffer containing protease inhibitors, β-mercaptoethanol, Tris-HCl 0.5M pH 7.6, NaCl 1M, EDTA 100 mM pH7, and 0.1% NP40. The protein suspension was centrifuged at 13,500 rpm for 20 min at 5 °C. The Oxyblot Protein Oxidation Detection Kit (purchased from Millipore, Vimodrone, Italy) was utilized to detect the protein carbonylation level, using reagents to detect carbonyl groups in the protein side chain. Six micrograms of protein lysate were denatured by adding 12% SDS for a final concentration of 6% SDS. Samples were derivatized, through incubation for 10 min with 2,4-dinitrophenylhydrazine (DNPH), to 2,4-dinitrophenylhydrazone (DNP hydrazone). Polyacrylamide gel electrophoresis was used to separate the DNP-derivatized protein samples (4–20% SDS precast gels, Bio-rad, Hercules, CA, USA), followed by Western blotting. The membranes were stained with Ponceau Red and then incubated with a primary antibody that was specific to the DNP moiety of the proteins, followed by an HRP-antibody conjugate directed against the primary antibody (secondary antibody: goat anti-rabbit IgG). Protein detection was performed using the Amersham ECL Select™ detection system (Cytiva Life Sciences, ex GE Healthcare, Marlborough, MA, USA), which highlights the HPR substrate through a chemiluminescent reaction. Membranes were gained through an analysis software, ImageQuant™ LAS 4000 (GE Healthcare Life Sciences, Milwaukee, WI, USA). Protein oxidation was quantified by defining the oxidative index (OI), i.e., the ratio between densitometric values of the OXYBLOT bands and those stained with Ponceau Red. The OI was expressed relative to control samples to compare different experiments.

### 4.5. Gene Expression Analysis

Total RNA, from diaphragm muscles, was extracted using the Promega SV Total RNA isolation kit; the concentration of RNA was evaluated by using NanoPhotometer N60/N50 (IMPLEN, Westlake Village, CA, USA). A 300 ng amount was reverse-transcribed with Super Script III reverse transcriptase (Invitrogen, Carlsbad, CA, USA) to obtain cDNA. The cDNA was analyzed by real-time PCR with the SyBR Green PCR kit (Applied Biosystem, Foster City, CA, USA), and the data were normalized to tubulin expression (Quantitect primer assay from QIAGEN, Hilden, Germany). Oligonucleotide primers used for real-time PCR are listed in Table 2. To identify genes that expressed differently, the default threshold of 6.0 was utilized. The difference between cycle threshold (Ct) values for each mRNA was calculated by taking the mean Ct of duplicate reactions and subtracting the mean Ct of duplicate reactions for the reference RNA measured on an aliquot from the same RT reaction (CΔt = Ct target gene − Ct reference gene). All samples were then normalized to the ΔCt value of a calibrator sample to obtain a ΔΔCt value (ΔCt target − ΔCt calibrator) (comparative method).

### 4.6. Western Blot Analysis

Diaphragm samples (stored at –80 °C) were pulverized with liquid nitrogen and suspended in a lysis buffer (1% triton × 100, 10% Glycerol, 20 mM TRIS-HCl, 5 mM EDTA, 150 mM NaCl, 100 mM Naf, 2 mM NaPPi, and 1 mM PMSF) supplemented with protease inhibitor cocktail and phosphatase inhibitor cocktail (Sigma-Aldrich, St. Louis, MO, USA). After 20 min on ice, the protein lysate was centrifuged at 18,000× $g$ at 4 °C for 20 min, and the supernatant was transferred to a clean Eppendorf tube and stored at –80 °C until it was ready to use. Protein concentration was determined using the RC DCTM protein

assay kit (Bio-rad Hercules, CA, USA). Equal amounts of protein sample (40 ug) were loaded on a polyacrylamide gel (Any kD precast gel—Biorad Hercules, CA, USA) and subjected to electrophoresis. Proteins were then electrotransferred to a membrane made of nitrocellulose at 35 mA O/N. After blocking in 5% milk in TBST for 1 h, the membranes were incubated O/N at 4 °C with the specific primary antibody appropriately diluted in a solution of TBST 1X containing 5% BSA or 5% fat-free milk (depending on specificities of antibodies in the datasheet (Table 3)). Lastly, the membranes were then incubated in HRP conjugated secondary antibody, goat-anti-rabbit (1: 10,000, from Millipore, St. Louis, MI. USA) or rabbit-anti-mouse (1:5000, from dako, Santa Clara, CA, USA), diluted in 5% milk, for 1 h at room temperature. The Amersham ECL Select™ detection system (Cytiva Life Sciences, Marlborough, MA, USA, ex GE Healthcare) was utilized to visualize the proteins, which highlights the HPR substrate by a chemiluminescent reaction. The target protein levels were normalized with respect to the amount of a housekeeping protein (tubulin); the phosphorylation levels of some proteins were evaluated by the ratio between phosphorylated and unphosphorylated total forms of the same protein.

**Table 2.** Oligonucleotide primers used for real-time PCR.

| | Forward Primer | Reverse Primer |
|---|---|---|
| *SERCA1* | TGTTTGTCCTATTTCGGGGTG | AATCCGCACAAGCAGGTCTTC |
| *SERCA2* | GAGAACGCTCACACAAAGACC | CAATTCGTTGGAGCCCCAT |
| *PGC1α* | ACCCCAGAGTCACCAAATGA | CGAAGCCTTGAAAGGGTTATC |
| *SIRT1* | CCGCGGATAGGTCCATATACT | AACAATCTGCCACAGCGTCA |
| *NRF1* | GCACCTTTGGAGAATGTGGT | CTGAGCCTGGGTCATTTTGT |
| *NRF2* | TTCTTTCAGCAGCATCCTCTCCAC | ACAGCCTTCAATAGTCCCGTCCAG |
| *BNIP3* | TTCCACTAGCACCTTCTGATGA | GAACACCGCATTTACAGAACAA |

### *4.7. Oxygraph-2k for High-Resolution Respirometry ($O_2$k HRR)*

For the measurements of mitochondrial respiration, the Oxygraph-2k ($O_2$k, OROBOROS Instruments, Innsbruck, Austria) was utilized. For each mouse, the diaphragm muscle was properly dissected and divided into two parts in ice-cold BIOPS buffer (biopsy preservation solution: 7.23 mM $K_2$EGTA, 5.77 mM $Na_2$ATP, 2.77 mM $CaK_2$EGTA, 6.56 mM $MgCl_2$•6 $H_2O$, 20 mM Taurine, 15 mM $Na_2$Phosphocreatine, 20 mM Imidazole, 0.5 mM Dithiothreitol (DTT), 50 mM MES, pH 7.1) at 0 °C. Both parts were used in order to perform the analysis in duplicate during the day. Pieces of diaphragm were washed in ice-cold BIOPS for 10 min, permeabilized with 20 µg/mL Saponin (Merck) in BIOPS in agitation at 4 °C, and finally washed with mMiR05 buffer (mitochondrial respiration medium: 3 mM $MgCl_2$, 60 mM lactobionic acid 0.5 mM EGTA, 20 mM taurine, 10 mM $KH_2PO_4$, 20 mM 4-(2-hydroxyethyl) piperazine-1-ethanesulfonic acid (HEPES), 110 mM D-sucrose, and 1 g·L-1 bovine serum albumin (pH 7.1)). Muscle samples were transferred into Oroboros-$O_2$k chambers; the experiments were performed in Mir05 solution, at 37 °C with an oxygen concentration between 400 and 250 µM to avoid $O_2$ limitation of respiration, and the medium was reoxygenated with pure gaseous $O_2$ when oxygen concentration decreased below the threshold of 250 µM. Moreover, the measurements were performed in the presence of Blebbistatin (a myosin II-ATPase inhibitor, 25 µM), dissolved in DMSO 5 mM stock [54] in order to avoid spontaneous contraction in the respiration medium of muscle samples. Calibration at air saturation was performed each day before starting experiments. Respiration was determined using substrate-uncoupler-inhibitor titration (SUIT) protocols previously described [55,56], with modifications. Glutamate and malate (10 mM and 4 mM, respectively) were added to measure non-phosphorylating resting mitochondrial respiration in the absence of adenylates, in order to evaluate the consumption of $O_2$, mainly determined by the leakage of protons through the inner mitochondrial membrane ("LEAK" respiration). Succinate (10 mM) was then used to support convergent electron flow into

the Q-junction through Complexes I and II (determining the LEAK of both Complexes I and II). ADP was added until reaching a 10 mM final saturating concentration, to obtain maximal ADP-stimulated mitochondrial respiration (OXPHOS capacity). Titrations with FCCP, the uncoupler protonophore carbonylcyanide-p trifluoromethoxyphenylhydrazone (a few steps of 1 µM), were performed to determine electron transfer system (ETS) capacity. Rotenone (Rot, 0.5 µM added to inhibit Complex I) and Antimycin A (AmA, 2.5 µM to inhibit Complex III and thus the mitochondrial respiratory chain) were added for the determination of maximal respiratory uncoupled efficiency and residual oxygen consumption (ROX) independently by mitochondria, respectively. Prior to AmA, Cytochrome C (10 µM) was added to the chambers to evaluate the outer mitochondrial membrane integrity: an increase in oxygen flux of more than 15% would indicate damaged organelles. At the end of each experiment, muscle samples were taken from the chambers, washed in PBS, and centrifuged for 10 min at 14,000× *g* at 4 °C, and frozen in liquid nitrogen to be stored at −80 °C until further determinations. All of the mitochondrial respiration parameters analyzed were corrected for $O_2$ flux resulting from residual $O_2$ consumption (ROX) and were normalized by the value of citrate synthase activity (see below) [57].

**Table 3.** Antibodies used for Western Blot Analysis.

| Primary Antibody | Species | Dilution | Supplier | Catalog Number |
|---|---|---|---|---|
| p-AMPK | Rabbit | 1:1000 | Cell Signaling | #4188 |
| AMPK | Rabbit | 1:1000 | Cell Signaling | #2532 |
| PGC1α | Rabbit | 1:1000 | Abcam | Ab54481 |
| TOM20 | Rabbit | 1:1000 | Santa Cruz | sc-11415 |
| OPA1 | Mouse | 1:3000 | Abcam | Ab157457 |
| MNF1 | Mouse | 1:1000 | Abcam | Ab57602 |
| MNF2 | Rabbit | 1:1000 | Abcam | Ab50843 |
| FIS1 | Rabbit | 1:1000 | Abcam | Ab71498 |
| DRP1 pSer616 | Rabbit | 1:1000 | Cell Signaling | #3455 |
| DRP1 pSer637 | Rabbit | 1:1000 | Cell Signaling | #4867 |
| DRP1 | Rabbit | 1:1000 | Cell Signaling | #8570 |
| SOD1 | Rabbit | 1:1000 | Abcam | Ab16831 |
| Catalase | Rabbit | 1:1000 | Abcam | Ab52477 |
| Hsp27 | Mouse | 1:1000 | Abcam | Ab2790 |
| Hsp70 | Mouse | 1:1000 | Abcam | Ab47455 |
| PRDX3 | Rabbit | 1:1000 | Abcam | Ab73349 |
| LC3B | Rabbit | 1:1000 | Sigma | L7543 |
| p62 | Rabbit | 1:2000 | Cell Signaling | #5114 |
| PINK1 | Rabbit | 1:1000 | Invitrogen | #PA1-16604 |
| PARKIN | Mouse | 1:2000 | Invitrogen | #39-0900 |
| Tubulin | Mouse | 1:2000 | Sigma | T6199 |
| OXPHOS | Mouse | 1:1000 | Abcam | Ab110413 |
| SERCA1 | Rabbit | 1:1000 | Cell Signaling | #12293 |
| SERCA2 | Rabbit | 1:1000 | Cell Signaling | #9580 |

### *4.8. Citrate Synthase Activity*

CS activity was assessed using the Citrate Synthase Activity Assay kit (Merck, Darmstadt, Germany). Muscle samples were homogenized in CS Assay Buffer provided by the kit

and centrifuged at 10,000× *g* for 20 min at 4 °C after being kept on ice for 40 min. RC-DC™ protein assay (Bio-rad Hercules, CA, USA) was used to determine protein concentration; 5 µg of protein lysate was used to test CS activity. The absorbance was measured at 412 nm at the initial time (Tinitial), after adding the appropriate Reaction Mix, with a plate reader (CLARIOstar Plus, BMG Labtech, Ortenberg, Germany), and then the measurement was followed for 45 min, taking an absorbance measurement (A412) every 5 min. CS enzyme activity was calculated by interpolating the value of the final time (Tfinal) on a standard curve whose points was scalar concentrations of a solution of known concentration (2 nmol/µL) of GSH standard solution. Values for citrate synthase activity were used to normalize the parameters evaluated by using $O_2$k HRR.

### *4.9. Electron Microscopy (EM)*

Intact diaphragms were fixed at room temperature with 3.5% glutaraldehyde in 0.1M Na Cacodylate buffer, pH 7.2 for several hours. Small pieces of fixed diaphragms were then processed, cut, and stained as in Boncompagni et al. 2009 [38]. Sections were viewed and photographed in a 120 kV JEM-1400 Flash Transmission Electron Microscope (Jeol Ltd., Tokyo, Japan) equipped with CMOS camera (Matataki and TEM Center software Ver. 1.7.22.2684 (Jeol Ltd., Tokyo, Japan)).

### *4.10. Statistical Analysis*

The data were expressed as mean ± S.D. The statistical significance of the differences between the averages was determined with the Student t-test; a probability of less than 5% ($p < 0.05$) was considered significant. The statistical analysis was performed using GraphPad Prism 9.0 software. The sample size was predetermined based on the published literature and chosen to use the fewest number of animals to achieve statistical significance.

## 5. Conclusions

Current pharmacological and cellular approaches, mainly focusing on motor neuron alterations, are only partially effective in ameliorating SMA clinical presentation. To achieve new and real expectations for SMA disease treatment in the future, it is necessary to develop alternative and parallel sites of intervention, especially for the patients who unfortunately already are not treatable with the newly discovered drugs (Spinraza, Risdiplam, and AVXS-101 (Zolgensma)). In particular, the improvement of diaphragm function could be useful to improve the quality of life of all patients with SMA.

The results obtained in the present study give the first demonstration of an intrinsic energetic imbalance and a significant ROS accumulation not scavenged by the antioxidant enzyme pool in the diaphragm of SMNΔ7 mice. Both conditions can contribute to muscle fatigue and, in the long run, lead to diaphragm wasting and respiratory failure. The significant increase in fatigue resistance of isolated diaphragm from SMA mice following ERGO exposure supports the rationale to test the effect of dietary supplementation with ERGO in SMA mice to improve their life quality and increase their lifespan.

**Supplementary Materials:** The following supporting information can be downloaded at: https://www.mdpi.com/article/10.3390/ijms241914953/s1.

**Author Contributions:** Conceptualization, M.C.; investigation, F.C., D.R., M.A., G.R., L.B.; resources, M.A.P., P.R.; writing—original draft preparation, M.C.; writing—review and editing, M.A.P., S.B.; funding acquisition, M.C. All authors have read and agreed to the published version of the manuscript.

**Funding:** This research was funded by Blue Sky Research (Call for University Research Found), BSR-15214 (2017–2019).

**Institutional Review Board Statement:** All procedures were approved by the University of Pavia's Animal Care and Use Committee (protocol reference n° 280/2021-PR) and, in accordance with Italian law, were communicated to the Ministry of Health and local authorities.

**Informed Consent Statement:** Not applicable.

**Data Availability Statement:** Not applicable.

**Acknowledgments:** We wish to thank Carlo Reggiani for discussion on the experimental work and valuable suggestions.

**Conflicts of Interest:** The authors declare no conflict of interest.

## References

1. Schroth, M.K. Special considerations in the respiratory management of spinal muscular atrophy. *Pediatrics* **2009**, *123* (Suppl. 4), S245–S249. [CrossRef] [PubMed]
2. Prior, T.W. Spinal muscular atrophy: A time for screening. *Curr. Opin. Pediatr.* **2010**, *22*, 696–702. [CrossRef]
3. Lefebvre, S.; Bürglen, L.; Reboullet, S.; Clermont, O.; Burlet, P.; Viollet, L.; Benichou, B.; Cruaud, C.; Millasseau, P.; Zeviani, M. Identification and characterization of a spinal muscular atrophy-determining gene. *Cell* **1995**, *80*, 155–165. [CrossRef]
4. Lorson, C.L.; Hahnen, E.; Androphy, E.J.; Wirth, B. A single nucleotide in the SMN gene regulates splicing and is responsible for spinal muscular atrophy. *Proc. Natl. Acad. Sci. USA* **1999**, *96*, 6307–6311. [CrossRef]
5. Yeo, C.J.J.; Darras, B.T. Overturning the Paradigm of Spinal Muscular Atrophy as Just a Motor Neuron Disease. *Pediatr. Neurol.* **2020**, *109*, 12–19. [CrossRef]
6. Nash, L.A.; Burns, J.K.; Chardon, J.W.; Kothary, R.; Parks, R.J. Spinal Muscular Atrophy: More than a Disease of Motor Neurons? *Curr. Mol. Med.* **2016**, *16*, 779–792. [CrossRef] [PubMed]
7. Simone, C.; Ramirez, A.; Bucchia, M.; Rinchetti, P.; Rideout, H.; Papadimitriou, D.; Re, D.B.; Corti, S. Is spinal muscular atrophy a disease of the motor neurons only: Pathogenesis and therapeutic implications? *Cell Mol. Life Sci.* **2016**, *73*, 1003–1020. [CrossRef] [PubMed]
8. Kim, J.K.; Jha, N.N.; Feng, Z.; Faleiro, M.R.; Chiriboga, C.A.; Wei-Lapierre, L.; Dirksen, R.T.; Ko, C.P.; Monani, U.R. Muscle-specific SMN reduction reveals motor neuron-independent disease in spinal muscular atrophy models. *J. Clin. Investig.* **2020**, *130*, 1271–1287. [CrossRef]
9. Lee, Y.I.; Mikesh, M.; Smith, I.; Rimer, M.; Thompson, W. Muscles in a mouse model of spinal muscular atrophy show profound defects in neuromuscular development even in the absence of failure in neuromuscular transmission or loss of motor neurons. *Dev. Biol.* **2011**, *356*, 432–444. [CrossRef]
10. Ripolone, M.; Ronchi, D.; Violano, R.; Vallejo, D.; Fagiolari, G.; Barca, E.; Lucchini, V.; Colombo, I.; Villa, L.; Berardinelli, A.; et al. Impaired Muscle Mitochondrial Biogenesis and Myogenesis in Spinal Muscular Atrophy. *JAMA Neurol.* **2015**, *72*, 666–675. [CrossRef]
11. James, R.; Chaytow, H.; Ledahawsky, L.M.; Gillingwater, T.H. Revisiting the role of mitochondria in spinal muscular atrophy. *Cell Mol. Life Sci.* **2021**, *78*, 4785–4804. [CrossRef]
12. Chemello, F.; Pozzobon, M.; Tsansizi, L.I.; Varanita, T.; Quintana-Cabrera, R.; Bonesso, D.; Piccoli, M.; Lanfranchi, G.; Giacomello, M.; Scorrano, L.; et al. Dysfunctional mitochondria accumulate in a skeletal muscle knockout model of Smn1, the causal gene of spinal muscular atrophy. *Cell Death Dis.* **2023**, *14*, 162. [CrossRef] [PubMed]
13. Durmus, H.; Yilmaz, R.; Gulsen-Parman, Y.; Oflazer-Serdaroglu, P.; Cuttini, M.; Dursun, M.; Deymeer, F. Muscle magnetic resonance imaging in spinal muscular atrophy type 3: Selective and progressive involvement. *Muscle Nerve* **2017**, *55*, 651–656. [CrossRef] [PubMed]
14. LoMauro, A.; Aliverti, A.; Mastella, C.; Arnoldi, M.T.; Banfi, P.; Baranello, G. Spontaneous Breathing Pattern as Respiratory Functional Outcome in Children with Spinal Muscular Atrophy (SMA). *PLoS ONE* **2016**, *11*, e0165818. [CrossRef] [PubMed]
15. Michaud, M.; Arnoux, T.; Bielli, S.; Durand, E.; Rotrou, Y.; Jablonka, S.; Robert, F.; Giraudon-Paoli, M.; Riessland, M.; Mattei, M.G.; et al. Neuromuscular defects and breathing disorders in a new mouse model of spinal muscular atrophy. *Neurobiol. Dis.* **2010**, *38*, 125–135. [CrossRef]
16. Fauroux, B.; Griffon, L.; Amaddeo, A.; Stremler, N.; Mazenq, J.; Khirani, S.; Baravalle-Einaudi, M. Respiratory management of children with spinal muscular atrophy (SMA). *Arch. Pediatr.* **2020**, *27*, 7S29–7S34. [CrossRef]
17. Kariya, S.; Park, G.H.; Maeno-Hikichi, Y.; Leykekhman, O.; Lutz, C.; Arkovitz, M.S.; Landmesser, L.T.; Monani, U.R. Reduced SMN protein impairs maturation of the neuromuscular junctions in mouse models of spinal muscular atrophy. *Hum. Mol. Genet.* **2008**, *17*, 2552–2569. [CrossRef]
18. Voigt, T.; Neve, A.; Schümperli, D. The craniosacral progression of muscle development influences the emergence of neuromuscular junction alterations in a severe murine model for spinal muscular atrophy. *Neuropathol. Appl. Neurobiol.* **2014**, *40*, 416–434. [CrossRef]
19. Neve, A.; Trüb, J.; Saxena, S.; Schümperli, D. Central and peripheral defects in motor units of the diaphragm of spinal muscular atrophy mice. *Mol. Cell Neurosci.* **2016**, *70*, 30–41. [CrossRef]
20. Le, T.T.; Pham, L.T.; Butchbach, M.E.; Zhang, H.L.; Monani, U.R.; Coovert, D.D.; Gavrilina, T.O.; Xing, L.; Bassell, G.J.; Burghes, A.H. SMNDelta7, the major product of the centromeric survival motor neuron (SMN2) gene, extends survival in mice with spinal muscular atrophy and associates with full-length SMN. *Hum. Mol. Genet.* **2005**, *14*, 845–857. [CrossRef]

21. Butchbach, M.E.; Edwards, J.D.; Burghes, A.H. Abnormal motor phenotype in the SMNDelta7 mouse model of spinal muscular atrophy. *Neurobiol. Dis.* **2007**, *27*, 207–219. [CrossRef]
22. Butchbach, M.E.; Rose, F.F.; Rhoades, S.; Marston, J.; McCrone, J.T.; Sinnott, R.; Lorson, C.L. Effect of diet on the survival and phenotype of a mouse model for spinal muscular atrophy. *Biochem. Biophys. Res. Commun.* **2010**, *391*, 835–840. [CrossRef] [PubMed]
23. Qaisar, R.; Pharaoh, G.; Bhaskaran, S.; Xu, H.; Ranjit, R.; Bian, J.; Ahn, B.; Georgescu, C.; Wren, J.D.; Van Remmen, H. Restoration of Sarcoplasmic Reticulum Ca. *Int. J. Mol. Sci.* **2020**, *22*, 37. [CrossRef] [PubMed]
24. Allen, D.G.; Lamb, G.D.; Westerblad, H. Skeletal muscle fatigue: Cellular mechanisms. *Physiol. Rev.* **2008**, *88*, 287–332. [CrossRef] [PubMed]
25. Kong, L.; Wang, X.; Choe, D.W.; Polley, M.; Burnett, B.G.; Bosch-Marcé, M.; Griffin, J.W.; Rich, M.M.; Sumner, C.J. Impaired synaptic vesicle release and immaturity of neuromuscular junctions in spinal muscular atrophy mice. *J. Neurosci.* **2009**, *29*, 842–851. [CrossRef]
26. Torres-Benito, L.; Neher, M.F.; Cano, R.; Ruiz, R.; Tabares, L. SMN requirement for synaptic vesicle, active zone and microtubule postnatal organization in motor nerve terminals. *PLoS ONE* **2011**, *6*, e26164. [CrossRef]
27. Acsadi, G.; Lee, I.; Li, X.; Khaidakov, M.; Pecinova, A.; Parker, G.C.; Hüttemann, M. Mitochondrial dysfunction in a neural cell model of spinal muscular atrophy. *J. Neurosci. Res.* **2009**, *87*, 2748–2756. [CrossRef]
28. Chan, D.C. Mitochondrial Dynamics and Its Involvement in Disease. *Annu. Rev. Pathol.* **2020**, *15*, 235–259. [CrossRef]
29. Favaro, G.; Romanello, V.; Varanita, T.; Andrea Desbats, M.; Morbidoni, V.; Tezze, C.; Albiero, M.; Canato, M.; Gherardi, G.; De Stefani, D.; et al. DRP1-mediated mitochondrial shape controls calcium homeostasis and muscle mass. *Nat. Commun.* **2019**, *10*, 2576. [CrossRef]
30. Xie, L.; Shi, F.; Li, Y.; Li, W.; Yu, X.; Zhao, L.; Zhou, M.; Hu, J.; Luo, X.; Tang, M.; et al. Drp1-dependent remodeling of mitochondrial morphology triggered by EBV-LMP1 increases cisplatin resistance. *Signal Transduct. Target. Ther.* **2020**, *5*, 56. [CrossRef]
31. Loh, J.K.; Lin, C.C.; Yang, M.C.; Chou, C.H.; Chen, W.S.; Hong, M.C.; Cho, C.L.; Hsu, C.M.; Cheng, J.T.; Chou, A.K.; et al. GSKIP- and GSK3-mediated anchoring strengthens cAMP/PKA/Drp1 axis signaling in the regulation of mitochondrial elongation. *Biochim. Biophys. Acta* **2015**, *1853*, 1796–1807. [CrossRef]
32. Gomes, L.C.; Di Benedetto, G.; Scorrano, L. During autophagy mitochondria elongate, are spared from degradation and sustain cell viability. *Nat. Cell Biol.* **2011**, *13*, 589–598. [CrossRef] [PubMed]
33. Navratil, M.; Terman, A.; Arriaga, E.A. Giant mitochondria do not fuse and exchange their contents with normal mitochondria. *Exp. Cell Res.* **2008**, *314*, 164–172. [CrossRef] [PubMed]
34. Leduc-Gaudet, J.P.; Picard, M.; St-Jean Pelletier, F.; Sgarioto, N.; Auger, M.J.; Vallée, J.; Robitaille, R.; St-Pierre, D.H.; Gouspillou, G. Mitochondrial morphology is altered in atrophied skeletal muscle of aged mice. *Oncotarget* **2015**, *6*, 17923–17937. [CrossRef] [PubMed]
35. Rambold, A.S.; Kostelecky, B.; Elia, N.; Lippincott-Schwartz, J. Tubular network formation protects mitochondria from autophagosomal degradation during nutrient starvation. *Proc. Natl. Acad. Sci. USA* **2011**, *108*, 10190–10195. [CrossRef] [PubMed]
36. Cantó-Santos, J.; Grau-Junyent, J.M.; Garrabou, G. The Impact of Mitochondrial Deficiencies in Neuromuscular Diseases. *Antioxidants* **2020**, *9*, 964. [CrossRef] [PubMed]
37. Marra, F.; Lunetti, P.; Curcio, R.; Lasorsa, F.M.; Capobianco, L.; Porcelli, V.; Dolce, V.; Fiermonte, G.; Scarcia, P. An Overview of Mitochondrial Protein Defects in Neuromuscular Diseases. *Biomolecules* **2021**, *11*, 1633. [CrossRef]
38. Boncompagni, S.; Rossi, A.E.; Micaroni, M.; Beznoussenko, G.V.; Polishchuk, R.S.; Dirksen, R.T.; Protasi, F. Mitochondria are linked to calcium stores in striated muscle by developmentally regulated tethering structures. *Mol. Biol. Cell* **2009**, *20*, 1058–1067. [CrossRef]
39. Bolaños, P.; Guillen, A.; Rojas, H.; Boncompagni, S.; Caputo, C. The use of CalciumOrange-5N as a specific marker of mitochondrial Ca2+ in mouse skeletal muscle fibers. *Pflugers Arch.* **2008**, *455*, 721–731. [CrossRef]
40. Rossi, A.E.; Boncompagni, S.; Dirksen, R.T. Sarcoplasmic reticulum-mitochondrial symbiosis: Bidirectional signaling in skeletal muscle. *Exerc. Sport. Sci. Rev.* **2009**, *37*, 29–35. [CrossRef]
41. Rossi, A.E.; Boncompagni, S.; Wei, L.; Protasi, F.; Dirksen, R.T. Differential impact of mitochondrial positioning on mitochondrial Ca(2+) uptake and Ca(2+) spark suppression in skeletal muscle. *Am. J. Physiol. Cell Physiol.* **2011**, *301*, C1128–C1139. [CrossRef] [PubMed]
42. Filomeni, G.; De Zio, D.; Cecconi, F. Oxidative stress and autophagy: The clash between damage and metabolic needs. *Cell Death Differ.* **2015**, *22*, 377–388. [CrossRef]
43. Brand, M.D.; Buckingham, J.A.; Esteves, T.C.; Green, K.; Lambert, A.J.; Miwa, S.; Murphy, M.P.; Pakay, J.L.; Talbot, D.A.; Echtay, K.S. Mitochondrial superoxide and aging: Uncoupling-protein activity and superoxide production. *Biochem. Soc. Symp.* **2004**, *71*, 203–213. [CrossRef]
44. Wonsey, D.R.; Zeller, K.I.; Dang, C.V. The c-Myc target gene PRDX3 is required for mitochondrial homeostasis and neoplastic transformation. *Proc. Natl. Acad. Sci. USA* **2002**, *99*, 6649–6654. [CrossRef]
45. Powers, S.K.; Jackson, M.J. Exercise-induced oxidative stress: Cellular mechanisms and impact on muscle force production. *Physiol. Rev.* **2008**, *88*, 1243–1276. [CrossRef] [PubMed]
46. Gruber, J.; Fong, S.; Chen, C.B.; Yoong, S.; Pastorin, G.; Schaffer, S.; Cheah, I.; Halliwell, B. Mitochondria-targeted antioxidants and metabolic modulators as pharmacological interventions to slow ageing. *Biotechnol. Adv.* **2013**, *31*, 563–592. [CrossRef]

47. Kerley, R.N.; McCarthy, C.; Kell, D.B.; Kenny, L.C. The potential therapeutic effects of ergothioneine in pre-eclampsia. *Free Radic. Biol. Med.* **2018**, *117*, 145–157. [CrossRef]
48. Rossi, R.; Bottinelli, R.; Sorrentino, V.; Reggiani, C. Response to caffeine and ryanodine receptor isoforms in mouse skeletal muscles. *Am. J. Physiol. Cell Physiol.* **2001**, *281*, C585–C594. [CrossRef]
49. Careccia, G.; Saclier, M.; Tirone, M.; Ruggieri, E.; Principi, E.; Raffaghello, L.; Torchio, S.; Recchia, D.; Canepari, M.; Gorzanelli, A.; et al. Rebalancing expression of HMGB1 redox isoforms to counteract muscular dystrophy. *Sci. Transl. Med.* **2021**, *13*, eaay8416. [CrossRef]
50. Mahmoodzadeh, S.; Koch, K.; Schriever, C.; Xu, J.; Steinecker, M.; Leber, J.; Dworatzek, E.; Purfürst, B.; Kunz, S.; Recchia, D.; et al. Age-related decline in murine heart and skeletal muscle performance is attenuated by reduced Ahnak1 expression. *J. Cachexia Sarcopenia Muscle* **2021**, *12*, 1249–1265. [CrossRef]
51. Halliwell, B.; Cheah, I.K.; Tang, R.M.Y. Ergothioneine—A diet-derived antioxidant with therapeutic potential. *FEBS Lett.* **2018**, *592*, 3357–3366. [CrossRef] [PubMed]
52. Borodina, I.; Kenny, L.C.; McCarthy, C.M.; Paramasivan, K.; Pretorius, E.; Roberts, T.J.; van der Hoek, S.A.; Kell, D.B. The biology of ergothioneine, an antioxidant nutraceutical. *Nutr. Res. Rev.* **2020**, *33*, 190–217. [CrossRef] [PubMed]
53. Roda, E.; Priori, E.C.; Ratto, D.; De Luca, F.; Di Iorio, C.; Angelone, P.; Locatelli, C.A.; Desiderio, A.; Goppa, L.; Savino, E.; et al. Neuroprotective Metabolites of. *Int. J. Mol. Sci.* **2021**, *22*, 6379. [CrossRef] [PubMed]
54. Perry, C.G.; Kane, D.A.; Lin, C.T.; Kozy, R.; Cathey, B.L.; Lark, D.S.; Kane, C.L.; Brophy, P.M.; Gavin, T.P.; Anderson, E.J.; et al. Inhibiting myosin-ATPase reveals a dynamic range of mitochondrial respiratory control in skeletal muscle. *Biochem. J.* **2011**, *437*, 215–222. [CrossRef]
55. Zuccarelli, L.; Baldassarre, G.; Magnesa, B.; Degano, C.; Comelli, M.; Gasparini, M.; Manferdelli, G.; Marzorati, M.; Mavelli, I.; Pilotto, A.; et al. Peripheral impairments of oxidative metabolism after a 10-day bed rest are upstream of mitochondrial respiration. *J. Physiol.* **2021**, *599*, 4813–4829. [CrossRef]
56. Makrecka-Kuka, M.; Krumschnabel, G.; Gnaiger, E. High-Resolution Respirometry for Simultaneous Measurement of Oxygen and Hydrogen Peroxide Fluxes in Permeabilized Cells, Tissue Homogenate and Isolated Mitochondria. *Biomolecules* **2015**, *5*, 1319–1338. [CrossRef]
57. Larsen, S.; Nielsen, J.; Hansen, C.N.; Nielsen, L.B.; Wibrand, F.; Stride, N.; Schroder, H.D.; Boushel, R.; Helge, J.W.; Dela, F.; et al. Biomarkers of mitochondrial content in skeletal muscle of healthy young human subjects. *J. Physiol.* **2012**, *590*, 3349–3360. [CrossRef]

# Results part II

The second aim of my Ph.D. thesis was to test the effect of ERGO on the SMNΔ7 mice model in vivo, in isolated diaphragm of 11 days old mice and on Neural Stem Cells (NSCs) in order to identify a supplement capable of improving the life quality in SMA patients.

## 1 Ex vivo Functional Analysis (TTP and TTR)

In the paper of Cadile and colleagues had been demonstrated a significant increase in fatigue resistance of isolated diaphragm from SMA mice following ERGO exposure.

During *ex vivo* functional experiments, the time to peak tension (TTP), and time to half relaxation (TTR) of the single twitch were also measured.

Both times were significantly increased in SMA in comparison with WT and after the exposition to ERGO returned to baseline levels (**Figure 17**).

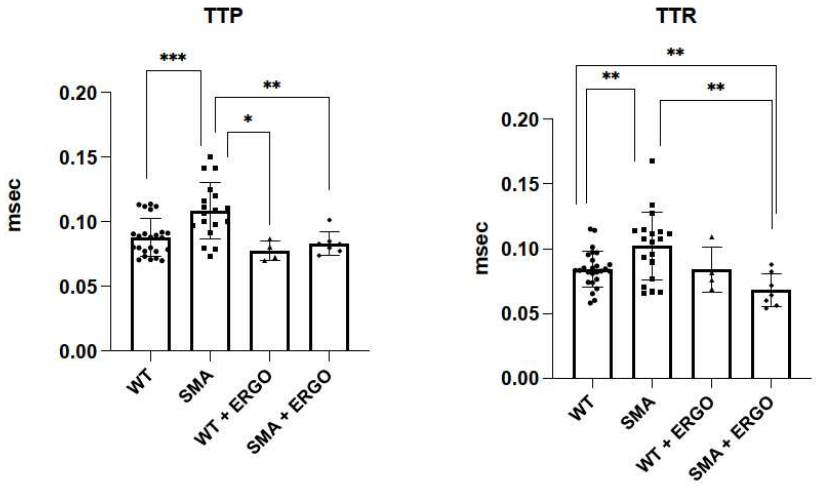


**Fig. 17** Mean values of twitch time to peak (TTP), twitch half relaxation time (TTR), determined in ex vivo functional analysis in the diaphragm muscles. TTP: (WT, n = 24 ; SMA, n = 18 ; WT + ERGO, n= 4 ;SMA + ERGO, n= 7). TTR: (WT, n = 26 ; SMA, n = 19 ; WT + ERGO, n= 4 ;SMA + ERGO, n= 7). * $p \leq 0.05$ ** $p \leq 0.01$, *** $p \leq 0.001$.

# 2 Survival and in Vivo Tests

Due to the encouraging preliminary results obtained through *ex-vivo* functional analysis, it was possible to formulate a rationale for testing the effect in vivo of ERGO administration on SMNΔ7 mice. ERGO supplementation was administered transplacentally to the fetus during the mother's pregnancy and feeding time.

## Kaplan-Meier Curve Survival

Kaplan-Meier survival curves were used to evaluate the survival of SMA +ERGO mice in comparison with SMA mice. The graph shows the number of days on the x-axis and the survival probability on the y-axis (**Figure 18**).

According to the literature, SMAΔ7 mice have an average lifespan of approximately 13 days (Le et al., 2005) and the treatment with ERGO was found able to extend their survival to up to 21 days. The difference in the overall survival was statistically significant (p=0.002) demonstrating the efficacy of treatment with ERGO in delaying the progression of debilitating symptoms of the disease and confirming the rationale for the treatment with antioxidants.

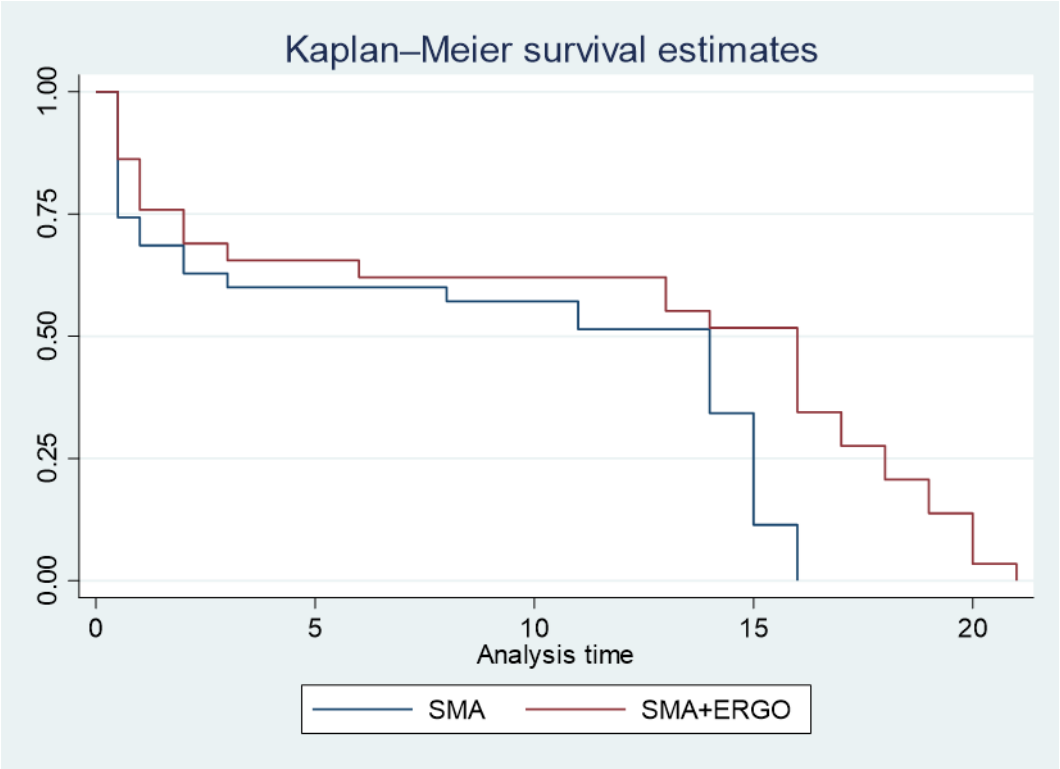


**Fig. 18 Kaplan Meier survival curve**. In blue SMA, n= 35; in red SMA + ERGO, n= 29.
The log-rank test was statistically significant (p=0.002).

## The Life's Quality Graph

In order to evaluate the overall quality of life of SMA + ERGO mice in comparison with SMA, we daily conducted *in vivo* measurements and tests from birth until day 11 of life.
The parameters considered were: the hind limb suspension test (**Figure 19**), weight and the presence of hair, the righting reflex, and the total distance in an open arena. It was immediately apparent that the SMA+ ERGO mice grew and developed much faster than the SMAs and were almost comparable to the WTs. The average difference in weight at 11 days was significant (SMA+ ERGO were 72,58% heavier than SMA). Among the parameters that were assessed daily, there was hair growth, which appeared at 7 days after birth in WT mice while SMA mice were hairless for almost all of the 11 days assessed.
Regarding motor performance, SMA + ERGO mice exhibited good motor skills, greater muscle strength, and fatigue resistance compared to the untreated mice.
These parameters were combined and represented as a single value named 'quality of life' (**Figure 20**). The total score can range from a minimum of 5 to a maximum of 18. WTs are in

the range from 15 to 18, SMA from 5 to 7, and SMA + ERGO from 8 to 17, and the differences among the groups were significant. The results showed that the SMA + ERGO mice had a better quality of life than the SMA mice.


**Fig. 19 The hindlimb suspension test** measures the capacity to develop force by the hind legs. SMA with an evident weakness (on the left) and SMA+ ERGO with normal posture (on the right).

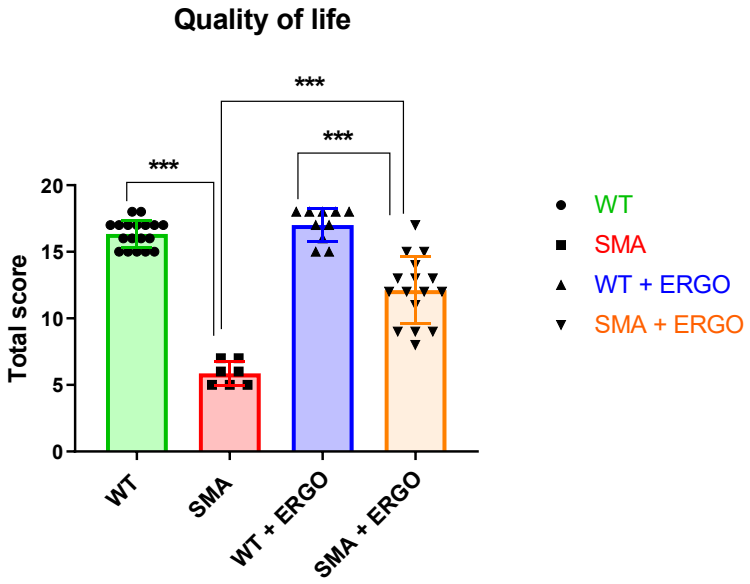


**Fig. 20 The life's quality graph** includes the in vivo parameters: weight, hindlimb suspension test, righting reflex, hair growth, and total distance in an open arena. (WT, n= 18; SMA, n= 7; WT + ERGO, n= 9; SMA + ERGO, n= 16). Bars represent means ± SD. Individual data are represented as scatter plots. $p \leq 0{,}01$ ***

# 3 WB analysis on the isolated diaphragm

Molecular analysis performed by WB experiment was repeated on the isolated diaphragms of SMNΔ7 mice 11 days old belonging to the 4 groups (SMA, WT, SMA + ERGO, WT+ ERGO). It is known the influence of calcium handling on fatigue, so the action of ERGO on the sarcoplasmic reticulum (SR) Ca2+ ATPase (SERCA1 and 2) pumps expression was assessed. The results indicate a restoration of the protein expression in SMA + ERGO compared to SMA (**Figure 21**) confirming the possibility of counteracting the isolated diaphragm fatigue by ERGO exposure.

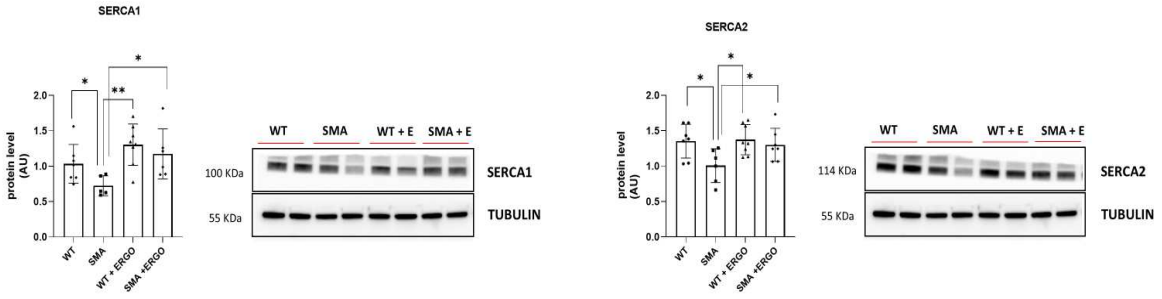


**Fig. 21** Western blot analysis of protein expression (WT, n = 7; SMA, n = 5; WT+ ERGO, n= 8; SMA+ ERGO, n= 6) of sarcoplasmic reticulum Ca2+ ATPase pumps (SERCA1) (WT, n = 7; SMA, n = 5; WT+ ERGO, n= 8; SMA+ ERGO, n= 6) and SERCA2 (WT, n = 7; SMA, n = 6; WT+ ERGO, n= 8; SMA+ ERGO, n= 7). The level of the protein target was normalized against the level of the housekeeping tubulin measured in the same blot. Representative Western blots are shown. Bars represent means± SD. Individual data are represented as scatter plots. * $p \leq 0.05$ ** $p \leq 0.01$

## 3.1 Energy Imbalance and Oxidative Metabolism

Unexpectedly, the energy imbalance observed in SMA seems to be maintained in SMA + ERGO. Specifically, ERGO seems to not affect the energy sensor AMPK and the mitochondrial biogenesis regulator PGC1α (**Figure 22 A, B**).

On the contrary, the mitochondrial mass which was increased in SMA (TOM-20 and PRDX3) was significantly normalized in SMA+ERGO, (**Figure 22 C, D**).

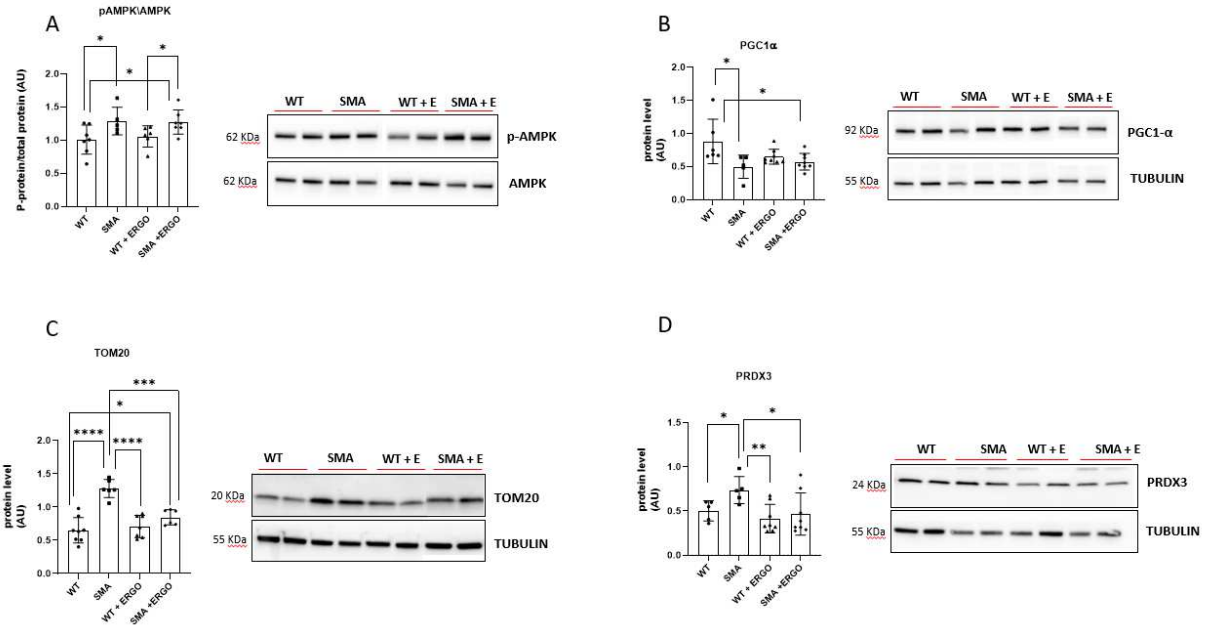


**Fig. 22 Effect of ERGO on energy balance**. (A) Mean values of the ratio between the content in the phosphorylated (p) and total forms for AMPK determined by Western blots (WT, n = 7; SMA, n = 5; WT+ ERGO, n= 6; SMA+ ERGO, n= 7). (B) Protein expression of PGC1α (WT, n =; 6 SMA, n = 5; WT+ ERGO, n= 8; SMA+ ERGO, n= 8) and (C) mitochondrial import receptor subunit TOM-20 (WT, n = 8; SMA, n = 6 ; WT+ ERGO, n= 7; SMA+ ERGO, n= 6) and (D) Piroxiredoxin 3 (PRDX3) (WT, n = 5; SMA, n = 5 ; WT+ ERGO, n= 8; SMA+ ERGO, n= 8), determined by Western blots. The level of each protein target was normalized against the level of the housekeeping tubulin measured in the same blot. Representative Western blots are shown. Bars represent means ± SD. Individual data are represented as scatter plots. * $p \leq 0.05$, ** $p \leq 0.01$, *** $p \leq 0.001$

The expression of specific proteins involved in mitochondrial dynamics was assessed. No significant difference following ERGO treatment was found (**Figure 23**).

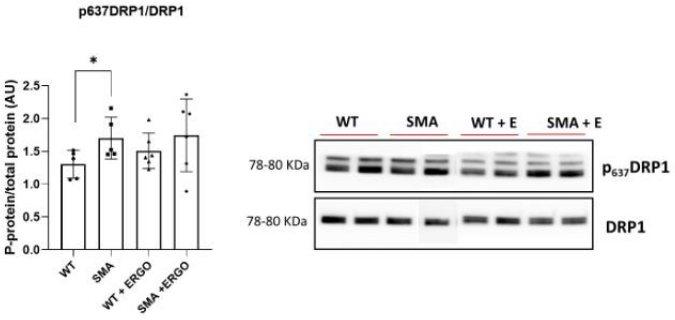


**Fig. 23 Effect of ERGO on mitochondrial dynamics.** Phosphorylation of serine 637 of DPR1 (WT, n = 5; SMA, n = 5; WT+ ERGO, n= 6; SMA+ ERGO, n= 6). Mean values of the ratio between the content in the phosphorylated ($p_{637}$) and total forms for DRP1 determined by Western blots. Bars represent means ± SD. Individual data are represented as scatter plots. * $p \leq 0.05$

## 3.2 Autophagy and Mitophagy

The significant induction in SMA of the active form LC3BII, along with the decrease in p62 expression, suggested the activation of the autophagy. Treatment with ERGO seems to maintain the autophagic activation (**Figure 24 A, B**). However, contrary to what happens in SMAs, the protein expression of Parkin is increased suggesting the activation of the mitophagy process (**Figure 24C**).

Based on this result and according to the reduction in mitochondria mass (TOM20 and PRDX3) it could suggest that the degradation of non-functional mitochondria by the mitophagy process occurs.

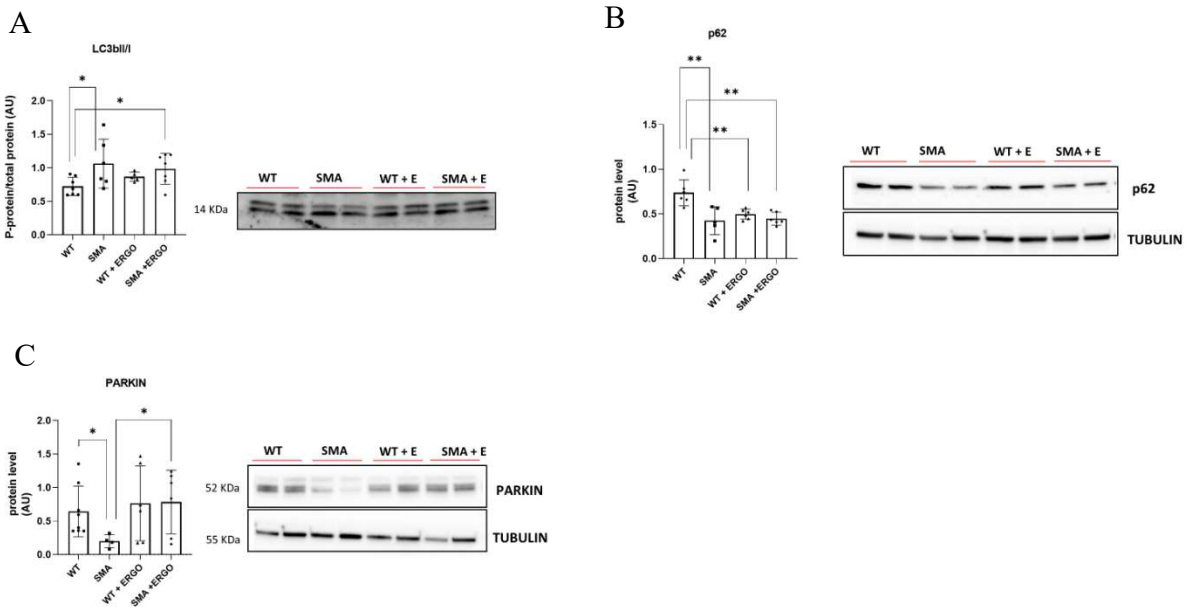


**Fig. 24 Effect of ERGO on Autophagy and Mitophagy** (A) The ratio between the active form and the inactive form of LC3B (LC3BII/LC3BI) (WT, n = 7; SMA, n = 6; WT+ ERGO, n= 5; SMA+ ERGO, n= 7), ) and (B) protein levels of p62 (WT, n = 6; SMA, n = 5; WT+ ERGO, n= 6; SMA+ ERGO, n= 6), determined by Western blots. (C) Protein levels of mitophagy maker PARKIN (WT, n = 8; SMA, n = 4; WT+ ERGO, n= 6; SMA+ ERGO, n= 6), determined by Western blots. The level of the protein target was normalized against the level of the housekeeping tubulin measured in the same blot. Representative Western blots are shown. Bars represent means ± SD. Individual data are represented as scatter plots. * $p \leq 0.05$ ** $p \leq 0.01$.

## 3.3 Redox imbalance

Oxyblot analysis showed a higher level of carbonylated protein in SMA compared to WT due to ROS accumulation since the main antioxidant systems (SOD1, Catalase) were not activated. ERGO administration seems to eliminate only partially the carbonylated proteins so that in comparison with SMAs no significant difference was found (**Figure 25A**)
but, even if ERGO did not affect the activation of SOD1 and catalase, it did significantly stimulate the activation of the GPX antioxidant system (**Figure 25D**).

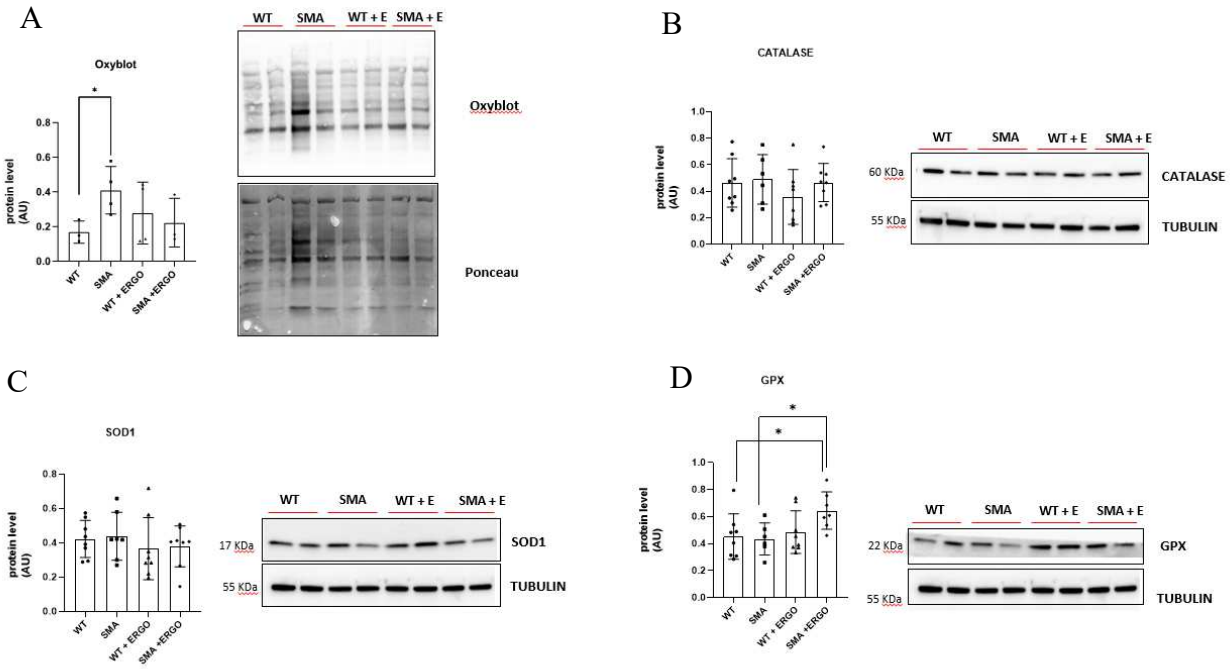


**Fig. 25 Effect of ERGO on redox imbalance** (A) Protein levels of carbonylated proteins revealed by Oxyblot analysis (WT, n = 6; SMA, n = 5; WT+ ERGO, n= 4; SMA+ ERGO, n= 3). Protein levels of (C) SOD1 (WT, n = 8; SMA, n = 7; WT+ ERGO, n= 8; SMA+ ERGO, n= 8), (B) Catalase (WT, n = 8; SMA, n = 6; WT+ ERGO, n= 8; SMA+ ERGO, n= 8), (D) GPX (WT, n = 8; SMA, n = 6; WT+ ERGO, n= 8; SMA+ ERGO, n= 7) determined by Western blots. The level of the protein target was normalized against the level of the housekeeping tubulin measured in the same blot. Representative Western blots are shown. Bars represent means ± SD. Individual data are represented as scatter plots. * $p \leq 0.05$ ** $p \leq 0.01$.

# 4 Electron Microscopy analysis of isolated diaphragm

Through collaboration with Prof. Boncompagni, we were able to study the morphology of the diaphragm's mitochondria through electron microscopy (EM) analysis.

Preliminary qualitative investigations on SMA diaphragms show the presence of mitochondria of variable shape often clustered in shorter columns scattered within the fiber interior (**Figures 26A, B, C and 27A, B**) and the lack of "triadic" mitochondria, i.e., mitochondria coupled to the Ca2+ Release Units (CRUs) or triads (**Figure 26E, F, G**),

supporting their misplaced and uneven distribution (Boncompagni et al., 2009). The proper "triadic" association is essential for the bi-directional cross-talk between the two organelles, as the $Ca^{2+}$ released from SR during EC coupling enters into the mitochondrial matrix, stimulating ATP production (Rossi et al., 2009 and 2011).

In SMA+ERGO mice frequency and distribution of mitochondria appear very similar to that described for WT mice: both roundly shaped and elongated mitochondria clustered to form longitudinal long rows that are quite evenly distributed between myofibrils (**Figure 26D**). Mitochondria coupled to CRUs are also present (**Figure 26H**).

To support the visual observation, the frequency and the size of mitochondria in WT, SMA, and SMA+ERGO mice were quantified. The number and the size of mitochondria are significantly decreased in the SMA diaphragm compared to WT and increase significantly in treated mice (**Table 12**).

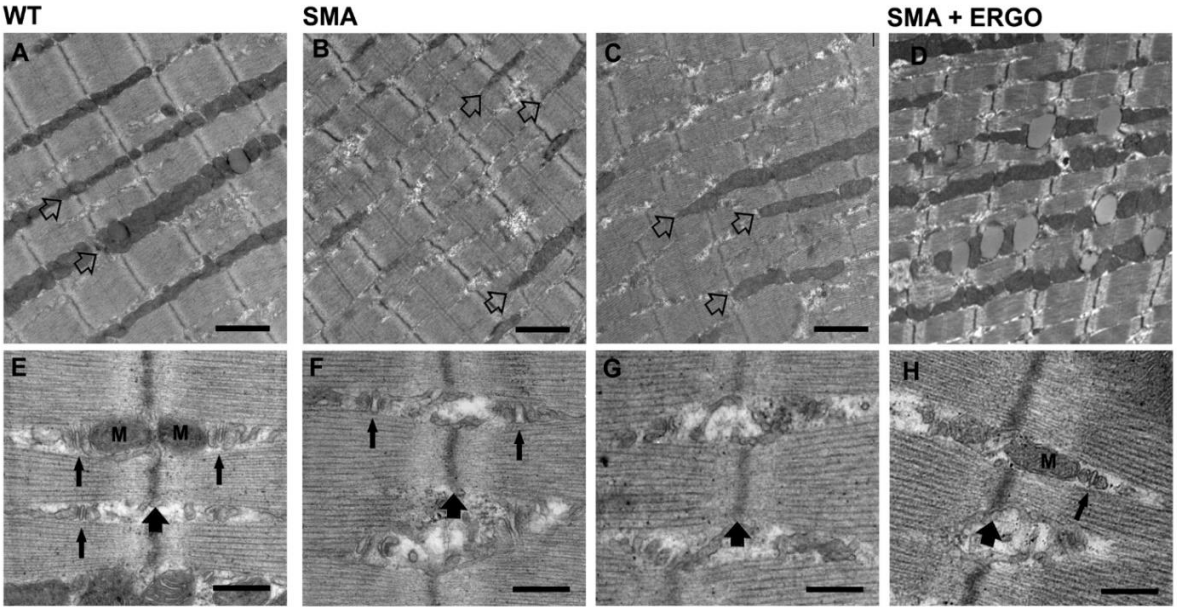


**Fig. 26 Mitochondria and CRUs distribution in muscle fibers from mice of the diaphragm at 11 days of age.** Representative EM images from WT (A and D) SMA (B and F) and SMA+ERGO (D and H) mice. *Labeling:* large empty arrows point to rows of mitochondria columns; small black arrows point to CRUs; large black arrows point to Z-line; M is for mitochondria. *Scale bars: A, B, C, and D: 2 µm; D, E, F, and H: 0.5 µm.*

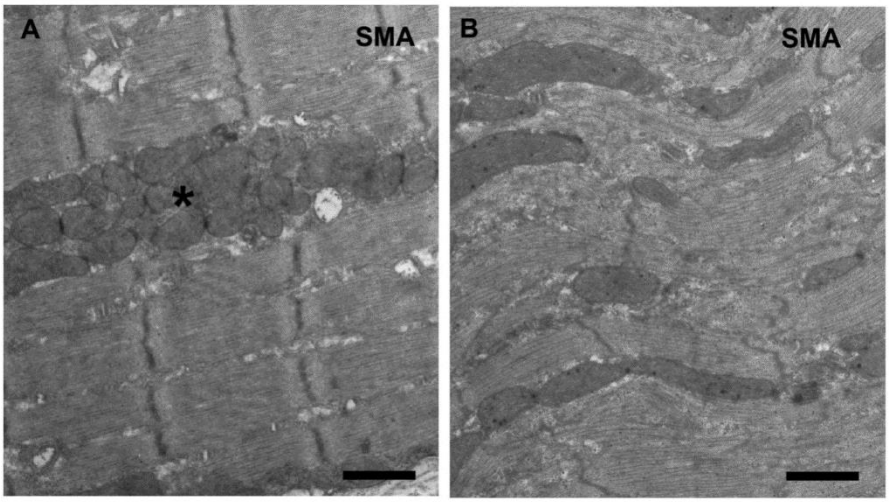


**Fig. 27 Additional ultrastructural observations of diaphragm fibers from mice at 11 days of age from SMA.** Representative EM images from SMA fibers show a large cluster of mitochondria (A, asterisk) and a completely degenerated fiber (B). Scale bars: A and B: 1 mm.

| | No. of Mitochondria /100 µm² | Average Mitochondria Size (µm²) |
|---|---|---|
| **WT** | 55.57 ± 13.1 | 0.5 ± 0.04 |
| **SMA** | 20.68 ± 4.0* | 0.6 ± 0.04 |
| **SMA + ERGO** | 41.57 ± 2.7‡ | 0.5 ± 0.04 |

**Table 12 Frequency and the size of mitochondria in diaphragm fibers from mice at 11 days of age.** Data are shown as mean ± SEM. *p<0.02 (SMA vs WT); ǂp<0.009 (SMA+ERGO vs SMA). Sample size: 24 fibers from 1 WT mice, 24 fibers from 1 SMA mice; 10 fibers from 1 SMA+ ERGO mice; 2 micrographs/fiber.

# 5 Neural Stem Cells Analysis

In collaboration with Dr. Bottai, molecular and cellular analyses on NSCs prepared from the subventricular zone of the brain of WT and SMA mice were performed. A significant difference in NSCs proliferation and self-renewal has been observed (**Figures 28 and 29**).

The effect of different concentrations of ERGO on NSCs proliferation was tested on NSCs from WT mice. The number of cells was measured at ERGO concentrations of 2.5, 5, 10, 20, 50, 100, and 200μM. At concentrations of 10 and 20μM, there was a significant increase in the proliferation capability of the NSCs, almost double that of the control group. At higher concentrations of 50, 100, and 200μM, ERGO treatment exhibited an inhibitory effect (**Figure 30**).

The 10μM concentration was used to conduct an MTT assay before and after ERGO treatment. The relative change in NSCs metabolic activity was compared between WT NSCs treated with ERGO and the WT NSCs control, as well as between the SMA NSCs treated with ERGO and the SMA NSCs control. The results indicate that ERGO is able to increase the metabolic activity of SMA NSCs more than WT NSCs (**Figure 31**).

Other experiments are to be performed to demonstrate the positive effect of ERGO on NSCs.

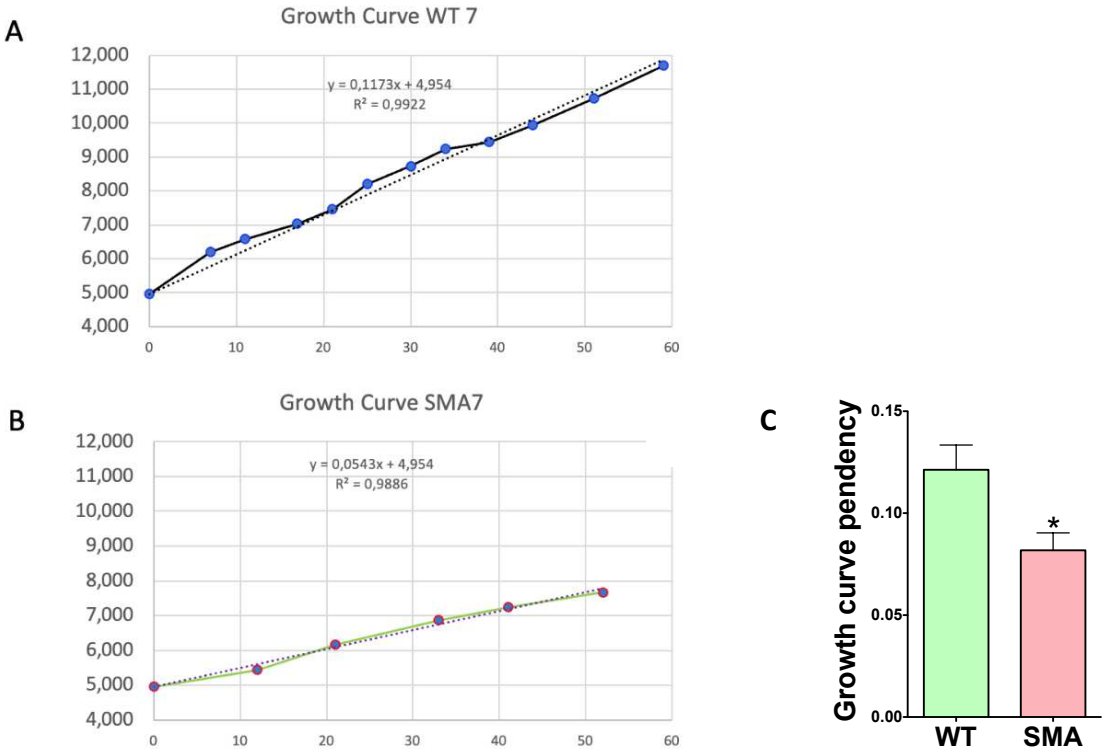


**Fig. 28 Impaired proliferation of SMA NSC cells.** NSCs from WT and SMA animals obtained from the subventricular zone (SVZ) proliferate exponentially. A and B are representative growth curves of WT and SMA NSCs. C The pendency of the growth curves is significantly lower in NSCs from SMA animals * $p<0.05$. N = 5 for each group.

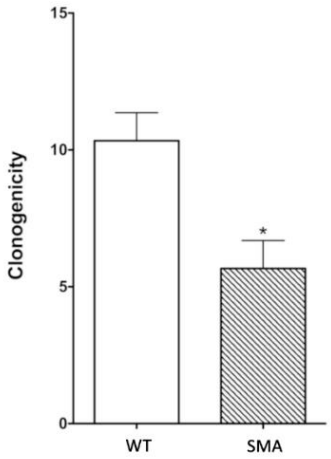


**Fig. 29 The clonogenicity of NSCs is decreased in SMA**. White: WT, green: SMA, * $p<0.05$; n =6 for each group.

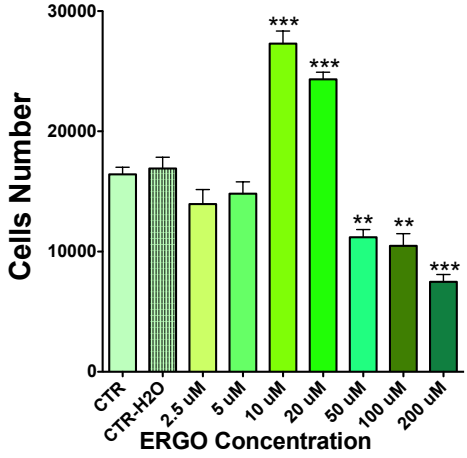


**Fig. 30 10 µM is the concentration of ERGO that allows the higher increase of NSCs proliferation.** Effect of different concentrations of Ergo on NSCs from WT animals. CRTs are untreated cells. CTR+$H_2O$ are the cells treated with vehicles. We ranged the concentration between 0 to 200 µM. At concentrations higher than 50 µM, we have found a significant decrease in the proliferation. ** $p<0.01$; ***$p< 0{,}001$

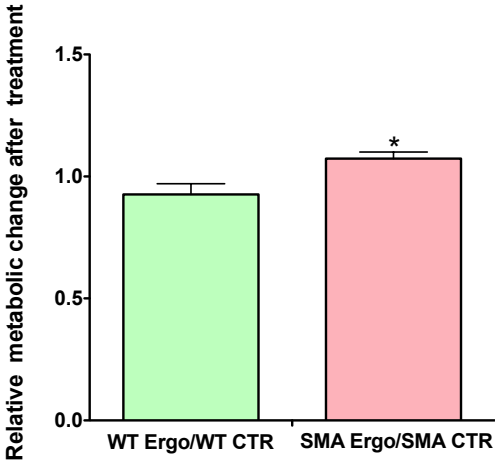


**Fig. 31 MTT assay.** ERGO is able to increase the metabolic activity of SMA NSC cells. Metabolic activity was compared before and after Ergo treatment in an MTT Assay. * $p<0.05$

# Discussion part II

## 1 Effect of ERGO administration

In the paper of Cadile and colleagues, a significant increase in fatigue resistance of isolated diaphragm from SMA mice following ERGO exposure was found. ERGO is a very potent natural antioxidant molecule that acts as a powerful scavenger of mitochondria-derived superoxide species and a protector of cell constituents from damage by ROS (Cheah et al., 2017). It is important to note that the time of exposure to ERGO was only 30 minutes. In this short time, it was impossible for ERGO to eliminate oxidized proteins present in the sample. ERGO is a histidine derivative that contains an imidazole ring. Its imidazole ring is suitable to function as a pH buffer (Holecek et al., 2020). In fact, histidine compounds such as carnosine, act as powerful buffers and attenuate changes in intracellular pH in muscles during anaerobic exercise (Abe et al., 2000). Based on this information, it is possible to assume that, within the organic bath, ERGO was able to bind $H^+$ ions derived from lactic acid that has accumulated following repeated high-frequency contractions. The accumulation of lactic acid in muscle has historically been suggested to be the major cause of muscle fatigue (Fitts et al., 1994).

Beyond that, ERGO, even if was not able to eliminate all the carbonylated proteins that have already been irreversibly modified, could protect the diaphragm's proteins from further oxidation by stimulating mitochondria function to reduce ROS formation and provide an adequate ATP amount in order to delay the onset of fatigue.

The availability of an adequate amount of ATP for SERCA pumps could also explain the reduction in both time-to-peak tension and time-to-half relaxation of a single twitch in SMA +ERGO (**Figure 17**). Moreover, the western blots experiments on the diaphragm of SMA +

ERGO indicate a restoration of SERCA pump protein expression (SERCA 1 and SERCA 2) compared to SMA (**Figure 21**).

So the alteration in contractile properties of isolated SMA diaphragm seems to be counteracted by ERGO and it could contribute to prolonging the onset time of respiratory failure in mice.

Based on the results obtained in an isolated diaphragm we wanted to test the effect of dietary supplementation with ERGO in SMA mice to assess its capacity to improve their life quality and possibly increase their lifespan. ERGO administrated at a dose of 20 μg/day to pregnant/mothers in drinking water during pregnancy and feeding time, was found to have a very powerful effect in vivo. ERGO was able to increase the pup's growth, motor performance, and in general life quality (**Figure 20)**. Very importantly, mice treated with ERGO managed to survive an average of 7 days longer (**Figure 18**).

Assuming that the in vivo ERGO effect was related to an antioxidant effect on the diaphragm muscle which in the absence of ROS is able to resist fatigue, improve the respiratory function of mice, and consequently increase their survival, the diaphragm of SMA +ERGO mice was analyzed at molecular level. At first, the effect of ERGO on energy imbalance was investigated. Surprisingly results showed that, despite ERGO administration, the energetic defect in SMA diaphragm persisted (**Figure 22A**). It could lead, in the long run, to respiratory failure.

The expression of mitochondrial import receptor subunit TOM-20 and the mitochondrial antioxidant protein PRDX3 (**Figure 22C, D**) were significantly decreased in SMA +ERGO in comparison with SMA mice even if the expression of TOM20 was still significantly higher than WT. As the low expression of PGC1α did not play in favor of an ERGO stimulation of mitochondria biogenesis (**Figure 22B**), the still high amount of mitochondrial proteins combined with the presence of an energy deficit suggests that some dysfunctional mitochondria could be still present.

Notwithstanding the presence of dysfunctional mitochondria was assumed, in SMA +ERGO a significant increase in Parkin protein expression was found, suggesting the stimulation of the mitophagic process by ERGO (**Figure 24C**). In addition, the autophagy process seems to remain activated as indicated by the maintenance of a significant increase in the protein level of LC3BII and a decrease in p62 protein expression (**Figure 24A, B**).

The EM analysis of the diaphragm of SMA +ERGO mice was a crucial step in supporting the results obtained at the molecular level. In SMA + ERGO diaphragm the shape, size, and

distribution of mitochondria appear very similar to WTs, and mitochondria coupled to CRUs are again present (**Figure 26 D, H**).

ERGO was found to increase GPX enzyme expression, with no impact on other antioxidant enzymes such as SOD1 and catalase (**Figure 25 B, C, D**) The main biological role of GPX is to protect the organism from oxidative damage. It is able to scavenge free radicals, aid in the prevention of lipid peroxidation, and in the maintenance of intracellular homeostasis and redox balance (Lubos et al., 2011).

This result led to the assumption of the elimination of ROS in the SMA diaphragm by ERGO but the Oxyblot analysis showed only a decreasing trend in carbonylated proteins amounts in SMA+ ERGO mice (**Figure 25A)**. It must be noted that a small number of samples were analyzed.

On the basis of the obtained results, it is not possible to say that in vivo ERGO effect can be only due to the antioxidant action on the diaphragm but other targets must be considered. SMA is primarily a neuromuscular disease and it is known that altered ROS levels and oxidative stress are present in SMA neural cells (Acsadi et al., 2009; Miller et al., 2016; Ando et al., 2020; James et al., 2021, Katsetos et al., 2013). Thanks to Dr. Bottai's collaboration, we were able to analyze NSCs from the subventricular zone of SMNΔ7 mice's brains. Preliminary results indicated a significant difference in NSCs proliferation and self-renewal capacity between SMA and WT (**Figure 28 and 29**). The presence of oxidative stress could be the reason for the lower growth curve of the NSCs in SMA (Hwang et al., 2021). Regarding the effect of ERGO, it has been observed that it could increase the metabolic activity of SMA NSCs, as determined by MTT assay, at a concentration of 10 μM (**Figure 31**). The same dose allowed a higher increase in NSCs proliferation and for this reason, has been chosen to perform future experiments (**Figure 30**). Although these are preliminary results, they are very encouraging and suggest that the observed in vivo effect of ERGO may not only be due to peripheral action but also achieved through concomitant action at a central level.

# Conclusions

The results obtained in the present study give the first evidence of an intrinsic energetic imbalance and significant accumulation of reactive oxygen species (ROS) that are not scavenged by the antioxidant enzyme pool in the diaphragm of SMNΔ7 mice. Both conditions can contribute to muscle fatigue, which can lead to diaphragm wasting and respiratory failure.

The significant increase in fatigue resistance of isolated diaphragm from SMA mice following ERGO (a very potent antioxidant molecule) exposure, supported the rationale to test the effect of dietary supplementation with ERGO in SMA mice in order to improve their life quality and increase their lifespan. In vivo tests demonstrated that ERGO treatment significantly enhanced the quality of life of SMA mice and extended their lifespan.
At the molecular level it has been observed that ERGO has the ability to stimulate mitophagy and increase the expression of the antioxidant GPX. It could result in a partial elimination of non-functional mitochondria and a reduction of oxidative stress in the diaphragm of SMNΔ7 mice. Supporting this hypothesis, electron microscopy showed an improvement in the morphology of the mitochondria in the treated mice, which are almost indistinguishable from the controls.

In conclusion, ERGO had positive effects on the SMNΔ7 mice, particularly evident in vivo. The antioxidant action of ERGO could partially counteract the redox imbalance in the SMA dipahragm but the improvement of motor skills and the increase in survival must be the result of an overall effect on multiple physiological systems. It can be hypothesized that the antioxidant action of ERGO takes place also in the locomotor muscles and at the central level. Preliminary analyses conducted on NSCs from the subventricular zone of the brain showed an increase in proliferation and an increase the metabolic activity in the treated mice compared to controls.
These results are very encouraging but much work needs to be done and the actions of ERGO should be further investigated.

To summarise, it has been demonstrated that ERGO is able to restore crucial alterations in SMA mice. Translating this information to the human level, ERGO could be effective in improving the quality of life in all SMA patients even if it cannot be the substitute for the newly available drugs. It could be also very useful in patients who do not respond to the therapies. Moreover, ERGO can be administered also during gestation (this cannot be done with the other approved drugs) so it could help to increase the window for the treatment.
The results of this research could open the possibility of a novel potential adjuvant to alleviate the symptoms of this serious neuromuscular disease.

# References


- Aartsma-Rus A. FDA Approval of Nusinersen for Spinal Muscular Atrophy Makes 2016 the Year of Splice Modulating Oligonucleotides. Nucleic Acid Ther. 2017 Apr;27(2):67-69. doi: 10.1089/nat.2017.0665. Epub 2017 Feb 21. PMID: 28346110.
- Abe H. Role of histidine-related compounds as intracellular proton buffering constituents in vertebrate muscle. Biochemistry (Mosc). 2000 Jul;65(7):757-65. PMID: 10951092.
- Acsadi G, Lee I, Li X, Khaidakov M, Pecinova A, Parker GC, Hüttemann M. Mitochondrial dysfunction in a neural cell model of spinal muscular atrophy. J Neurosci Res. 2009 Sep;87(12):2748-56. doi: 10.1002/jnr.22106. PMID: 19437551.
- Adami R, Pagano J, Colombo M, Platonova N, Recchia D, Chiaramonte R, Bottinelli R, Canepari M, Bottai D. Reduction of Movement in Neurological Diseases: Effects on Neural Stem Cells Characteristics. Front Neurosci. 2018 May 23;12:336. doi: 10.3389/fnins.2018.00336. PMID: 29875623; PMCID: PMC5974544.
- Ahmadian-Moghadam H, Sadat-Shirazi MS, Zarrindast MR. Therapeutic potential of stem cells for treatment of neurodegenerative diseases. Biotechnol Lett. 2020 Jul;42(7):1073-1101. doi: 10.1007/s10529-020-02886-1. Epub 2020 Apr 27. PMID: 32342435.
- Ames BN. Prolonging healthy aging: Longevity vitamins and proteins. Proc Natl Acad Sci U S A. 2018 Oct 23;115(43):10836-10844. doi: 10.1073/pnas.1809045115. Epub 2018 Oct 15. PMID: 30322941; PMCID: PMC6205492.
- Ando S, Osanai D, Takahashi K, Nakamura S, Shimazawa M, Hara H. Survival motor neuron protein regulates oxidative stress and inflammatory response in microglia of the spinal cord in spinal muscular atrophy. J Pharmacol Sci. 2020 Dec;144(4):204-211. doi: 10.1016/j.jphs.2020.09.001. Epub 2020 Sep 10. PMID: 33070839.
- Arnold AS, Gueye M, Guettier-Sigrist S, Courdier-Fruh I, Coupin G, Poindron P, Gies JP. Reduced expression of nicotinic AChRs in myotubes from spinal muscular atrophy I patients. Lab Invest. 2004 Oct;84(10):1271-8. doi: 10.1038/labinvest.3700163. PMID: 15322565.
- Axente M, Shelby ES, Mirea A, Sporea C, Badina M, Padure L, Ion DA. Clinical features and genetics in non-5q spinal muscular atrophy caused by acid ceramidase deficiency. J Med Life. 2021 May-Jun;14(3):424-428. doi: 10.25122/jml-2021-0147. PMID: 34377212; PMCID: PMC8321613.
- Bagli E, Zikou AK, Agnantis N, Kitsos G. Mitochondrial Membrane Dynamics and Inherited Optic Neuropathies. In Vivo. 2017 Jul-Aug;31(4):511-525. doi: 10.21873/invivo.11090. PMID: 28652416; PMCID: PMC5566899.
- Barrett D, Bilic S, Chyung Y, Cote SM, Iarrobino R, Kacena K, Kalra A, Long K, Nomikos G, Place A, Still JG, Vrishabhendra L. A Randomized Phase 1 Safety, Pharmacokinetic and Pharmacodynamic Study of the Novel Myostatin Inhibitor Apitegromab (SRK-015): A Potential Treatment for Spinal Muscular Atrophy. Adv Ther.

2021 Jun;38(6):3203-3222. doi: 10.1007/s12325-021-01757-z. Epub 2021 May 8. PMID: 33963971; PMCID: PMC8189951.

- Bennett CF, Krainer AR, Cleveland DW. Antisense Oligonucleotide Therapies for Neurodegenerative Diseases. Annu Rev Neurosci. 2019 Jul 8;42:385-406. doi: 10.1146/annurev-neuro-070918-050501. PMID: 31283897; PMCID: PMC7427431.
- Bianchi L, Sframeli M, Vantaggiato L, Vita GL, Ciranni A, Polito F, Oteri R, Gitto E, Di Giuseppe F, Angelucci S, Versaci A, Messina S, Vita G, Bini L, Aguennouz M. Nusinersen Modulates Proteomics Profiles of Cerebrospinal Fluid in Spinal Muscular Atrophy Type 1 Patients. Int J Mol Sci. 2021 Apr 21;22(9):4329. doi: 10.3390/ijms22094329. PMID: 33919289; PMCID: PMC8122268.
- Blair HA. Onasemnogene Abeparvovec: A Review in Spinal Muscular Atrophy. CNS Drugs. 2022 Sep;36(9):995-1005. doi: 10.1007/s40263-022-00941-1. Epub 2022 Aug 12. PMID: 35960489.
- Boido M, Vercelli A. Neuromuscular Junctions as Key Contributors and Therapeutic Targets in Spinal Muscular Atrophy. Front Neuroanat. 2016 Feb 3;10:6. doi: 10.3389/fnana.2016.00006. PMID: 26869891; PMCID: PMC4737916.
- Boncompagni S, Rossi AE, Micaroni M, Beznoussenko GV, Polishchuk RS, Dirksen RT, Protasi F. Mitochondria are linked to calcium stores in striated muscle by developmentally regulated tethering structures. Mol Biol Cell. 2009 Feb;20(3):1058-67. doi: 10.1091/mbc.e08-07-0783. Epub 2008 Nov 26. PMID: 19037102; PMCID: PMC2633377.
- Bordet T, Berna P, Abitbol JL, Pruss RM. Olesoxime (TRO19622): A Novel Mitochondrial-Targeted Neuroprotective Compound. Pharmaceuticals (Basel). 2010 Jan 28;3(2):345-368. doi: 10.3390/ph3020345. PMID: 27713255; PMCID: PMC4033913.
- Bottai D, Adami R. Spinal muscular atrophy: new findings for an old pathology. Brain Pathol. 2013 Nov;23(6):613-22. doi: 10.1111/bpa.12071. Epub 2013 Jun 28. PMID: 23750936; PMCID: PMC8029454.
- Bottai D, Fiocco R, Gelain F, Defilippis L, Galli R, Gritti A, Vescovi LA. Neural stem cells in the adult nervous system. J Hematother Stem Cell Res. 2003 Dec;12(6):655-70. doi: 10.1089/15258160360732687. PMID: 14977475.
- Bottai D, Madaschi L, Di Giulio AM, Gorio A. Viability-dependent promoting action of adult neural precursors in spinal cord injury. Mol Med. 2008 Sep-Oct;14(9-10):634-44. doi: 10.2119/2008-00077.Bottai. PMID: 18654659; PMCID: PMC2480612.
- Bowerman M, Murray LM, Boyer JG, Anderson CL, Kothary R. Fasudil improves survival and promotes skeletal muscle development in a mouse model of spinal muscular atrophy. BMC Med. 2012 Mar 7;10:24. doi: 10.1186/1741-7015-10-24. PMID: 22397316; PMCID: PMC3310724.
- Brandalise F, Cesaroni V, Gregori A, Repetti M, Romano C, Orrù G, Botta L, Girometta C, Guglielminetti ML, Savino E, Rossi P. Dietary Supplementation of *Hericium erinaceus* Increases Mossy Fiber-CA3 Hippocampal Neurotransmission and Recognition Memory in Wild-Type Mice. Evid Based Complement Alternat Med. 2017;2017:3864340. doi: 10.1155/2017/3864340. Epub 2017 Jan 1. PMID: 28115973; PMCID: PMC5237458.
- Braun S, Croizat B, Lagrange MC, Warter JM, Poindron P. Constitutive muscular abnormalities in culture in spinal muscular atrophy. Lancet. 1995 Mar 18;345(8951):694-5. doi: 10.1016/s0140-6736(95)90869-2. Erratum in: Lancet 1995 Apr 22;345(8956):1060. PMID: 7741893.

- Brzustowicz LM, Lehner T, Castilla LH, Penchaszadeh GK, Wilhelmsen KC, Daniels R, Davies KE, Leppert M, Ziter F, Wood D, et al. Genetic mapping of chronic childhood-onset spinal muscular atrophy to chromosome 5q11.2-13.3. Nature. 1990 Apr 5;344(6266):540-1. doi: 10.1038/344540a0. PMID: 2320125.
- Burghes AH, Beattie CE. Spinal muscular atrophy: why do low levels of survival motor neuron protein make motor neurons sick? Nat Rev Neurosci. 2009 Aug;10(8):597-609. doi: 10.1038/nrn2670. Epub 2009 Jul 8. PMID: 19584893; PMCID: PMC2853768.
- Burr P, Reddivari AKR. Spinal Muscle Atrophy. 2023 Jul 17. In: StatPearls [Internet]. Treasure Island (FL): StatPearls Publishing; 2023 Jan–. PMID: 32809522.
- Butchbach ME, Edwards JD, Burghes AH. Abnormal motor phenotype in the SMNDelta7 mouse model of spinal muscular atrophy. Neurobiol Dis. 2007 Aug;27(2):207-19. doi: 10.1016/j.nbd.2007.04.009. Epub 2007 May 5. PMID: 17561409; PMCID: PMC2700002.
- Cadile F, Recchia D, Ansaldo M, Rossi P, Rastelli G, Boncompagni S, Brocca L, Pellegrino MA, Canepari M. Diaphragm Fatigue in SMNΔ7 Mice and Its Molecular Determinants: An Underestimated Issue. Int J Mol Sci. 2023 Oct 6;24(19):14953. doi: 10.3390/ijms241914953. PMID: 37834400; PMCID: PMC10574014.
- Careccia G, Saclier M, Tirone M, Ruggieri E, Principi E, Raffaghello L, Torchio S, Recchia D, Canepari M, Gorzanelli A, Ferrara M, Castellani P, Rubartelli A, Rovere-Querini P, Casalgrandi M, Preti A, Lorenzetti I, Bruno C, Bottinelli R, Brunelli S, Previtali SC, Bianchi ME, Messina G, Vénéreau E. Rebalancing expression of HMGB1 redox isoforms to counteract muscular dystrophy. Sci Transl Med. 2021 Jun 2;13(596):eaay8416. doi: 10.1126/scitranslmed.aay8416. PMID: 34078746.
- Chaytow H, Faller KME, Huang YT, Gillingwater TH. Spinal muscular atrophy: From approved therapies to future therapeutic targets for personalized medicine. Cell Rep Med. 2021 Jul 21;2(7):100346. doi: 10.1016/j.xcrm.2021.100346. PMID: 34337562; PMCID: PMC8324491.
- Chaytow H, Huang YT, Gillingwater TH, Faller KME. The role of survival motor neuron protein (SMN) in protein homeostasis. Cell Mol Life Sci. 2018 Nov;75(21):3877-3894. doi: 10.1007/s00018-018-2849-1. Epub 2018 Jun 5. PMID: 29872871; PMCID: PMC6182345.
- Cheah IK, Halliwell B. Ergothioneine, recent developments. Redox Biol. 2021 Jun;42:101868. doi: 10.1016/j.redox.2021.101868. Epub 2021 Jan 26. PMID: 33558182; PMCID: PMC8113028.
- Cheah IK, Tang RM, Yew TS, Lim KH, Halliwell B. Administration of Pure Ergothioneine to Healthy Human Subjects: Uptake, Metabolism, and Effects on Biomarkers of Oxidative Damage and Inflammation. Antioxid Redox Signal. 2017 Feb 10;26(5):193-206. doi: 10.1089/ars.2016.6778. Epub 2016 Sep 7. PMID: 27488221.
- Chemello F, Pozzobon M, Tsansizi LI, Varanita T, Quintana-Cabrera R, Bonesso D, Piccoli M, Lanfranchi G, Giacomello M, Scorrano L, Bean C. Dysfunctional mitochondria accumulate in a skeletal muscle knockout model of Smn1, the causal gene of spinal muscular atrophy. Cell Death Dis. 2023 Feb 27;14(2):162. doi: 10.1038/s41419-023-05573-x. PMID: 36849544; PMCID: PMC9971247.
- Chiriboga CA, Swoboda KJ, Darras BT, Iannaccone ST, Montes J, De Vivo DC, Norris DA, Bennett CF, Bishop KM. Results from a phase 1 study of nusinersen (ISIS-SMN(Rx)) in children with spinal muscular atrophy. Neurology. 2016 Mar 8;86(10):890-7. doi: 10.1212/WNL.0000000000002445. Epub 2016 Feb 10. PMID: 26865511; PMCID: PMC4782111.

- Cifuentes-Diaz C, Frugier T, Tiziano FD, Lacène E, Roblot N, Joshi V, Moreau MH, Melki J. Deletion of murine SMN exon 7 directed to skeletal muscle leads to severe muscular dystrophy. J Cell Biol. 2001 Mar 5;152(5):1107-14. doi: 10.1083/jcb.152.5.1107. PMID: 11238465; PMCID: PMC2198815.
- Coovert DD, Le TT, McAndrew PE, Strasswimmer J, Crawford TO, Mendell JR, Coulson SE, Androphy EJ, Prior TW, Burghes AH. The survival motor neuron protein in spinal muscular atrophy. Hum Mol Genet. 1997 Aug;6(8):1205-14. doi: 10.1093/hmg/6.8.1205. PMID: 9259265.
- Crawford, T.O. ( 2003) *Spinal muscular atrophies*, In: Jones, R.H., De Vivo, D.C. and Darras, B.T. (eds). *Neuromuscular Disorders of Infancy, Childhood, and Adolescence: A Clinician's Approach*, Butterworth Heinemann: Philadelphia, PA, pp. 145-166.
- D'Amico A, Mercuri E, Tiziano FD, Bertini E. Spinal muscular atrophy. Orphanet J Rare Dis. 2011 Nov 2;6:71. doi: 10.1186/1750-1172-6-71. PMID: 22047105; PMCID: PMC3231874.
- Daniela F, Vescovi AL, Bottai D. The stem cells as a potential treatment for neurodegeneration. Methods Mol Biol. 2007;399:199-213. doi: 10.1007/978-1-59745-504-6_14. PMID: 18309934.
- Darras BT. Spinal muscular atrophies. Pediatr Clin North Am. 2015 Jun;62(3):743-66. doi: 10.1016/j.pcl.2015.03.010. Epub 2015 Apr 11. PMID: 26022173.
- DiDonato CJ, Chen XN, Noya D, Korenberg JR, Nadeau JH, Simard LR. Cloning, characterization, and copy number of the murine survival motor neuron gene: homolog of the spinal muscular atrophy-determining gene. Genome Res. 1997 Apr;7(4):339-52. doi: 10.1101/gr.7.4.339. PMID: 9110173.
- Durmus H, Yilmaz R, Gulsen-Parman Y, Oflazer-Serdaroglu P, Cuttini M, Dursun M, Deymeer F. Muscle magnetic resonance imaging in spinal muscular atrophy type 3: Selective and progressive involvement. Muscle Nerve. 2017 May;55(5):651-656. doi: 10.1002/mus.25385. Epub 2017 Jan 5. PMID: 27543937.
- Edens BM, Ajroud-Driss S, Ma L, Ma YC. Molecular mechanisms and animal models of spinal muscular atrophy. Biochim Biophys Acta. 2015 Apr;1852(4):685-92. doi: 10.1016/j.bbadis.2014.07.024. Epub 2014 Aug 1. PMID: 25088406.
- El-Khodor BF, Edgar N, Chen A, Winberg ML, Joyce C, Brunner D, Suárez-Fariñas M, Heyes MP. Identification of a battery of tests for drug candidate evaluation in the SMNDelta7 neonate model of spinal muscular atrophy. Exp Neurol. 2008 Jul;212(1):29-43. doi: 10.1016/j.expneurol.2008.02.025. Epub 2008 Mar 18. PMID: 18455159.
- Fallini C, Bassell GJ, Rossoll W. Spinal muscular atrophy: the role of SMN in axonal mRNA regulation. Brain Res. 2012 Jun 26;1462:81-92. doi: 10.1016/j.brainres.2012.01.044. Epub 2012 Jan 28. PMID: 22330725; PMCID: PMC3360984.
- Fauroux B, Griffon L, Amaddeo A, Stremler N, Mazenq J, Khirani S, Baravalle-Einaudi M. Respiratory management of children with spinal muscular atrophy (SMA). Arch Pediatr. 2020 Dec;27(7S):7S29-7S34. doi: 10.1016/S0929-693X(20)30274-8. PMID: 33357594.
- Feather-Schussler DN, Ferguson TS. A Battery of Motor Tests in a Neonatal Mouse Model of Cerebral Palsy. J Vis Exp. 2016 Nov 3;(117):53569. doi: 10.3791/53569. PMID: 27842358; PMCID: PMC5226120.
- Feldkötter M, Schwarzer V, Wirth R, Wienker TF, Wirth B. Quantitative analyses of SMN1 and SMN2 based on real-time lightCycler PCR: fast and highly reliable carrier testing and prediction of severity of spinal muscular

atrophy. Am J Hum Genet. 2002 Feb;70(2):358-68. doi: 10.1086/338627. Epub 2001 Dec 21. PMID: 11791208; PMCID: PMC419987.

- Finkel RS, Mercuri E, Darras BT, Connolly AM, Kuntz NL, Kirschner J, Chiriboga CA, Saito K, Servais L, Tizzano E, Topaloglu H, Tulinius M, Montes J, Glanzman AM, Bishop K, Zhong ZJ, Gheuens S, Bennett CF, Schneider E, Farwell W, De Vivo DC; ENDEAR Study Group. Nusinersen versus Sham Control in Infantile-Onset Spinal Muscular Atrophy. N Engl J Med. 2017 Nov 2;377(18):1723-1732. doi: 10.1056/NEJMoa1702752. PMID: 29091570.
- Fitts RH. Cellular mechanisms of muscle fatigue. Physiol Rev. 1994 Jan;74(1):49-94. doi: 10.1152/physrev.1994.74.1.49. PMID: 8295935.
- Gavrilov DK, Shi X, Das K, Gilliam TC, Wang CH. Differential SMN2 expression associated with SMA severity. Nat Genet. 1998 Nov;20(3):230-1. doi: 10.1038/3030. PMID: 9806538.
- Gennarelli M, Lucarelli M, Capon F, Pizzuti A, Merlini L, Angelini C, Novelli G, Dallapiccola B. Survival motor neuron gene transcript analysis in muscles from spinal muscular atrophy patients. Biochem Biophys Res Commun. 1995 Aug 4;213(1):342-8. doi: 10.1006/bbrc.1995.2135. PMID: 7639755.
- Gidaro T, Servais L. Nusinersen treatment of spinal muscular atrophy: current knowledge and existing gaps. Dev Med Child Neurol. 2019 Jan;61(1):19-24. doi: 10.1111/dmcn.14027. Epub 2018 Sep 17. PMID: 30221755.
- Gogliotti RG, Quinlan KA, Barlow CB, Heier CR, Heckman CJ, Didonato CJ. Motor neuron rescue in spinal muscular atrophy mice demonstrates that sensory-motor defects are a consequence, not a cause, of motor neuron dysfunction. J Neurosci. 2012 Mar 14;32(11):3818-29. doi: 10.1523/JNEUROSCI.5775-11.2012. PMID: 22423102; PMCID: PMC3679185.
- Gondin J, Brocca L, Bellinzona E, D'Antona G, Maffiuletti NA, Miotti D, Pellegrino MA, Bottinelli R. Neuromuscular electrical stimulation training induces atypical adaptations of the human skeletal muscle phenotype: a functional and proteomic analysis. J Appl Physiol (1985). 2011 Feb;110(2):433-50. doi: 10.1152/japplphysiol.00914.2010. Epub 2010 Dec 2. PMID: 21127206.
- Gravina AG, Pellegrino R, Auletta S, Palladino G, Brandimarte G, D'Onofrio R, Arboretto G, Imperio G, Ventura A, Cipullo M, Romano M, Federico A. *Hericium erinaceus*, a medicinal fungus with a centuries-old history: Evidence in gastrointestinal diseases. World J Gastroenterol. 2023 May 28;29(20):3048-3065. doi: 10.3748/wjg.v29.i20.3048. PMID: 37346156; PMCID: PMC10280799.
- Guettier-Sigrist S, Hugel B, Coupin G, Freyssinet JM, Poindron P, Warter JM. Possible pathogenic role of muscle cell dysfunction in motor neuron death in spinal muscular atrophy. Muscle Nerve. 2002 May;25(5):700-708. doi: 10.1002/mus.10081. PMID: 11994964.
- Halliwell B, Cheah IK, Tang RMY. Ergothioneine - a diet-derived antioxidant with therapeutic potential. FEBS Lett. 2018 Oct;592(20):3357-3366. doi: 10.1002/1873-3468.13123. Epub 2018 Jun 15. PMID: 29851075.
- Hayashi M, Araki S, Arai N, Kumada S, Itoh M, Tamagawa K, Oda M, Morimatsu Y. Oxidative stress and disturbed glutamate transport in spinal muscular atrophy. Brain Dev. 2002 Dec;24(8):770-5. doi: 10.1016/s0387-7604(02)00103-1. PMID: 12453601.
- Hayhurst M, Wagner AK, Cerletti M, Wagers AJ, Rubin LL. A cell-autonomous defect in skeletal muscle satellite cells expressing low levels of survival of motor neuron protein. Dev Biol. 2012 Aug 15;368(2):323-34. doi: 10.1016/j.ydbio.2012.05.037. Epub 2012 Jun 15. PMID: 22705478; PMCID: PMC3851302.

- Hebert MD, Szymczyk PW, Shpargel KB, Matera AG. Coilin forms the bridge between Cajal bodies and SMN, the spinal muscular atrophy protein. Genes Dev. 2001 Oct 15;15(20):2720-9. doi: 10.1101/gad.908401. PMID: 11641277; PMCID: PMC312817.
- Hoffmann J. Uber chronische spinale Muskelatrophie im Kindersalter auf familiarer Basis. DeutZeitsch Nervenheilkd. 1893; 3(6):427–470.10.1007/BF01668496.
- Holeček M. Histidine in Health and Disease: Metabolism, Physiological Importance, and Use as a Supplement. Nutrients. 2020 Mar 22;12(3):848. doi: 10.3390/nu12030848. PMID: 32235743; PMCID: PMC7146355.
- Hwang I, Tang D, Paik J. Oxidative stress sensing and response in neural stem cell fate. Free Radic Biol Med. 2021 Jun;169:74-83. doi: 10.1016/j.freeradbiomed.2021.03.043. Epub 2021 Apr 18. PMID: 33862161; PMCID: PMC9594080.
- Hwee DT, Kennedy A, Ryans J, Russell AJ, Jia Z, Hinken AC, Morgans DJ, Malik FI, Jasper JR. Fast skeletal muscle troponin activator tirasemtiv increases muscle function and performance in the B6SJL-SOD1G93A ALS mouse model. PLoS One. 2014 May 7;9(5):e96921. doi: 10.1371/journal.pone.0096921. PMID: 24805850; PMCID: PMC4013064.
- Iftikhar M, Frey J, Shohan MJ, Malek S, Mousa SA. Current and emerging therapies for Duchenne muscular dystrophy and spinal muscular atrophy. Pharmacol Ther. 2021 Apr;220:107719. doi: 10.1016/j.pharmthera.2020.107719. Epub 2020 Oct 29. PMID: 33130193.
- Ivanov I, Atkinson D, Litvinenko I, Angelova L, Andonova S, Mumdjiev H, Pacheva I, Panova M, Yordanova R, Belovejdov V, Petrova A, Bosheva M, Shmilev T, Savov A, Jordanova A. Pontocerebellar hypoplasia type 1 for the neuropediatrician: Genotype-phenotype correlations and diagnostic guidelines based on new cases and overview of the literature. Eur J Paediatr Neurol. 2018 Jul;22(4):674-681. doi: 10.1016/j.ejpn.2018.03.011. Epub 2018 Apr 3. PMID: 29656927.
- Iyer CC, McGovern VL, Wise DO, Glass DJ, Burghes AH. Deletion of atrophy enhancing genes fails to ameliorate the phenotype in a mouse model of spinal muscular atrophy. Neuromuscul Disord. 2014 May;24(5):436-44. doi: 10.1016/j.nmd.2014.02.007. Epub 2014 Feb 25. PMID: 24656734; PMCID: PMC4005840.
- Jablonka S, Beck M, Lechner BD, Mayer C, Sendtner M. Defective Ca2+ channel clustering in axon terminals disturbs excitability in motoneurons in spinal muscular atrophy. J Cell Biol. 2007 Oct 8;179(1):139-49. doi: 10.1083/jcb.200703187. PMID: 17923533; PMCID: PMC2064743.
- Jager KJ, van Dijk PC, Zoccali C, Dekker FW. The analysis of survival data: the Kaplan-Meier method. Kidney Int. 2008 Sep;74(5):560-5. doi: 10.1038/ki.2008.217. Epub 2008 Jul 2. PMID: 18596735.
- James R, Chaytow H, Ledahawsky LM, Gillingwater TH. Revisiting the role of mitochondria in spinal muscular atrophy. Cell Mol Life Sci. 2021 May;78(10):4785-4804. doi: 10.1007/s00018-021-03819-5. Epub 2021 Apr 5. PMID: 33821292; PMCID: PMC8195803.
- Jurcau A. Insights into the Pathogenesis of Neurodegenerative Diseases: Focus on Mitochondrial Dysfunction and Oxidative Stress. Int J Mol Sci. 2021 Oct 31;22(21):11847. doi: 10.3390/ijms222111847. PMID: 34769277; PMCID: PMC8584731.
- Kariya S, Park GH, Maeno-Hikichi Y, Leykekhman O, Lutz C, Arkovitz MS, Landmesser LT, Monani UR. Reduced SMN protein impairs maturation of the neuromuscular junctions in mouse models of spinal muscular

atrophy. Hum Mol Genet. 2008 Aug 15;17(16):2552-69. doi: 10.1093/hmg/ddn156. Epub 2008 May 20. PMID: 18492800; PMCID: PMC2722888.

- Katsetos C. D., Koutzaki S., Melvin J. J. (2013). Mitochondrial dysfunction in neuromuscular disorders. *Semin. Pediatr. Neurol.* 20, 202–215. 10.1016/j.spen.2013.10.010
- Khirani S, Colella M, Caldarelli V, Aubertin G, Boulé M, Forin V, Ramirez A, Fauroux B. Longitudinal course of lung function and respiratory muscle strength in spinal muscular atrophy type 2 and 3. Eur J Paediatr Neurol. 2013 Nov;17(6):552-60. doi: 10.1016/j.ejpn.2013.04.004. Epub 2013 May 11. PMID: 23672834.
- Kim JK, Jha NN, Feng Z, Faleiro MR, Chiriboga CA, Wei-Lapierre L, Dirksen RT, Ko CP, Monani UR. Muscle-specific SMN reduction reveals motor neuron-independent disease in spinal muscular atrophy models. J Clin Invest. 2020 Mar 2;130(3):1271-1287. doi: 10.1172/JCI131989. PMID: 32039917; PMCID: PMC7269591.
- Kolb SJ, Coffey CS, Yankey JW, Krosschell K, Arnold WD, Rutkove SB, Swoboda KJ, Reyna SP, Sakonju A, Darras BT, Shell R, Kuntz N, Castro D, Iannaccone ST, Parsons J, Connolly AM, Chiriboga CA, McDonald C, Burnette WB, Werner K, Thangarajh M, Shieh PB, Finanger E, Cudkowicz ME, McGovern MM, McNeil DE, Finkel R, Kaye E, Kingsley A, Renusch SR, McGovern VL, Wang X, Zaworski PG, Prior TW, Burghes AH, Bartlett A, Kissel JT; NeuroNEXT Clinical Trial Network and on behalf of the NN101 SMA Biomarker Investigators. Baseline results of the NeuroNEXT spinal muscular atrophy infant biomarker study. Ann Clin Transl Neurol. 2016 Jan 21;3(2):132-45. doi: 10.1002/acn3.283. PMID: 26900585; PMCID: PMC4748311.
- Komiya Y, Nakamura T, Ishii M, Shimizu K, Hiraki E, Kawabata F, Nakamura M, Tatsumi R, Ikeuchi Y, Mizunoya W. Increase in muscle endurance in mice by dietary Yamabushitake mushroom (Hericium erinaceus) possibly via activation of PPARδ. Anim Sci J. 2019 Jun;90(6):781-789. doi: 10.1111/asj.13199. Epub 2019 Apr 1. PMID: 30938015; PMCID: PMC6594082.
- Kong L, Wang X, Choe DW, Polley M, Burnett BG, Bosch-Marcé M, Griffin JW, Rich MM, Sumner CJ. Impaired synaptic vesicle release and immaturity of neuromuscular junctions in spinal muscular atrophy mice. J Neurosci. 2009 Jan 21;29(3):842-51. doi: 10.1523/JNEUROSCI.4434-08.2009. PMID: 19158308; PMCID: PMC2746673.
- Larsen S, Nielsen J, Hansen CN, Nielsen LB, Wibrand F, Stride N, Schroder HD, Boushel R, Helge JW, Dela F, Hey-Mogensen M. Biomarkers of mitochondrial content in skeletal muscle of healthy young human subjects. J Physiol. 2012 Jul 15;590(14):3349-60. doi: 10.1113/jphysiol.2012.230185. Epub 2012 May 14. PMID: 22586215; PMCID: PMC3459047.
- Le TT, Pham LT, Butchbach ME, Zhang HL, Monani UR, Coovert DD, Gavrilina TO, Xing L, Bassell GJ, Burghes AH. SMNDelta7, the major product of the centromeric survival motor neuron (SMN2) gene, extends survival in mice with spinal muscular atrophy and associates with full-length SMN. Hum Mol Genet. 2005 Mar 15;14(6):845-57. doi: 10.1093/hmg/ddi078. Epub 2005 Feb 9. PMID: 15703193.
- Lee YI, Mikesh M, Smith I, Rimer M, Thompson W. Muscles in a mouse model of spinal muscular atrophy show profound defects in neuromuscular development even in the absence of failure in neuromuscular transmission or loss of motor neurons. Dev Biol. 2011 Aug 15;356(2):432-44. doi: 10.1016/j.ydbio.2011.05.667. Epub 2011 May 30. PMID: 21658376; PMCID: PMC3143211.

- Lefebvre S, Bürglen L, Reboullet S, Clermont O, Burlet P, Viollet L, Benichou B, Cruaud C, Millasseau P, Zeviani M, et al. Identification and characterization of a spinal muscular atrophy-determining gene. Cell. 1995 Jan 13;80(1):155-65. doi: 10.1016/0092-8674(95)90460-3. PMID: 7813012.
- Li Q. Nusinersen as a Therapeutic Agent for Spinal Muscular Atrophy. Yonsei Med J. 2020 Apr;61(4):273-283. doi: 10.3349/ymj.2020.61.4.273. PMID: 32233169; PMCID: PMC7105407.
- Ling KK, Gibbs RM, Feng Z, Ko CP. Severe neuromuscular denervation of clinically relevant muscles in a mouse model of spinal muscular atrophy. Hum Mol Genet. 2012 Jan 1;21(1):185-95. doi: 10.1093/hmg/ddr453. Epub 2011 Oct 3. PMID: 21968514; PMCID: PMC3235013.
- Ling KK, Lin MY, Zingg B, Feng Z, Ko CP. Synaptic defects in the spinal and neuromuscular circuitry in a mouse model of spinal muscular atrophy. PLoS One. 2010 Nov 11;5(11):e15457. doi: 10.1371/journal.pone.0015457. PMID: 21085654; PMCID: PMC2978709.
- Liu Q, Dreyfuss G. A novel nuclear structure containing the survival of motor neurons protein. EMBO J. 1996 Jul 15;15(14):3555-65. PMID: 8670859; PMCID: PMC451956.
- LoMauro A, Aliverti A, Mastella C, Arnoldi MT, Banfi P, Baranello G. Spontaneous Breathing Pattern as Respiratory Functional Outcome in Children with Spinal Muscular Atrophy (SMA). PLoS One. 2016 Nov 7;11(11):e0165818. doi: 10.1371/journal.pone.0165818. PMID: 27820869; PMCID: PMC5098831.
- Lomonte P, Baklouti F, Binda O. The Biochemistry of Survival Motor Neuron Protein Is Paving the Way to Novel Therapies for Spinal Muscle Atrophy. Biochemistry. 2020 Apr 14;59(14):1391-1397. doi: 10.1021/acs.biochem.9b01124. Epub 2020 Apr 2. PMID: 32227847.
- Long KK, O'Shea KM, Khairallah RJ, Howell K, Paushkin S, Chen KS, Cote SM, Webster MT, Stains JP, Treece E, Buckler A, Donovan A. Specific inhibition of myostatin activation is beneficial in mouse models of SMA therapy. Hum Mol Genet. 2019 Apr 1;28(7):1076-1089. doi: 10.1093/hmg/ddy382. PMID: 30481286; PMCID: PMC6423420.
- Lorson CL, Hahnen E, Androphy EJ, Wirth B. A single nucleotide in the SMN gene regulates splicing and is responsible for spinal muscular atrophy. Proc Natl Acad Sci U S A. 1999 May 25;96(11):6307-11. doi: 10.1073/pnas.96.11.6307. PMID: 10339583; PMCID: PMC26877.
- Lubos E, Loscalzo J, Handy DE. Glutathione peroxidase-1 in health and disease: from molecular mechanisms to therapeutic opportunities. Antioxid Redox Signal. 2011 Oct 1;15(7):1957-97. doi: 10.1089/ars.2010.3586. Epub 2011 Apr 10. PMID: 21087145; PMCID: PMC3159114.
- Lunn MR, Wang CH. Spinal muscular atrophy. Lancet. 2008 Jun 21;371(9630):2120-33. doi: 10.1016/S0140-6736(08)60921-6. PMID: 18572081.
- Mahmoodzadeh S, Koch K, Schriever C, Xu J, Steinecker M, Leber J, Dworatzek E, Purfürst B, Kunz S, Recchia D, Canepari M, Heuser A, Di Francescantonio S, Morano I. Age-related decline in murine heart and skeletal muscle performance is attenuated by reduced Ahnak1 expression. J Cachexia Sarcopenia Muscle. 2021 Oct;12(5):1249-1265. doi: 10.1002/jcsm.12749. Epub 2021 Jul 1. PMID: 34212535; PMCID: PMC8517348.
- Makrecka-Kuka M, Krumschnabel G, Gnaiger E. High-Resolution Respirometry for Simultaneous Measurement of Oxygen and Hydrogen Peroxide Fluxes in Permeabilized Cells, Tissue Homogenate and Isolated Mitochondria. Biomolecules. 2015 Jun 29;5(3):1319-38. doi: 10.3390/biom5031319. PMID: 26131977; PMCID: PMC4598754.

- Martínez-Hernández R, Soler-Botija C, Also E, Alias L, Caselles L, Gich I, Bernal S, Tizzano EF. The developmental pattern of myotubes in spinal muscular atrophy indicates prenatal delay of muscle maturation. J Neuropathol Exp Neurol. 2009 May;68(5):474-81. doi: 10.1097/NEN.0b013e3181a10ea1. PMID: 19525895.
- Mastaglia, F. L. and Walton, J. N. (1971). Histological and histochemical changes in skeletal muscle from cases of chronic juvenile and early adult spinal muscular atrophy (the Kugelberg-Welander syndrome). *J. Neurol. Sci.*, **12**, 15–44
- McGovern VL, Gavrilina TO, Beattie CE, Burghes AH. Embryonic motor axon development in the severe SMA mouse. Hum Mol Genet. 2008 Sep 15;17(18):2900-9. doi: 10.1093/hmg/ddn189. Epub 2008 Jul 3. PMID: 18603534; PMCID: PMC2722893.
- Meftahi GH, Bahari Z, Zarei Mahmoudabadi A, Iman M, Jangravi Z. Applications of western blot technique: From bench to bedside. Biochem Mol Biol Educ. 2021 Jul;49(4):509-517. doi: 10.1002/bmb.21516. Epub 2021 Apr 13. PMID: 33847452.
- Mercuri E, Sumner C.J, Muntoni F, Darras B.T & Finkel R.S. Spinal muscular Atrophy Nature reviews. Disease primers, 2022 Aug.
- Messina S, Sframeli M, Maggi L, D'Amico A, Bruno C, Comi G, Mercuri E. Spinal muscular atrophy: state of the art and new therapeutic strategies. Neurol Sci. 2022 Dec;43(Suppl 2):615-624. doi: 10.1007/s10072-021-05258-3. Epub 2021 Apr 19. PMID: 33871750.
- Michaud M, Arnoux T, Bielli S, Durand E, Rotrou Y, Jablonka S, Robert F, Giraudon-Paoli M, Riessland M, Mattei MG, Andriambeloson E, Wirth B, Sendtner M, Gallego J, Pruss RM, Bordet T. Neuromuscular defects and breathing disorders in a new mouse model of spinal muscular atrophy. Neurobiol Dis. 2010 Apr;38(1):125-35. doi: 10.1016/j.nbd.2010.01.006. Epub 2010 Jan 18. PMID: 20085811.
- Miguel-Aliaga I, Culetto E, Walker DS, Baylis HA, Sattelle DB, Davies KE. The Caenorhabditis elegans orthologue of the human gene responsible for spinal muscular atrophy is a maternal product critical for germline maturation and embryonic viability. Hum Mol Genet. 1999 Nov;8(12):2133-43. doi: 10.1093/hmg/8.12.2133. PMID: 10545592.
- Miller N, Shi H, Zelikovich AS, Ma YC. Motor neuron mitochondrial dysfunction in spinal muscular atrophy. Hum Mol Genet. 2016 Aug 15;25(16):3395-3406. doi: 10.1093/hmg/ddw262. Epub 2016 Aug 3. PMID: 27488123; PMCID: PMC5179954.
- Mohseni J, Zabidi-Hussin ZA, Sasongko TH. Histone deacetylase inhibitors as potential treatment for spinal muscular atrophy. Genet Mol Biol. 2013 Sep;36(3):299-307. doi: 10.1590/S1415-47572013000300001. Epub 2013 Aug 30. PMID: 24130434; PMCID: PMC3795173.
- Monani UR, Lorson CL, Parsons DW, Prior TW, Androphy EJ, Burghes AH, McPherson JD. A single nucleotide difference that alters splicing patterns distinguishes the SMA gene SMN1 from the copy gene SMN2. Hum Mol Genet. 1999 Jul;8(7):1177-83. doi: 10.1093/hmg/8.7.1177. PMID: 10369862.
- Montes J, Garber CE, Kramer SS, Montgomery MJ, Dunaway S, Kamil-Rosenberg S, Carr B, Cruz R, Strauss NE, Sproule D, De Vivo DC. Single-Blind, Randomized, Controlled Clinical Trial of Exercise in Ambulatory Spinal Muscular Atrophy: Why are the Results Negative? J Neuromuscul Dis. 2015 Oct 7;2(4):463-470. doi: 10.3233/JND-150101. PMID: 27858749; PMCID: PMC5240606.

- Montes J, Goodwin AM, McDermott MP, Uher D, Hernandez FM, Coutts K, Cocchi J, Hauschildt M, Cornett KM, Rao AK, Monani UR, Ewing Garber C, De Vivo DC. Diminished muscle oxygen uptake and fatigue in spinal muscular atrophy. Ann Clin Transl Neurol. 2021 May;8(5):1086-1095. doi: 10.1002/acn3.51353. Epub 2021 Mar 31. PMID: 33788421; PMCID: PMC8108417.
- Muntoni F, Bertini E, Comi G, Kirschner J, Lusakowska A, Mercuri E, Scoto M, van der Pol WL, Vuillerot C, Burdeska A, El-Khairi M, Fontoura P, Ives J, Gorni K, Reid C, Fuerst-Recktenwald S; OLEOS Study Group. Long-term follow-up of patients with type 2 and non-ambulant type 3 spinal muscular atrophy (SMA) treated with olesoxime in the OLEOS trial. Neuromuscul Disord. 2020 Dec;30(12):959-969. doi: 10.1016/j.nmd.2020.10.008. Epub 2020 Nov 5. PMID: 33246887.
- Murray LM, Comley LH, Thomson D, Parkinson N, Talbot K, Gillingwater TH. Selective vulnerability of motor neurons and dissociation of pre- and post-synaptic pathology at the neuromuscular junction in mouse models of spinal muscular atrophy. Hum Mol Genet. 2008 Apr 1;17(7):949-62. doi: 10.1093/hmg/ddm367. Epub 2007 Dec 8. PMID: 18065780.
- Mutsaers CA, Wishart TM, Lamont DJ, Riessland M, Schreml J, Comley LH, Murray LM, Parson SH, Lochmüller H, Wirth B, Talbot K, Gillingwater TH. Reversible molecular pathology of skeletal muscle in spinal muscular atrophy. Hum Mol Genet. 2011 Nov 15;20(22):4334-44. doi: 10.1093/hmg/ddr360. Epub 2011 Aug 12. PMID: 21840928.
- Namba T, Aberfeld D.C. & Grob D. Chronic spinal muscular atrophy. Journal of the Neurological Sciences, 11, 401. 1970.
- Naveed A, Calderon H. Onasemnogene Abeparvovec (AVXS-101) for the Treatment of Spinal Muscular Atrophy. J Pediatr Pharmacol Ther. 2021;26(5):437-444. doi: 10.5863/1551-6776-26.5.437. Epub 2021 Jun 28. PMID: 34239394; PMCID: PMC8244960.
- Neve A, Trüb J, Saxena S, Schümperli D. Central and peripheral defects in motor units of the diaphragm of spinal muscular atrophy mice. Mol Cell Neurosci. 2016 Jan;70:30-41. doi: 10.1016/j.mcn.2015.11.007. Epub 2015 Nov 24. PMID: 26621405.
- Parente V, Corti S. Advances in spinal muscular atrophy therapeutics. Ther Adv Neurol Disord. 2018 Feb 5;11:1756285618754501. doi: 10.1177/1756285618754501. PMID: 29434670; PMCID: PMC5802612.
- Paushkin S, Charroux B, Abel L, Perkinson RA, Pellizzoni L, Dreyfuss G. The survival motor neuron protein of Schizosacharomyces pombe. Conservation of survival motor neuron interaction domains in divergent organisms. J Biol Chem. 2000 Aug 4;275(31):23841-6. doi: 10.1074/jbc.M001441200. PMID: 10816558.
- Pedersen BK. Muscles and their myokines. J Exp Biol. 2011 Jan 15;214(Pt 2):337-46. doi: 10.1242/jeb.048074. PMID: 21177953.
- Peeters K, Chamova T, Jordanova A. Clinical and genetic diversity of SMN1-negative proximal spinal muscular atrophies. Brain. 2014 Nov;137(Pt 11):2879-96. doi: 10.1093/brain/awu169. Epub 2014 Jun 25. PMID: 24970098; PMCID: PMC4208460.
- Perego MGL, Galli N, Nizzardo M, Govoni A, Taiana M, Bresolin N, Comi GP, Corti S. Current understanding of and emerging treatment options for spinal muscular atrophy with respiratory distress type 1 (SMARD1). Cell Mol Life Sci. 2020 Sep;77(17):3351-3367. doi: 10.1007/s00018-020-03492-0. Epub 2020 Mar 2. PMID: 32123965.

- Perry CG, Kane DA, Lin CT, Kozy R, Cathey BL, Lark DS, Kane CL, Brophy PM, Gavin TP, Anderson EJ, Neufer PD. Inhibiting myosin-ATPase reveals a dynamic range of mitochondrial respiratory control in skeletal muscle. Biochem J. 2011 Jul 15;437(2):215-22. doi: 10.1042/BJ20110366. PMID: 21554250; PMCID: PMC3863643.
- Pino MG, Rich KA, Kolb SJ. Update on Biomarkers in Spinal Muscular Atrophy. *Biomarker Insights*. 2021;16. doi:10.1177/11772719211035643
- Piras A, Schiaffino L, Boido M, Valsecchi V, Guglielmotto M, De Amicis E, Puyal J, Garcera A, Tamagno E, Soler RM, Vercelli A. Inhibition of autophagy delays motoneuron degeneration and extends lifespan in a mouse model of spinal muscular atrophy. Cell Death Dis. 2017 Dec 20;8(12):3223. doi: 10.1038/s41419-017-0086-4. PMID: 29259166; PMCID: PMC5870600.
- Pogmore JP, Uehling D, Andrews DW. Pharmacological Targeting of Executioner Proteins: Controlling Life and Death. J Med Chem. 2021 May 13;64(9):5276-5290. doi: 10.1021/acs.jmedchem.0c02200. Epub 2021 May 3. PMID: 33939407.
- Rafii, S., O'Regan, P., Xinarianos, G., Azmy, I., Stephenson, T., Reed, M., Meuth, M., Thacker, J., & Cox, A. (2002). Neurofilament accumulation at the motor endplate and lack of axonal sprouting in a spinal muscular atrophy mouse model. Human Molecular Genetics, 11(12). https://doi.org/10.1093/hmg/11.12.1439.
- Ratni H, Scalco RS, Stephan AH. Risdiplam, the First Approved Small Molecule Splicing Modifier Drug as a Blueprint for Future Transformative Medicines. ACS Med Chem Lett. 2021 Jan 28;12(6):874-877. doi: 10.1021/acsmedchemlett.0c00659. PMID: 34141064; PMCID: PMC8201486.
- Ratto D, Corana F, Mannucci B, Priori EC, Cobelli F, Roda E, Ferrari B, Occhinegro A, Di Iorio C, De Luca F, Cesaroni V, Girometta C, Bottone MG, Savino E, Kawagishi H, Rossi P. *Hericium erinaceus* Improves Recognition Memory and Induces Hippocampal and Cerebellar Neurogenesis in Frail Mice during Aging. Nutrients. 2019 Mar 27;11(4):715. doi: 10.3390/nu11040715. PMID: 30934760; PMCID: PMC6521003.
- Ripolone M, Ronchi D, Violano R, Vallejo D, Fagiolari G, Barca E, Lucchini V, Colombo I, Villa L, Berardinelli A, Balottin U, Morandi L, Mora M, Bordoni A, Fortunato F, Corti S, Parisi D, Toscano A, Sciacco M, DiMauro S, Comi GP, Moggio M. Impaired Muscle Mitochondrial Biogenesis and Myogenesis in Spinal Muscular Atrophy. JAMA Neurol. 2015 Jun;72(6):666-75. doi: 10.1001/jamaneurol.2015.0178. Erratum in: JAMA Neurol. 2015 Oct;72(10):1210. PMID: 25844556; PMCID: PMC4944827.
- Roda E, Priori EC, Ratto D, De Luca F, Di Iorio C, Angelone P, Locatelli CA, Desiderio A, Goppa L, Savino E, Bottone MG, Rossi P. Neuroprotective Metabolites of *Hericium erinaceus* Promote Neuro-Healthy Aging. Int J Mol Sci. 2021 Jun 15;22(12):6379. doi: 10.3390/ijms22126379. PMID: 34203691; PMCID: PMC8232141.
- Rossi AE, Boncompagni S, Dirksen RT. Sarcoplasmic reticulum-mitochondrial symbiosis: bidirectional signaling in skeletal muscle. Exerc Sport Sci Rev. 2009 Jan;37(1):29-35. doi: 10.1097/JES.0b013e3181911fa4. PMID: 19098522; PMCID: PMC2740713.
- Rossi AE, Boncompagni S, Wei L, Protasi F, Dirksen RT. Differential impact of mitochondrial positioning on mitochondrial Ca(2+) uptake and Ca(2+) spark suppression in skeletal muscle. Am J Physiol Cell Physiol. 2011 Nov;301(5):C1128-39. doi: 10.1152/ajpcell.00194.2011. Epub 2011 Aug 17. PMID: 21849670; PMCID: PMC3213917.

- Rossi P, Cesaroni V, Brandalise F, Occhinegro A, Ratto D, Perrucci F, Lanaia V, Girometta C, Orrù G, Savino E. Dietary Supplementation of Lion's Mane Medicinal Mushroom, Hericium erinaceus (Agaricomycetes), and Spatial Memory in Wild-Type Mice. Int J Med Mushrooms. 2018;20(5):485-494. doi: 10.1615/IntJMedMushrooms.2018026241. PMID: 29953363.
- Rossi R, Bottinelli R, Sorrentino V, Reggiani C. Response to caffeine and ryanodine receptor isoforms in mouse skeletal muscles. Am J Physiol Cell Physiol. 2001 Aug;281(2):C585-94. doi: 10.1152/ajpcell.2001.281.2.C585. PMID: 11443058.
- Rudnik-Schöneborn S, Berg C, Zerres K, Betzler C, Grimm T, Eggermann T, Eggermann K, R Wirth, Wirth B, Heller R. Genotype–phenotype studies in infantile spinal muscular atrophy (SMA) type I in Germany: implications for clinical trials and genetic counselling. Clin Genet 2009: 76: 168–178. doi: 10.1111/j.1399-0004.2009.01200.x
- Ruiz R, Casañas JJ, Torres-Benito L, Cano R, Tabares L. Altered intracellular Ca2+ homeostasis in nerve terminals of severe spinal muscular atrophy mice. J Neurosci. 2010 Jan 20;30(3):849-57. doi: 10.1523/JNEUROSCI.4496-09.2010. PMID: 20089893; PMCID: PMC6633088.
- Schiaffino S, Reggiani C. Fiber types in mammalian skeletal muscles. Physiol Rev. 2011 Oct;91(4):1447-531. doi: 10.1152/physrev.00031.2010. PMID: 22013216.
- Schrank B, Götz R, Gunnersen JM, Ure JM, Toyka KV, Smith AG, Sendtner M. Inactivation of the survival motor neuron gene, a candidate gene for human spinal muscular atrophy, leads to massive cell death in early mouse embryos. Proc Natl Acad Sci U S A. 1997 Sep 2;94(18):9920-5. doi: 10.1073/pnas.94.18.9920. PMID: 9275227; PMCID: PMC23295.
- Schroth MK. Special considerations in the respiratory management of spinal muscular atrophy. Pediatrics. 2009 May;123 Suppl 4:S245-9. doi: 10.1542/peds.2008-2952K. PMID: 19420154.
- Seo J, Singh NN, Ottesen EW, Sivanesan S, Shishimorova M, Singh RN. Oxidative Stress Triggers Body-Wide Skipping of Multiple Exons of the Spinal Muscular Atrophy Gene. PLoS One. 2016 Apr 25;11(4):e0154390. doi: 10.1371/journal.pone.0154390. PMID: 27111068; PMCID: PMC4844106.
- Shababi M, Lorson CL, Rudnik-Schöneborn SS. Spinal muscular atrophy: a motor neuron disorder or a multi-organ disease? J Anat. 2014 Jan;224(1):15-28. doi: 10.1111/joa.12083. Epub 2013 Jul 22. PMID: 23876144; PMCID: PMC3867883.
- Simone C, Ramirez A, Bucchia M, Rinchetti P, Rideout H, Papadimitriou D, Re DB, Corti S. Is spinal muscular atrophy a disease of the motor neurons only: pathogenesis and therapeutic implications? Cell Mol Life Sci. 2016 Mar;73(5):1003-20. doi: 10.1007/s00018-015-2106-9. Epub 2015 Dec 18. PMID: 26681261; PMCID: PMC4756905.
- Singh NN, Hoffman S, Reddi PP, Singh RN. Spinal muscular atrophy: Broad disease spectrum and sex-specific phenotypes. Biochim Biophys Acta Mol Basis Dis. 2021 Apr 1;1867(4):166063. doi: 10.1016/j.bbadis.2020.166063. Epub 2021 Jan 5. PMID: 33412266; PMCID: PMC7867633.
- Singh RN, Howell MD, Ottesen EW, Singh NN. Diverse role of survival motor neuron protein. Biochim Biophys Acta Gene Regul Mech. 2017 Mar;1860(3):299-315. doi: 10.1016/j.bbagrm.2016.12.008. Epub 2017 Jan 15. PMID: 28095296; PMCID: PMC5325804.

- Singh RN. More is needed to complement the available therapies of spinal muscular atrophy. Future Med Chem. 2019 Nov;11(22):2873-2876. doi: 10.4155/fmc-2019-0239. Epub 2019 Oct 31. PMID: 31668092.
- Sleigh JN, Gillingwater TH, Talbot K. The contribution of mouse models to understanding the pathogenesis of spinal muscular atrophy. Dis Model Mech. 2011 Jul;4(4):457-67. doi: 10.1242/dmm.007245. PMID: 21708901; PMCID: PMC3124050.
- Smeriglio P, Langard P, Querin G, Biferi MG. The Identification of Novel Biomarkers Is Required to Improve Adult SMA Patient Stratification, Diagnosis and Treatment. J Pers Med. 2020 Jul 29;10(3):75. doi: 10.3390/jpm10030075. PMID: 32751151; PMCID: PMC7564782.
- Tang RMY, Cheah IK, Yew TSK, Halliwell B. Distribution and accumulation of dietary ergothioneine and its metabolites in mouse tissues. Sci Rep. 2018 Jan 25;8(1):1601. doi: 10.1038/s41598-018-20021-z. PMID: 29371632; PMCID: PMC5785509.
- Torres-Benito L, Neher MF, Cano R, Ruiz R, Tabares L. SMN requirement for synaptic vesicle, active zone and microtubule postnatal organization in motor nerve terminals. PLoS One. 2011;6(10):e26164. doi: 10.1371/journal.pone.0026164. Epub 2011 Oct 12. PMID: 22022549; PMCID: PMC3192162.
- Viollet L, Bertrandy S, Bueno Brunialti AL, Lefebvre S, Burlet P, Clermont O, Cruaud C, Guénet JL, Munnich A, Melki J. cDNA isolation, expression, and chromosomal localization of the mouse survival motor neuron gene (Smn). Genomics. 1997 Feb 15;40(1):185-8. doi: 10.1006/geno.1996.4551. PMID: 9070939.
- Voigt T, Meyer K, Baum O, Schümperli D. Ultrastructural changes in diaphragm neuromuscular junctions in a severe mouse model for Spinal Muscular Atrophy and their prevention by bifunctional U7 snRNA correcting SMN2 splicing. Neuromuscul Disord. 2010 Nov;20(11):744-52. doi: 10.1016/j.nmd.2010.06.010. Epub 2010 Sep 15. PMID: 20832308.
- Voigt T, Neve A, Schümperli D. The craniosacral progression of muscle development influences the emergence of neuromuscular junction alterations in a severe murine model for spinal muscular atrophy. Neuropathol Appl Neurobiol. 2014 Jun;40(4):416-34. doi: 10.1111/nan.12064. PMID: 23718187.
- Vu-Han TL, Reisener MJ, Putzier M, Pumberger M. Skoliose bei spinaler Muskelatrophie [Scoliosis in spinal muscular atrophy]. Orthopade. 2021 Aug;50(8):657-663. German. doi: 10.1007/s00132-021-04131-7. Epub 2021 Jul 7. PMID: 34232342.
- Wan JJ, Qin Z, Wang PY, Sun Y, Liu X. Muscle fatigue: general understanding and treatment. Exp Mol Med. 2017 Oct 6;49(10):e384. doi: 10.1038/emm.2017.194. PMID: 28983090; PMCID: PMC5668469.
- Werdnig G. Two early infantile hereditary cases of progressive muscular atrophy simulating dystrophy, but on a neural basis. 1891. Arch Neurol. 1971 Sep;25(3):276-8. doi: 10.1001/archneur.1971.00490030102014. PMID: 4952838.
- Wishart TM, Huang JP, Murray LM, Lamont DJ, Mutsaers CA, Ross J, Geldsetzer P, Ansorge O, Talbot K, Parson SH, Gillingwater TH. SMN deficiency disrupts brain development in a mouse model of severe spinal muscular atrophy. Hum Mol Genet. 2010 Nov 1;19(21):4216-28. doi: 10.1093/hmg/ddq340. Epub 2010 Aug 12. PMID: 20705736; PMCID: PMC2951867.
- Zambon AA, Pini V, Bosco L, Falzone YM, Munot P, Muntoni F, Previtali SC. Early onset hereditary neuronopathies: an update on non-5q motor neuron diseases. Brain. 2023 Mar 1;146(3):806-822. doi: 10.1093/brain/awac452. PMID: 36445400; PMCID: PMC9976982.

- Zanetta C, Riboldi G, Nizzardo M, Simone C, Faravelli I, Bresolin N, Comi GP, Corti S. Molecular, genetic and stem cell-mediated therapeutic strategies for spinal muscular atrophy (SMA). J Cell Mol Med. 2014 Feb;18(2):187-96. doi: 10.1111/jcmm.12224. Epub 2014 Jan 8. PMID: 24400925; PMCID: PMC3930406.
- Zeng W, Kong X, Alamana C, Liu Y, Guzman J, Pang PD, Day JW, Wu JC. Generation of two induced pluripotent stem cell lines from spinal muscular atrophy type 1 patients carrying no functional copies of SMN1 gene. Stem Cell Res. 2023 Jun;69:103095. doi: 10.1016/j.scr.2023.103095. Epub 2023 Apr 17. PMID: 37087898.
- Zerres K, Rudnik-Schöneborn S, Forrest E, Lusakowska A, Borkowska J, Hausmanowa-Petrusewicz I. A collaborative study on the natural history of childhood and juvenile onset proximal spinal muscular atrophy (type II and III SMA): 569 patients. J Neurol Sci. 1997 Feb 27;146(1):67-72. doi: 10.1016/s0022-510x(96)00284-5. PMID: 9077498.
- Zerres K, Rudnik-Schöneborn S. 93rd ENMC international workshop: non-5q-spinal muscular atrophies (SMA) - clinical picture (6-8 April 2001, Naarden, The Netherlands). Neuromuscul Disord. 2003 Feb;13(2):179-83. doi: 10.1016/s0960-8966(02)00211-0. PMID: 12565918.
- Zilio E, Piano V, Wirth B. Mitochondrial Dysfunction in Spinal Muscular Atrophy. Int J Mol Sci. 2022 Sep 17;23(18):10878. doi: 10.3390/ijms231810878. PMID: 36142791; PMCID: PMC9503857.
- Zuccarelli L, Baldassarre G, Magnesa B, Degano C, Comelli M, Gasparini M, Manferdelli G, Marzorati M, Mavelli I, Pilotto A, Porcelli S, Rasica L, Šimunič B, Pišot R, Narici M, Grassi B. Peripheral impairments of oxidative metabolism after a 10-day bed rest are upstream of mitochondrial respiration. J Physiol. 2021 Nov;599(21):4813-4829. doi: 10.1113/JP281800. Epub 2021 Sep 28. PMID: 34505290; PMCID: PMC9293208.


.